

# POLITECNICO DI TORINO

Department of Mechanical and Aerospace Engineering

Master's Degree in Mechanical Engineering



**Politecnico  
di Torino**



**NTNU**

Norwegian University of  
Science and Technology

Master's Degree Thesis

---

## **Residual service life assessment in steel railway bridges using the updated FE model of an existing bridge**

---

**Supervisor**

Prof. Marco Domaneschi

**Co-Supervisors**

Prof. Anders Rønnquist

Prof. Gunnstein Thomas Frøseth

**Candidate**

Pier Luca Todesco

December 2021



---

# Abstract

Promoting railways as a sustainable, innovative, interconnected and safe means of transport, of both passengers and goods, and strengthening its contribution to the economy, industry and trade are some of the priorities which have involved the whole world in the last decades.

Nowadays, on Norwegian soil, approximately 50 to 90 per cent of the goods are transported on rails over the entire territory.

Because of increasing service loads and train speeds, rail authorities are therefore paying attention to predict and possibly extend the remaining service life of railway infrastructures.

Accordingly, the aim of this study is to estimate the condition of an existing historical steel railway bridge in order to define cost-effective maintenance strategies and avoid the sudden interruption of the regular service with considerable economic losses.

Railway bridges are indeed subjected to repetitive high stress due to the live loads acting on them, so they have to be examined to point out a possible fatigue failure. Real time structural health monitoring, however, may not always be available for maintenance purposes and for reporting progressive damage conditions up to failure.

In this regard, a simple finite element model of the bridge is developed and employed as a simulation tool for numerical analyses. Moreover, a more accurate model is also prepared in parallel.

The Modal Assurance Criterion (*MAC*) for the evaluation of mode shapes is exploited with the purpose of validate the two models respect to each other.

In the absence of monitoring data on the real structure, a comparison between the previously developed models and others coming from independent studies is also performed. From that, it has been shown that the quality and the level of detail of a numerical model are a function of engineer's sensitivity and background and that modelling discrepancies can affect the results.

Furthermore, the Late Acceptance Hill Climbing (*LAHC*) model updating algorithm is implemented with the aim of minimizing the disparities in behaviour of the models, improving consequently the fatigue life assessment of the bridge. The effect of model uncertainties is investigated on the most stressed components.

Afterwards, the updated model is employed to evaluate the capacity losses of the bridges during its service period.

---

An influence line analysis is conducted in the most critical sections in terms of shape equivalence and stresses magnitude.

Lastly, taking into account eight different trains, Miner's cumulative damage law and S-N curves are used to assess the most damaged components and the most damaging trains.

Hence, it is proven that, by exploiting simulations conducted on an optimized numerical model and the theory of fatigue, the estimation of the health of the structure is achievable.

---

# Table of contents

Abstract.....	i
Index of figures.....	v
Table index.....	vii
1 Introduction .....	1
1.1 Background .....	2
1.1.1 Railway transportation system in Norway.....	2
1.1.2 Reasons behind the survey.....	3
1.2 Material fatigue and fatigue analysis .....	4
1.3 Aim of the study .....	5
1.4 Outline .....	5
2 Development of the numerical models.....	6
2.1 Identification of the geometry and of the bridge characteristics.....	7
2.2 CAD model exploiting <i>Ansys SpaceClaim</i> .....	11
2.3 FE model exploiting <i>Ansys Mechanical APDL</i> .....	15
2.3.1 FEM model creation, simplifications and modelling uncertainties .....	15
2.3.2 Model developed by the consulting company .....	20
3 Definition of railway trainsets.....	22
4 Identification of disparities and similarities between models.....	26
4.1 Comparisons on the static behaviour of the bridge - Influence Line analysis .....	26
4.1.1 Theory.....	26
4.1.2 Definition of the three loading conditions .....	27
4.1.3 Consulting company's IL calculation .....	30
4.1.4 IL computation on self-made models .....	33
4.1.5 Shape equivalence .....	40
4.1.6 Stresses magnitude comparative .....	45
4.2 Comparisons on the dynamic behaviour of the bridge - Modal Assurance Criterion.....	56
4.2.1 Theory.....	56
4.2.2 Applying the model .....	57
5 Damage evaluation on critical components .....	59
5.1 Miner's linear damage summation rule.....	59
5.2 Discrepancies between the three models .....	61
6 Model Updating.....	68
6.1 FE model modification .....	69
6.1.1 Evaluation of the parameters that influence fatigue behaviour: model uncertainties .....	69
6.1.2 Modification of the connections between critical components.....	70

---

6.2	Late Acceptance Hill Climbing algorithm .....	72
6.2.1	How the algorithm works .....	72
6.2.2	Definition of move and objective functions .....	75
6.2.3	Identification of the three most damaged components to be analysed .....	76
6.2.4	Optimal values of the considered parameters .....	77
6.2.5	LAHC efficiency and effectiveness.....	79
7	Conclusions.....	83
8	References.....	84

---

# Index of figures

Figure 1 Bridge over Sokna stream.....	1
Figure 2 Norwegian transport infrastructure.....	2
Figure 3 Bridge over Sokna stream.....	6
Figure 4 Bridge drawings - side view.....	7
Figure 5 Bridge drawings - top view.....	7
Figure 6 Bridge drawings - side view.....	7
Figure 7 Gusset plates.....	8
Figure 8 Rail track curvature.....	8
Figure 9 Cross girder - stringer intersection.....	8
Figure 10 Wind bracers.....	9
Figure 11 Subsystem.....	9
Figure 12 Constraints at lower chords ends.....	10
Figure 13 Picture depicting the constraint conditions at the end of the lower chords.....	10
Figure 14 Picture depicting the constraint conditions at the end of the stringers.....	10
Figure 15 Constraints at the stringers ends.....	11
Figure 16 CAD simple model.....	11
Figure 17 Side view on xz plane - wireframe simple model.....	12
Figure 18 Top view - wireframe simple model.....	12
Figure 19 Side view on yz plane - wireframe simple model.....	13
Figure 20 CAD complete model.....	13
Figure 21 Side view on xz plane - wireframe complete model.....	14
Figure 22 Top view - wireframe complete model.....	14
Figure 23 Side view on yz plane - wireframe complete model.....	14
Figure 24 FEM model and detail - Simple model.....	15
Figure 25 FEM model and detail - Complete model.....	16
Figure 26 Element BEAM188 Ansys.....	18
Figure 27 Element SHELL63 Ansys.....	18
Figure 28 Lines discretization - Simple and complete models.....	19
Figure 29 Element creation - Simple and complete model.....	19
Figure 30 Constraints - Simple and complete model.....	20
Figure 31 Johs Holt's FEM model.....	20
Figure 32 Johs Holt's constraint definition.....	21
Figure 33 Bogie wagon.....	23
Figure 34 Two axle wagon.....	23
Figure 35 Load vector associated to Train1.....	24
Figure 36 Load vector associated to Train2.....	24
Figure 37 Load vector associated to Train3.....	24
Figure 38 Load vector associated to Train4.....	24
Figure 39 Load vector associated to Train5.....	25
Figure 40 Load vector associated to Train6.....	25
Figure 41 Load vector associated to Train7.....	25
Figure 42 Load vector associated to Train8.....	25
Figure 43 Inclination of the rail track plane with respect to the horizontal one.....	28
Figure 44 Application of unit loads and their distribution to the wheel-track contact.....	28
Figure 45 Johs Holt FEM model.....	30
Figure 46 First company's load condition: $R_v$ .....	31
Figure 47 Second company's load condition: $R_t$ .....	31
Figure 48 Third company's load condition: $R_h$ .....	31
Figure 49 Internal forces and moments, for the simpler model, due to the self-weight of the structure.....	34
Figure 50 Considered elements position and number - Simple model.....	36

---

<i>Figure 51 Most stressed point on the section</i> .....	39
Figure 52 Normal stress <i>IL</i> per unit load comparison - Stringer: elem. 102 simple, elem. 102 complete .....	41
<i>Figure 53 Normal stress IL per unit load comparison - Subsystem: elem. 1154 simple, elem. 1884 complete</i> .....	41
Figure 54 Normal stress <i>IL</i> per unit load comparison - Cross girder: elem. 829 simple, elem. 1049 complete.....	42
Figure 55 Normal stress <i>IL</i> per unit load comparison - Cross girder: elem. 844 simple, elem. 1064 complete.....	42
Figure 56 Normal stress <i>IL</i> per unit load comparison - Cross girder: elem. 879 simple, elem. 1618 complete.....	43
Figure 57 Normal stress <i>IL</i> per unit load comparison - Cross girder: elem. 929 simple, elem. 1249 complete.....	43
Figure 58 Normal stress <i>IL</i> per unit load comparison - Vertical 9: elem. 1327 simple, elem. 2380 complete .....	43
<i>Figure 59 Normal stress IL per unit load comparison - Vertical 1: elem. 1390 simple, elem. 2696 complete</i> .....	43
Figure 60 Normal stress <i>IL</i> per unit load comparison - Diagonal 1/0: elem. 620 simple, elem. 817 complete.....	44
Figure 61 Normal stress <i>IL</i> per unit load comparison - Diagonal 9/11: elem. 617 simple, elem. 847 complete.....	44
Figure 62 Normal stress <i>IL</i> per unit load comparison- Upper chord: elem. 533 simple, elem. 13766 complete .....	44
Figure 63 Normal stress <i>IL</i> per unit load comparison - Lower chord: elem. 426 simple, elem. 13846 complete .....	44
<i>Figure 64 Resultant force exerts more against the outside rail than the inside rail</i> .....	47
Figure 65 Normal stress <i>IL</i> comparison - Diagonal 1/0: elem. 620 simple, elem. 817 complete. T8.....	53
Figure 66 Normal stress <i>IL</i> comparison - Stringer: elem. 102 simple, elem. 102 complete. T8.....	54
Figure 67 Normal stress <i>IL</i> comparison - Cross girder: elem. 844 simple, elem. 1064 complete. T8.....	54
Figure 68 Normal stress <i>IL</i> comparison - Lower chord: elem. 426 simple, elem. 13846 complete. T8.....	55
Figure 69 MAC matrix .....	58
Figure 70 Linear endurance curve .....	60
Figure 71 Element COMBIN14 Ansys .....	70
Figure 72 LAHC example.....	72
Figure 73 Hill climbing functioning .....	73
Figure 74 Late acceptance hill climbing functioning .....	74
Figure 75 Energy vs number of steps - Attempt 1 .....	80
Figure 76 Energy vs number of steps - Attempt 2 .....	80
Figure 77 Energy vs number of steps - Attempt 3 .....	80
Figure 78 Energy vs number of steps - Attempt 4 .....	81
Figure 79 Energy vs number of steps - Attempt 5 .....	81
Figure 80 Energy vs number of steps - Attempt 6 .....	81
Figure 81 Energy vs number of steps - Attempt 7 .....	82

---

# Table index

Table 1 Elements and node selected and their geometrical properties - Simple model.....	17
Table 2 Elements and node selected and their geometrical properties - Complete model.....	17
Table 3 Material properties.....	18
Table 4 Trains characteristics.....	23
Table 5 Normal stress <b>IL</b> per unit load univocal names.....	34
Table 6 Elements and nodes correspondence.....	35
Table 7 Correspondence between the position of the origin of the RFs for the self-made models and Johs Holt's one.....	35
Table 8 Local and global RF correspondence - Simple model.....	35
Table 9 Local and global RF correspondence - Complete model.....	35
Table 10 Forces, moments and stresses for element 102, simple model, unit vertical load on a single stringer.....	38
Table 11 Normal stress <b>IL</b> shape equivalence.....	40
Table 12 Normal stress <b>IL</b> shape equivalence - Different section points evaluation.....	41
Table 13 Normal stress <b>IL</b> univocal names.....	45
Table 14 Maximum difference between the absolute values of normal stress <b>IL</b> - Train 1.....	48
Table 15 Maximum difference between the absolute values of normal stress <b>IL</b> - Train 2.....	49
Table 16 Maximum difference between the absolute values of normal stress <b>IL</b> - Train 3.....	49
Table 17 Maximum difference between the absolute values of normal stress <b>IL</b> - Train 4.....	50
Table 18 Maximum difference between the absolute values of normal stress <b>IL</b> - Train 5.....	50
Table 19 Maximum difference between the absolute values of normal stress <b>IL</b> - Train 6.....	51
Table 20 Maximum difference between the absolute values of normal stress <b>IL</b> - Train 7.....	51
Table 21 Maximum difference between the absolute values of normal stress <b>IL</b> - Train 8.....	52
Table 22 Matched mode shapes.....	57
Table 23 Most damaged elements and most damaging trains.....	61
Table 24 Damages and damage differences - Train 1.....	62
Table 25 Damages and damage differences - Train 2.....	63
Table 26 Damages and damage differences - Train 3.....	64
Table 27 Damages and damage differences - Train 4.....	64
Table 28 Damages and damage differences - Train 5.....	65
Table 29 Damages and damage differences - Train 6.....	65
Table 30 Damages and damage differences - Train 7.....	66
Table 31 Damages and damage differences - Train 8.....	66
Table 32 Damages and damage differences - Train 8 - elem. 844.....	67
Table 33 Normal stress differences, damages and damage differences - Train 8.....	76
Table 34 Results of the model updating procedure.....	78

---

# 1 Introduction

The object of the study is the railway bridge over the Sokna stream in Lundamo, in the municipality of Melhus in Trøndelag county, Norway. A picture of the bridge is illustrated in Figure 1.

This bridge is part of the Dovre line on the section Støren-Trondheim.

It was built in 1917. A subsequent reinforcement, assumed to be definitive for the entire life of the structure, was carried out in 1942.



*Figure 1 Bridge over Sokna stream*

In 2018, the railway infrastructure owner commissioned the consulting company Johs Holt to conduct an investigation aimed at determining the condition of the structure and its remaining fatigue life.

The numerical model created by the company and the results obtained by them will be taken as a reference in order to evaluate the effect of structural modelling on the estimated service life of the structure and in order to validate the conclusions drawn from the analyzes conducted on the self-made models.

The remaining fatigue life was estimated using a finite element model of the structure, a fatigue load model and the S-N curve methodology.

The quality of the data and the validity of all the models used in the fatigue life estimation, has a large influence on the accuracy of the estimated fatigue life [1], [2]. Recently, much work has been carried out to improve load modelling [2] and fatigue modelling of riveted structures [3]. It has also been shown that the structural model can be inaccurate to estimate the stress response in key components of steel railway bridges [4].

Another important aspect in regards to structural modelling is the fact that a structural model is subjective to the engineer(s) that establishes them, i.e. a structural model established by one engineer is in general different from

a structural model developed by another engineer. This aspect has potentially a huge impact on the estimated fatigue life of steel bridges, and has not been thoroughly investigated in this domain before.

This thesis considers the influence of structural modelling on fatigue life analysis of steel railway bridges. A finite element model of the Sokna bridge is established. This finite element model is then compared to the finite element model developed in the fatigue life project from 2018 by the Norwegian infrastructure owner. Furthermore, this thesis establishes a framework for updating a finite element model for fatigue analysis with measurement data to ensure more accurate and reliable fatigue life estimates can be obtained.

## 1.1 Background

### 1.1.1 Railway transportation system in Norway

The Norwegian railway system, shown in Figure 2, consists of a railway network more than 4000 km long, of which about 2600 are electrified. The Norwegian, state-owned, company Bane NOR is responsible for the construction, monitoring, maintenance and renewing of the infrastructure.

The first railway line dates back to 1854, connecting Oslo and Eidsvoll. Between the end of the nineteenth and the beginning of the twentieth century, much of the Norwegian railway infrastructure developed. The Dovre line was inaugurated in 1920.



Figure 2 Norwegian transport infrastructure

The Norwegian government has made available, on the basis of the national transport plan for the period 2018-2029 [5], substantial funding, in particular for new constructions and the renovation of the current infrastructure. In recent years, there has been a sharp increase in demand: consequently, an enhancement in the offer for rail passengers, particularly in the most densely populated areas, is necessary.

The aim is to standardize and modernize the rail system. This consists of many old infrastructures. The railways in the Nordland region are among the first routes to undergo this modernization process.

Having said that, the need to screen the entire railway infrastructure in order to assess and monitor its condition is even more stringent. In this way you are able to identify the structures that require corrective action and those that need to be replaced because they have reached the end of life.

With regard to railway infrastructure, bridges are a primary element. Due to the topology of Norway, with its large number of mountains, ridges, valleys, creeks and rivers, the presence of numerous railway bridges is necessary. On Norwegian soil there are more than 2700.

### 1.1.2 Reasons behind the survey

Most of the railway bridges in Norway were built in the early 1900s and the 40% of these bridges are made entirely of steel.

These structures were therefore designed on the basis of the requirements and on the railway vehicles of the time.

However, the load conditions to which the rail network is subject have changed over the decades.

The design, axle loads, speeds and frequency of passages of both freight and passenger trains has changed several times since the time these infrastructures were conceived.

Generally, the new load conditions are more damaging.

In recent decades, there has been an increase in population and an increase in rail trade that have led to an increase in demand on the ageing railway infrastructure.

By focusing on railway bridges, which are essential in railway infrastructure, the combination of historical and modern loads, which are not always necessarily most severe, has resulted in a loss of structural capacity and a progressive increase in damage.

Railway bridges are generally characterized by very long service lives. Since these structures are entirely made of steel, or have at least numerous components in this material, the most typical damage phenomenon is that resulting from fatigue. The entire history load, difficult to identify since much data on historical load conditions are missing, to which the bridge is subject will contribute in the rise and subsequent extension of fatigue cracks.

The condition of these bridges must therefore be verified, especially in a condition of increased operational demands, in order to ensure a safe use of the infrastructure.

It follows that you need to be able to estimate the remaining service life of railway bridges and improve this estimation.

When systematic and periodic monitoring in the field, by means of sensors, is not possible or is considered not to be economically affordable, it is essential to develop numerical, reliable, models that allow to predict the conditions at which each component of the bridge stands.

## 1.2 Material fatigue and fatigue analysis

As mentioned above, fatigue phenomena are the main reason of damage in steel railway bridges, causing the loss of structural capacity and eventually the collapse of the structure.

Fatigue is a dynamic phenomenon and manifests itself in two subsequent phases: the initiation, which includes nucleation and growth, and the propagation of a crack. The formation of the crack generally occurs on the surface (at points of maximum tension for example or due to the surface roughness) and/or where there is concentration of tensions.

Usually the final collapse consists of a fracture, failure due to fragile behavior, at the residual section of the component due to the achievement by the crack of a critical length. The fracture represents the final event of the fatigue phenomenon and occurs very quickly.

In the fracture zone, the initiation point of the defect, the bench marks and the fracture area can be identified.

The fatigue of the material is caused by the application of cyclic loads, as it is for the bridges under consideration continuously subject to load cycles due to the passage of convoys.

The cyclic load, in fact, causes an inter-granular movement of the dislocations, called slip, where high tensions and cyclic shear tensions/deformations occur.

The movement of the dislocations involves the formation of slip bands, that is, a modification of the microstructural characteristics of the material occurs.

As a result of the formation of slip bands, as they propagate towards the surface, micro-cracks are formed.

Such micro-cracks, later, grow in the direction of maximum shear tension, namely along the grains that make up the microstructure of the material. At this point there are cracks visible with the naked eye.

Due to the high normal stresses, with respect to the component surface and shear ones on the grains, fatigue cracks propagate until they lead to the yielding of the net section or to fracture.

The longer the fatigue phenomenon lasts, the more the phase of formation of the crack predominates over that of propagation.

There are also two families of fatigue behavior:

- fatigue for high number of cycles: high fatigue durations and small plastic deformations
- fatigue due to low number of cycles: reduced fatigue life and high plastic deformations

In the case of railway bridges you generally speak of high cycle fatigue.

One of the first methods developed for the study of *HCF* was the fatigue endurance model introduced by Wöhler, which introduces the concept of fatigue limit and  $\sigma - N$  diagrams.

Through this model, the number of cycles that elapse from an immaculate condition of the material to a condition of fatigue failure are identified, thus defining the entire life of the component under examination, when it is subject to load cycles at constant amplitude.

In assessing the fatigue damage in the bridge under analysis, the endurance curves of the material will be used.

Using the theory of fracture mechanics it is possible to estimate the remaining fatigue life of the structure. However, this requires that the initial size of the crack is known and that the phenomenon of fatigue develops during the growth of the crack itself.

Often, however, it is not possible to identify and measure a crack because accurate and periodic inspections of the bridge would be necessary.

As a result, other theories are exploited to estimate fatigue life. One of these, the one used in this discussion, is the linear damage summation rule formulated by Miner, which will be described in detail in the chapter on damage.

Having no information about the state of the fatigue mechanism of the structure, both the period of formation and that of growth of the crack are considered.

The fatigue life is therefore determined by combining the fatigue endurance model and a damage accumulation model, which takes into account the application of load histories at variable amplitudes.

It is essential, in order to monitor bridges, to be able to control and predict the state of fatigue of the material to avoid the failure of the structure, which would lead to economic losses and, potentially, affect the well-being of people or things.

Fatigue life assessment is therefore essential in order to have a well-managed railway network, which does not involve a waste of money linked to the interruption of rail traffic, reliable and safe.

## 1.3 Aim of the study

The focus of this thesis is to consider the influence of the engineer on modelling of steel railway and to develop a framework for model updating of a finite element model by measurement of bridge response.

In order to do this, in the absence of monitoring data, two models are developed and to validate them mutual comparisons and comparisons with a model developed by a consulting company are performed.

Subsequently, chosen to analyse only one of the two models, a model updating procedure is followed in order to reduce the gap, in terms of estimated damage, with the Johs Holt Consultant Eng. model taken as a reference.

## 1.4 Outline

Chapter two describes the steps that led to the identification of the configuration of the bridge and the hypotheses made in order to create a simplified *CAD* model first and a *FEM* model then. A comparison is then made with respect to the assumptions made by Johs Holt Consultant Eng..

Chapter three explains how the load functions associated with the trains examined are constructed.

The fourth chapter deals with a series of comparisons made between the three models in possession. Formerly, the static behavior of the three models are compared through the study of stress influence lines. A comparison in terms of the shape and magnitude of these curves is made.

Subsequently, a comparison of the dynamic behavior, eigenfrequencies and mode shapes, is conducted using the two simple models in order to validate them with respect to each other.

The chapter in which the occurred damage in the critical components of the bridge is evaluated is the fifth. Miner's linear summation rule is exploited.

In the last chapter, the sixth, the Late Acceptance Hill Climbing algorithm is illustrated and executed, aimed at optimizing the stress and strain responses of the model.

## 2 Development of the numerical models

The first step of the study is focused on the examination of the geometry of the bridge.

In order to do this, the available technical drawings and the examination done in the field are exploited. The picture in Figure 3 is taken during the inspection.



*Figure 3 Bridge over Sokna stream*

During the development of the models, the report written by the consulting company was not taken into consideration so as to create independent modeling, whose results will be compared with those of Johs Holt Consultant Eng. at the end of the modelling process.

In this way, it is avoided being influenced by the assumptions and simplifications they made.

Indeed one of the goals of the study is to demonstrate how a different sensitivity of the engineer can lead to the adoption of different modelling choices that may produce disparities in terms of results.

## 2.1 Identification of the geometry and of the bridge characteristics

The bridge over the Sokna stream is a steel frame structure rather standard in the field of railway bridges (Figures 4-6). The truss/beam framework follows the Pratt scheme, noticeable in Figure 4. According to this configuration, the upper chord is expected to be subject to compression, the lower chord to traction. Even verticals should be subject to compression, odd ones should be unloaded.

The structure consists of three identical truss bridges with 20 m span each, the total length hence reaches 60 m. For the purposes of the analysis, the focus will therefore be put on a single section of the bridge.



Figure 4 Bridge drawings - side view

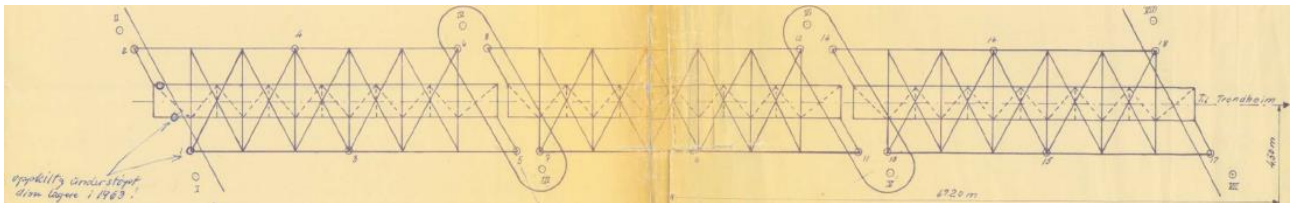


Figure 5 Bridge drawings - top view

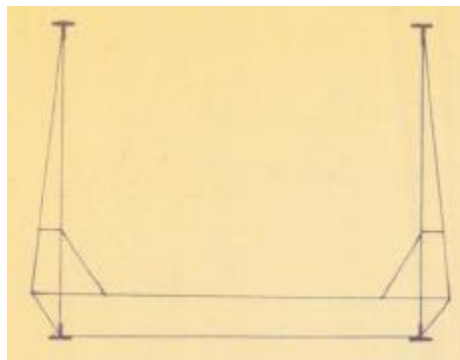


Figure 6 Bridge drawings - side view

The three spans are centrally supported by means of two pylons lying on the riverbed. An ensemble of slender beams, characterized by sections with different profiles, joined by means of rivets, represents the supporting structure of the bridge. Above the grid consisting of cross girders and stringers, lie transversely arranged wooden beams and the rail tracks.

At most of the joints between truss members and beams, where an additional support is required to withstand stress, there are gusset plates, made of cold-rolled steel, showed in Figure 7. Gusset plates are fastened to permanent members only by means of rivets and are painted as all the other elements of the bridge frame to give an extra layer of protection against corrosion.



Figure 7 Gusset plates

The viability on the bridge is guaranteed in both directions, but only one pair of tracks is present. The axis of the bridge turns out to be straight, unlike that of the rail track. The tracks have in fact a curvature whose radius amounts to  $500\text{ m}$ , as evident in Figure 8. In defining the load conditions to which the structure is subject, the effect of this aspect will be taken into account.

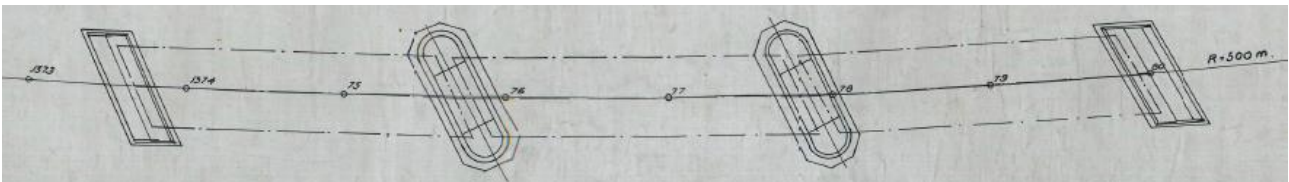


Figure 8 Rail track curvature

The main components of the structure are:

- Lower chords
- Upper chords: subject to compression when a train passes
- Stringers and cross girders. Their intersection is displayed in Figure 9.



Figure 9 Cross girder - stringer intersection

- Verticals: counteract the phenomenon of buckling at the upper chords when these are under load

- Diagonals
- Wind bracers, Figure 10: they brace the deck in the plane avoiding the sliding due to shear effects and act as a load divider, then as reinforcement



*Figure 10 Wind bracers*

- Subsystems, Figure 11, located in the transversal direction that reinforce the grid consisting of cross girders and stringers



*Figure 11 Subsystem*

On the basis of the examination of the technical drawings and on the basis of the personal inspection of the bridge, the support systems were identified.

Each of the two lower chords is bound at its extremities. An end is totally bound to translation in the three directions in space.

The other end is instead bound to the translation in the vertical and transverse direction, but not to the longitudinal one in order not to have a hyperstatic structure. Release along the longitudinal axis is allowed by means of roller bearings as shown in Figure 12 and Figure 13.

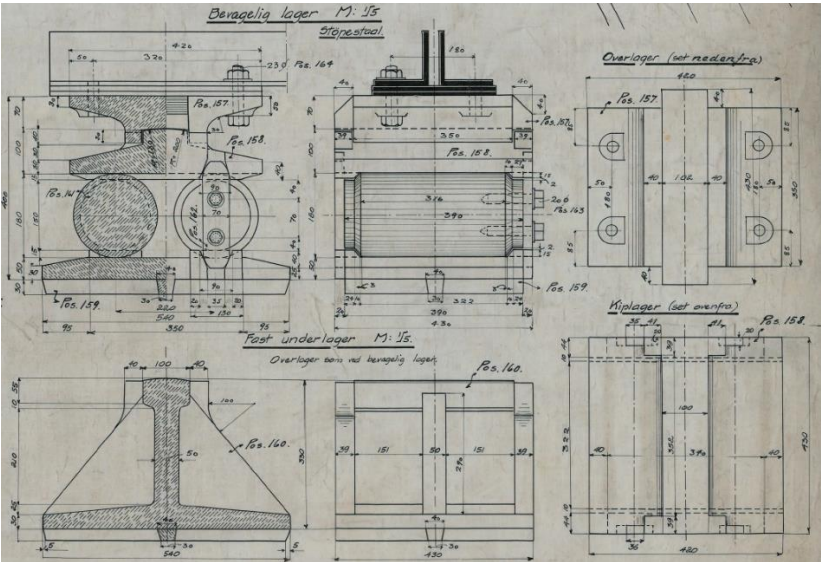


Figure 12 Constraints at lower chords ends



Figure 13 Picture depicting the constraint conditions at the end of the lower chords

Other constraint conditions appear at the ends of the stringers. As highlighted by the pictures in Figure 14 and Figure 15, the stringers lean on supports that prevent their translation in a vertical direction but allow them to move in a longitudinal direction.

Focusing on the translation along the transverse axis, this is also constrained by means of cast iron elements. It will be expected in subsequent analyses, therefore, that the value assumed by the stress influence lines at the two ends of the stringers, for loads applied in a vertical and transverse direction, is equal to zero.



Figure 14 Picture depicting the constraint conditions at the end of the stringers



Therefore, in this first phase, the presence of two-dimensional elements, such as shells or plates, or three-dimensional elements is not intended.

This simplifying hypothesis refers to the simple geometry of the structure. It will be demonstrated later how the simplified model is able to represent quite faithfully the behaviour of the bridge, especially for the study that is intended to be conducted on it, without consequently complicating the realization of the model and increasing the computational effort.

In order to create a simplified model of the bridge, it is necessary to understand what are the load carrying systems of the structure. Two are distinguished:

- Primary load carrying system: the components belonging to this set, redirect the loads to the supports, where consequently they are discharged. The elements that are part of it are the diagonals, the verticals, upper and lower chords and the bottom wind bracers.
- Secondary load carrying system: these elements redirect the load to the primary system. This includes stringers, cross girders and wind bracers at the rail track level.

By defining the simplified model, an assumption is made: you assume to condense the two load carrying systems obtaining a simplified geometry of the structure. Upper wind bracers, lower wind bracers, subsystems, cross girders and stringers now all lie in the same plane and equivalent section profiles are defined.

It is intended to show that this geometric simplification leads to a model that is still able to simulate the behavior of the structure with good precision.

It has been necessary to define equivalent section profiles, trying to match the original values of areas and second moments of inertia.

The wireframe of the bridge is represented in Figure 17 - Figure 19.

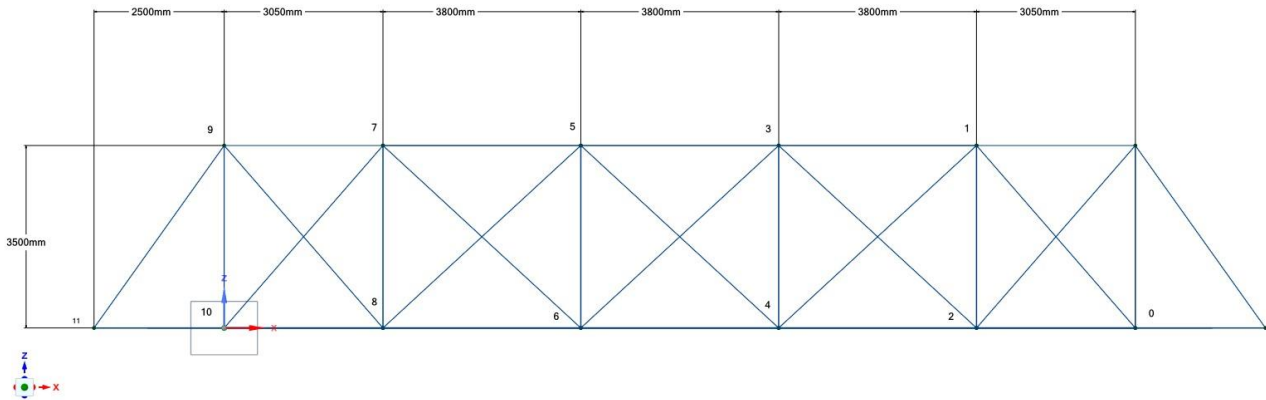


Figure 17 Side view on xz plane - wireframe simple model

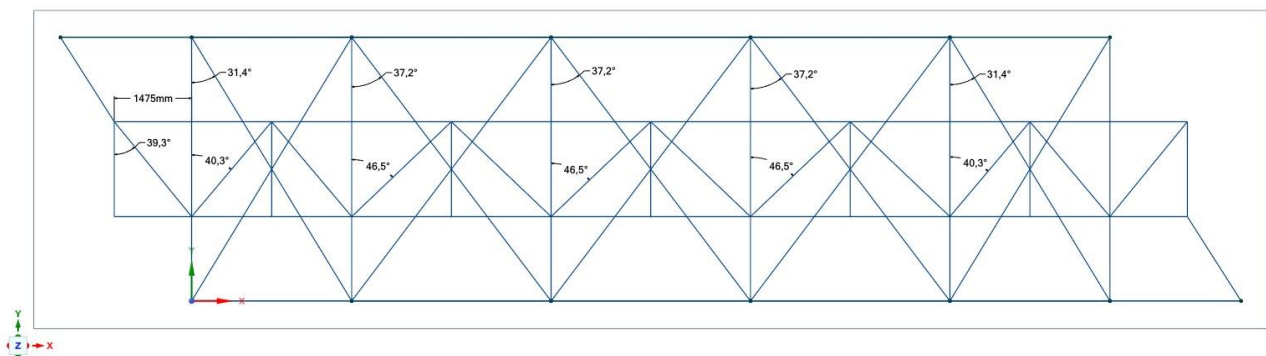


Figure 18 Top view - wireframe simple model

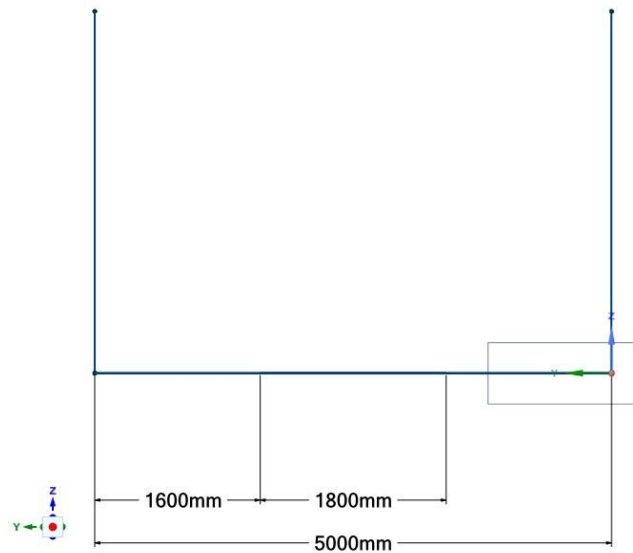


Figure 19 Side view on yz plane - wireframe simple model

Once the first simulations have been carried out on the simplified model, in particular those aimed at determining the influence lines, a sensitivity analysis is carried out to assess whether an update of the model is required.

A second model, Figure 20, has been then prepared for comparison with respect to the simplified one. The second model is aimed to evaluate whether the geometric simplifications previously made and the definition of equivalent sections can lead to differences in terms of output.

The refined model, which will be named in the discussion as *complete*, has a geometry much more consistent to the real bridge:

- The two load carrying systems are no longer compressed
- Stringers and cross girders are represented as they are in reality: slender beams joined by a plate element
- The subsystems are represented as in the actual structure, without bringing them back to an equivalent beam with a C-profile
- Addition of reinforcing components in the verticals, which however proved not being useful for a structural purpose
- Almost all the section profiles used are the same as those defined by the technical drawings except for a few exceptions

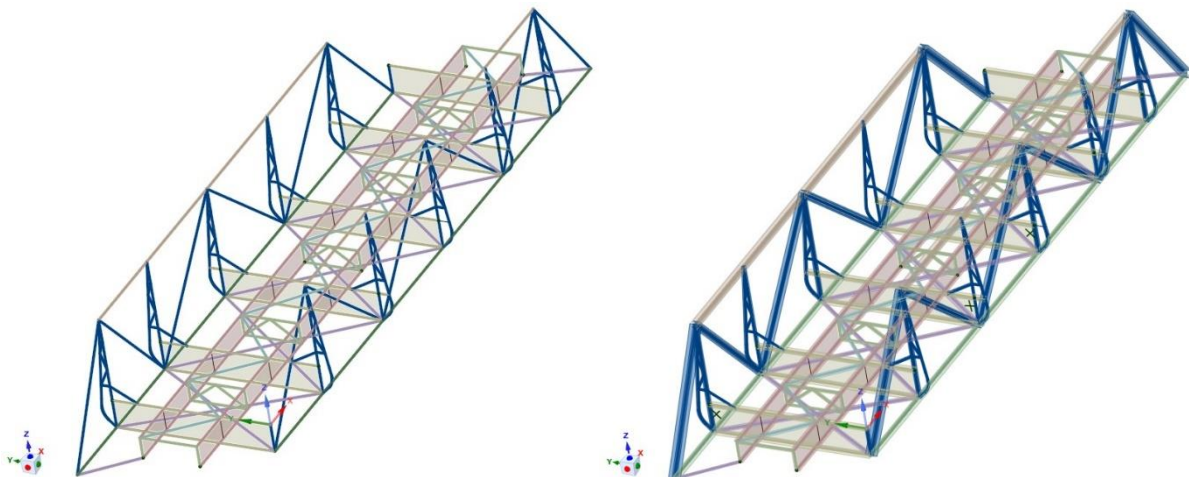


Figure 20 CAD complete model

The resulting geometry is illustrated in the following figures, Figure 21 - Figure 23:

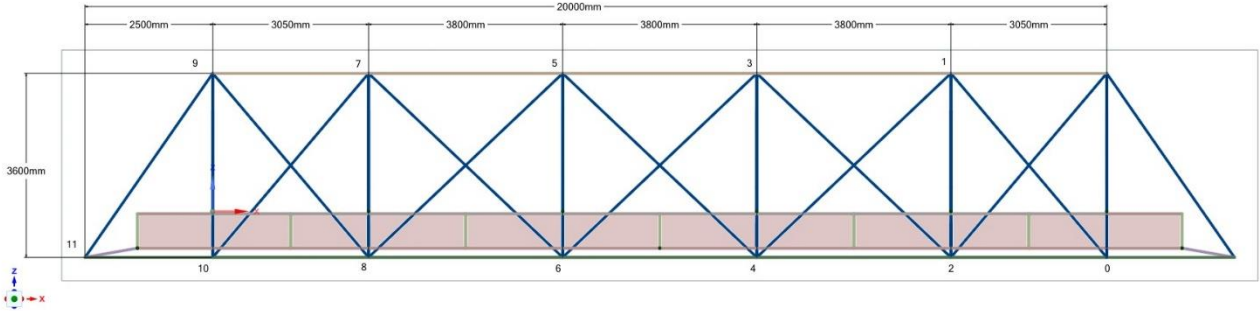


Figure 21 Side view on xz plane - wireframe complete model

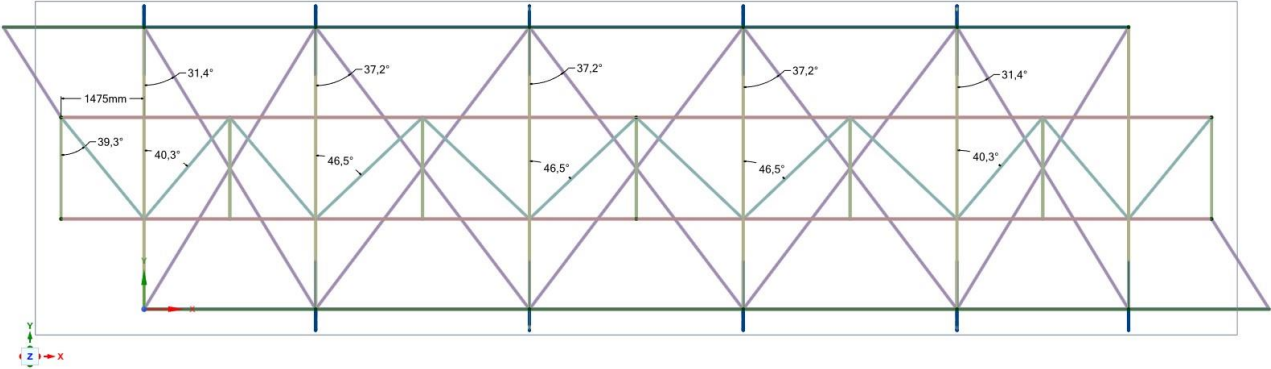


Figure 22 Top view - wireframe complete model

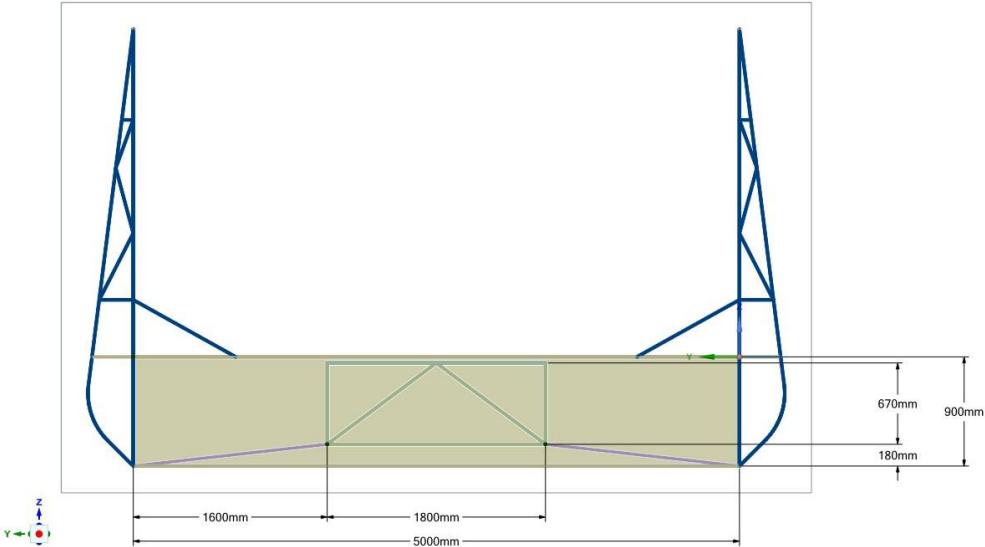


Figure 23 Side view on yz plane - wireframe complete model

## 2.3 FE model exploiting *Ansys Mechanical APDL*

### 2.3.1 FEM model creation, simplifications and modelling uncertainties

*FEM* modeling was performed exploiting *Ansys Mechanical APDL* software.

*Ansys Mechanical APDL* is a finite element solver that allows you to conduct simulations of various kinds (structural, thermal, acoustic, electrostatic, etc.) on numerical models.

Models and simulations have been performed using the *Ansys Parametric Design Language*. A parametric writing of the code allows to quickly introduce changes on the model and on the load conditions.

A first simplified model, Figure 24, is built using only one-dimensional elements in space, therefore systematically structured with a division of nodes and beam elements.

Specifically, *BEAM188* elements [6] were used to model each component of the frame.

Through the use of these elements it was possible to create cross sections with conventional profiles.

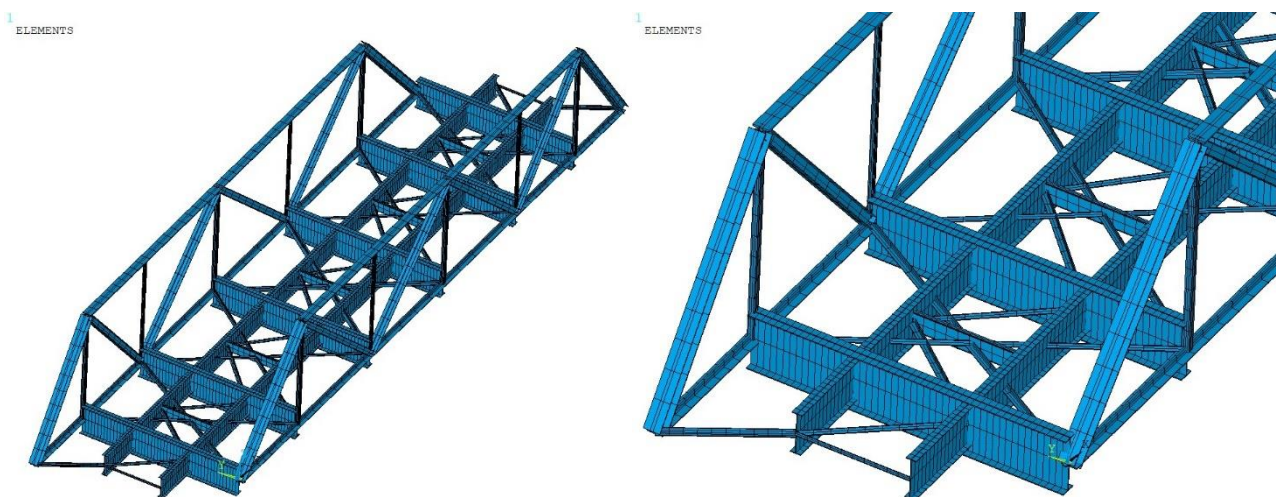


Figure 24 FEM model and detail - Simple model

The simplified model is based on the establishing of some hypotheses:

- Definition of equivalent sections where necessary. For components subject mainly to axial and flexural loads, it is sufficient that the equivalent sections present the same area and the same second moments of inertia of the original sections.
- Condensation of the two load carrying systems: stringers, cross girders and wind bracers lie on the same z coordinate and the subsystem is reduced to a beam element with equivalent C-section
- Junction between the individual components made by means of fully fixed joints (with infinite stiffness). The stiffness in correspondence of the connections, in particular the critical ones, is an aspect to be taken into account. It is expected that these stiffnesses, decrease the greater the damage that incurs.

The second model, Figure 25, has been prepared afterwards the comparisons made between the influence lines of the simple model and the one developed by the consulting agency.

Therefore, the geometry of the bridge has been reproduced as accurately as possible with respect to the real one.

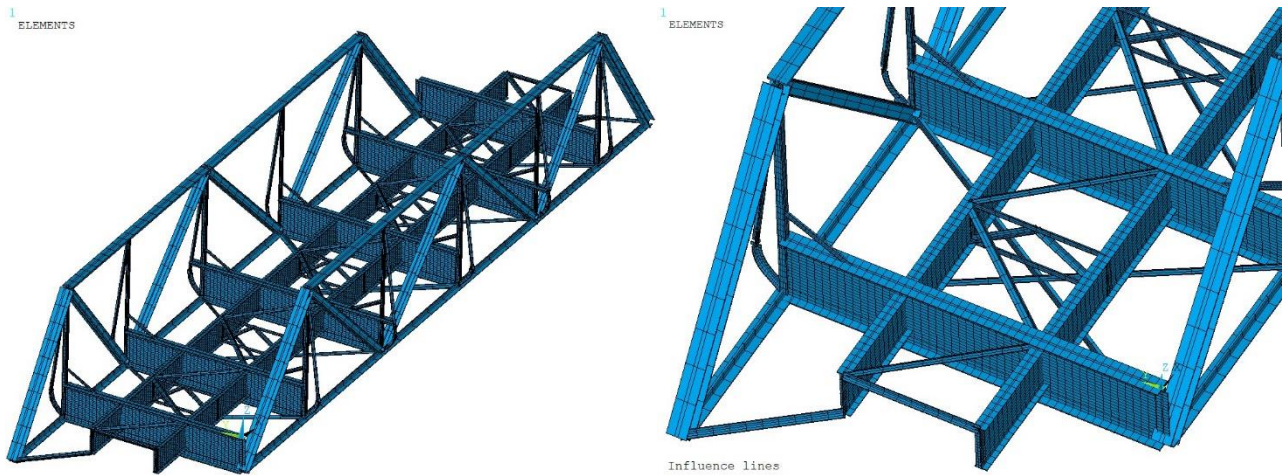


Figure 25 FEM model and detail - Complete model

As mentioned, stringers, cross girders and subsystems are no longer represented by equivalent components, but are now modeled as they really are.

Stringers and cross girders, in particular, consist of L-profile beams and thin-thickness panels. The subsystem is no longer traced back to a beam with equivalent C-section, but is represented in its ensemble of L-profile beams. All the profiles of the bridge constituents are now the actual ones except those of the verticals and the upper chord.

Given the geometrical simplicity of the frame, it was considered sufficient to re-model each beam component as one-dimensional elements with two nodes and 12 degrees of freedom (*DOF*) overall (*BEAM 188*) and model the reinforcement plates with *SHELL63* elements [6].

Therefore, you did not want to increase the complexity of the model and the computational efforts by using two- or three-dimensional elements throughout the structure. The results obtained with the simple model are already satisfactory and an analysis on the benefits that a certain type of element or a certain refinement of the mesh could have was not considered relevant for the purposes of the study.

The intent to build a second model, therefore, arose rather from the desire to evaluate the effect of the geometrical simplification.

In the analysis conducted, only some elements and therefore some specific sections of the bridge will be considered. The choice follows the desire to study the behavior in some specific points of the bridge that could be critical for fatigue damage.

Table 1 and Table 2 exhibit the number of elements and nodes taken into account and the geometric characteristics of those sections.

Simple model												
Location	Elem.	Node	Section type	Sectional area [mm <sup>2</sup> ]	I <sub>zz</sub> [mm <sup>4</sup> ]	I <sub>yy</sub> [mm <sup>4</sup> ]	TKZ [mm]	TKY [mm]	Area average [mm <sup>2</sup> ]	smin [mm]	smax [mm]	Σa <sup>3</sup> s <sup>3</sup> [mm <sup>4</sup> ]
Stinger	102	104	I equivalent	11000.00	6.92E+06	6.23E+08	670.00	160.00		10.00	12.00	1.44E+06
Subsystem	1154	799	C equivalent	4992.00	1.66E+06	5.59E+07	300.00	108.48		12.00	12.00	8.52E+05
Cross girder (CG-vertical 9 junction)	829	412	I equivalent	17602.00	3.01E+07	1.95E+09	750.00	13.00		13.00	13.00	1.65E+06
Cross girder (CG-stringer junction)	844	207	I equivalent	17602.00	3.01E+07	1.95E+09	750.00	13.00		13.00	13.00	1.65E+06

Cross girder (CG- diagonal 9/8 junction)	879	422	I equivalent	17602.00	3.01E+07	1.95E+09	750.00	13.00		13.00	13.00	1.65E+06
Vertical 9	1327	1296	Square equivalent	6001.40	6.92E+06	6.92E+06	99.60	99.60	6001.40	18.50	18.50	
Vertical 1	1390	1351	Square equivalent	7104.36	8.36E+06	8.36E+06	103.00	103.00	7104.36	21.90	21.90	
Diagonal 1/0	620	622	I	16604.00	3.98E+07	1.25E+08	240.00	260.00		13.00	46.00	2.20E+07
Diagonal 9/11	617	621	I	16604.00	3.98E+07	1.25E+08	240.00	260.00		13.00	46.00	2.20E+07
Upper chord	533	539	T equivalent	14594.00	4.23E+07	4.78E+07	252.28	46.00		28.00	46.00	2.28E+07
Lower chord	426	431	T equivalent	5902.00	1.51E+07	7.99E+06	170.44	26.00		13.00	26.00	2.82E+06
Cross girder (CG-vertical 5 junction)	929	428	I equivalent	17602.00	3.01E+07	1.95E+09	750.00	13.00		13.00	13.00	1.65E+06

Table 1 Elements and node selected and their geometrical properties - Simple model

Complete model												
Location	Elem.	Node	Section type	Sectional area [mm <sup>2</sup> ]	I <sub>zz</sub> [mm <sup>4</sup> ]	I <sub>yy</sub> [mm <sup>4</sup> ]	TKZ [mm]	TKY [mm]	Area average [mm <sup>2</sup> ]	s <sub>min</sub> [mm]	s <sub>max</sub> [mm]	Σa * s <sup>3</sup> [mm <sup>4</sup> ]
Stinger	102	103	T	3000.00	3.46E+06	1.78E+06	47.33	160.00		10.00	20.00	4.59E+05
Subsystem	1884	1857	L	1179.00	5.34E+05	5.34E+05	41.60	98.40		9.00	9.00	9.55E+04
Cross girder (CG-vertical 9 junction)	1049	1044	T	5902.00	1.51E+07	7.99E+06	157.44	26.00		13.00	26.00	2.60E+06
Cross girder (CG- stringer junction)	1064	1061	T	5902.00	1.51E+07	7.99E+06	157.44	26.00		13.00	26.00	2.60E+06
Cross girder (CG- diagonal 9/8 junction)	1618	867	T	5902.00	1.51E+07	7.99E+06	157.44	26.00		13.00	26.00	2.60E+06
Vertical 9	2380	2326	Square equivalent	6001.40	6.92E+06	6.92E+06	99.60	99.60	6001.40	18.50	18.50	
Vertical 1	2696	2619	Square equivalent	7104.36	8.36E+06	8.36E+06	103.00	103.00	7104.36	21.90	21.90	
Diagonal 1/0	817	822	I	16604.00	3.98E+07	1.25E+08	240.00	260.00		13.00	46.00	2.20E+07
Diagonal 9/11	847	856	I	16604.00	3.98E+07	1.25E+08	240.00	260.00		13.00	46.00	2.20E+07
Upper chord	13766	12759	T equivalent	14594.00	4.23E+07	4.78E+07	252.28	46.00		28.00	46.00	2.28E+07
Lower chord	13846	12828	T	5902.00	1.51E+07	7.99E+06	170.44	26.00		13.00	26.00	2.82E+06
Cross girder (CG-vertical 5 junction)	1249	1248	T	5902.00	1.51E+07	7.99E+06	157.44	26.00		13.00	26.00	2.60E+06

Table 2 Elements and node selected and their geometrical properties - Complete model

Where:

- $Area_{average} = chord * s_{min}$
- $a$ : is the mean section length
- $s$ : is the thickness of the section
- $s_{max}$  is the maximum thickness of the rectangles that make up the section

The modeling procedure, the same for both self-made models, can be summarized as follows:

- Importing of the bridge wireframe in the form of an *IGES* file.  
Definition of the properties of the material that makes up the structure and creation of the associated *material property*. The structure is entirely made of steel.  
All components of the frame, except the gusset plates, are made of *s355* steel with the following characteristics:

Steel s355		
Density, $\rho$	7.85E-03	g/mm <sup>3</sup>
Young's modulus, E	2.10E+05	MPa
Shear modulus, G	8.10E+04	MPa
Poisson's modulus, $\nu$	0.30	
Yield strength, $\sigma_y$	355.00	MPa
Ultimate strength, $\sigma_u$	490.00	MPa

Table 3 Material properties

The gusset plates are in cold-rolled steel.

- Indication of the element types used.  
As mentioned, for the simple model only *BEAM188* elements are used (Figure 26).

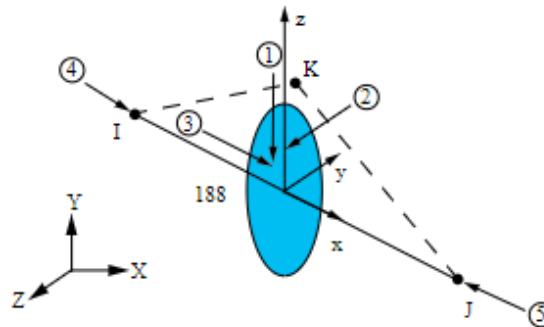


Figure 26 Element BEAM188 Ansys

*BEAM188* is ideal for the study of slender beam structures. The element is based on Timoshenko beam theory which includes shear-deformation effects, although the effect of shear forces is not taken into account in this discussion.

It is a two-node one-dimensional element with behaviour in space characterized by six *DOF* per node (three translational and three rotational), used here in its option with linear behaviour. It also allows the definition of sections with standard profile of various types.

The complete model, on the other hand, also makes use of *SHELL63* elements (Figure 27).

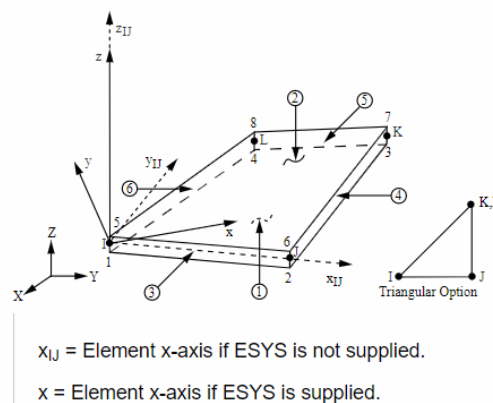


Figure 27 Element SHELL63 Ansys

Such an element is a four-node two-dimensional element with six *DOF* per node (three translational and three rotational).

For the *SHELL63* element, you must first define a *real constant* that associates the thickness information to the element.

Finite elements are based on the choice of *DOF* in nodes: in this case both the beam element in space and the shell element have the same *DOF* in the nodes. It is therefore not necessary to impose further kinematic relations. Their assembly is consistent from the point of view of *DOF*.

The *CP* command ensures that the corresponding *DOF* are connected.

- Construction of the mesh.

Discretization of the lines constituting the model, as shown in Figure 28, and for the 2D elements discretization of the previously created areas.

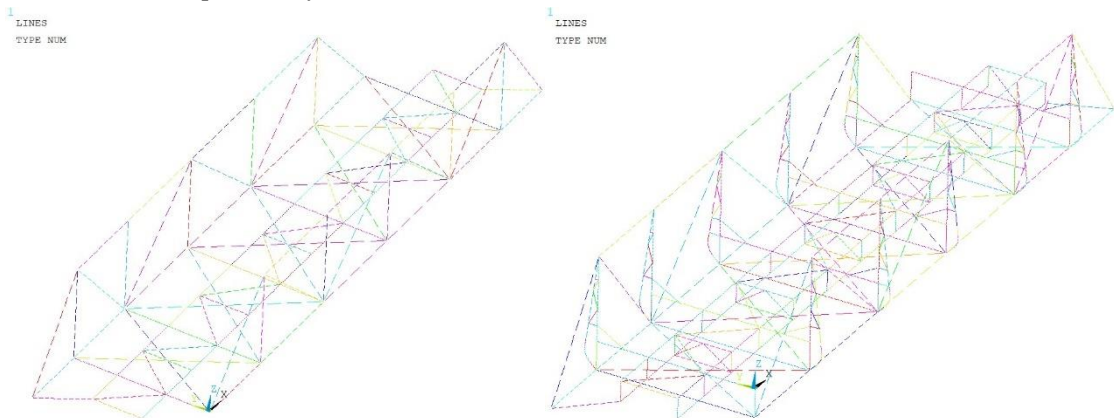


Figure 28 Lines discretization - Simple and complete models

Definition of section profiles for beam elements and association of *element types*, *real constants* and *material properties* to the mesh. The result of the element creation is illustrated in Figure 29.

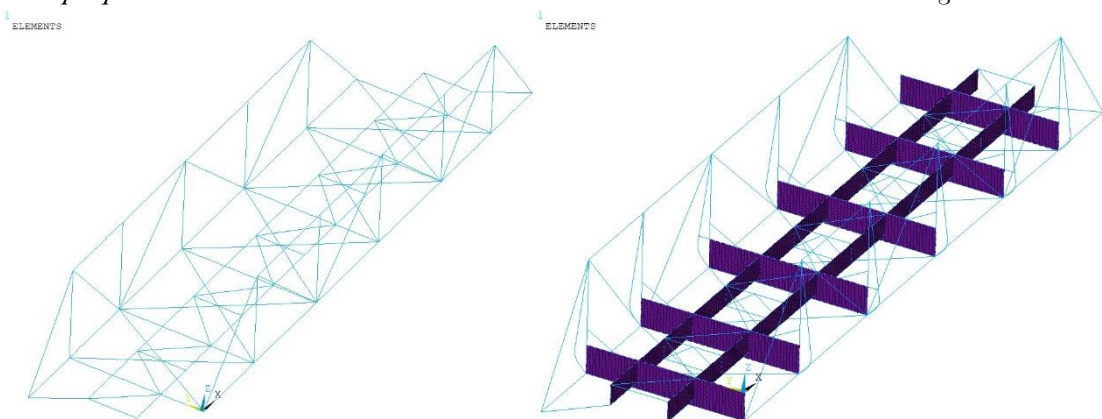


Figure 29 Element creation - Simple and complete model

It should be noted that the discretization of the main longitudinal beams follows the load conditions to which the structure is intended to be subjected in order to determine the stress influence lines.

In reality, the loads are exchanged between the wheels of the convoy and the rail tracks. However, since the rails lie exactly above the stringers, separated only by means of the transverse wooden beams, it is considered appropriate to apply the loads directly on the stringers themselves.

The load vector associated with the eight trains examined is discretized in space every 10 *cm*. The influence lines will require the same subdivision, consequently a discretization of the stringers every 10 *cm* is defined.

- Definition of constraint conditions (displayed in Figure 30).  
For both self-made models, the stringers are constrained, at both ends, not to translate in a vertical and transverse direction.  
The lower chords at one end see all the translations prevented, in the other only translation in the longitudinal direction is allowed.

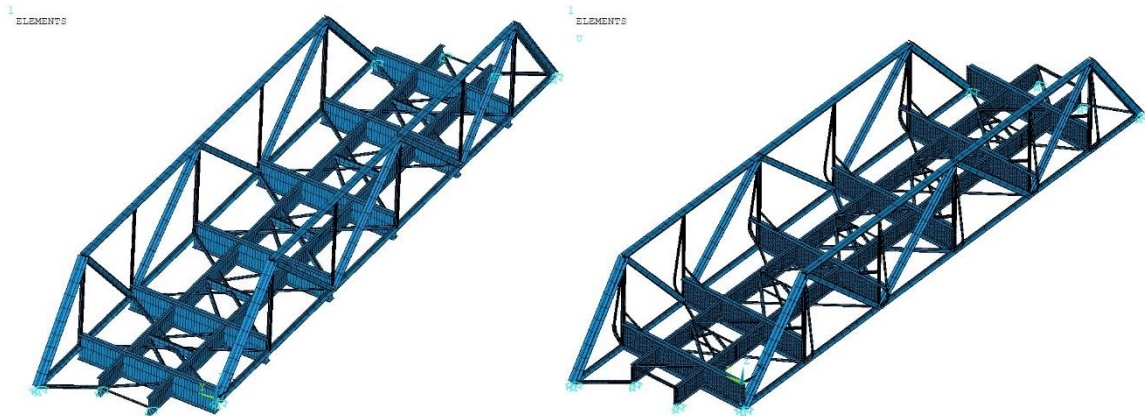


Figure 30 Constraints - Simple and complete model

### 2.3.2 Model developed by the consulting company

The individual element cross-sections of the bridge are computed in *Excel* by the consulting company. In the analysis, the gross cross-section is used, instead when calculating stresses the net cross-section is adopted with deduction for nail holes in the relative section.

As for the self-made models, this foresight was not followed because it would have been a supplement to the discussion.

The analysis model made by Johs Holt Consultant Eng., Figure 31, consists of, as the two self-made models, the two truss walls on each side, rotated with respect to each other, wind bracers in the lower belt bridge, longitudinal and transverse beams and transverse subsystems as a reinforcement. The software used by the company for the modeling is *Sofistik*.

The simplifications and the assumptions made by the consulting company are listed:

- Geometry and cross section after reinforcement are assumed for the entire life of the bridge
- Joints between transverse elements and verticals are assumed rigid.
- The center of gravity of the individual bridge elements is assumed to lay on their axis
- For larger eccentricities, rigid coupling springs are used.
- The eccentricity between the mid-plane of the track and the mid-plane of the bridge is assumed to be constant along the bridge.

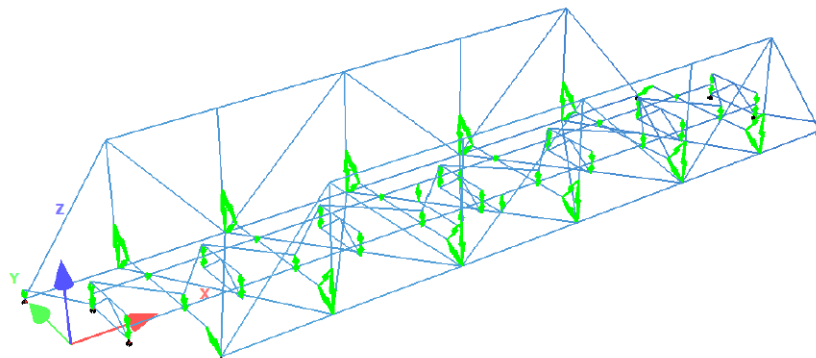
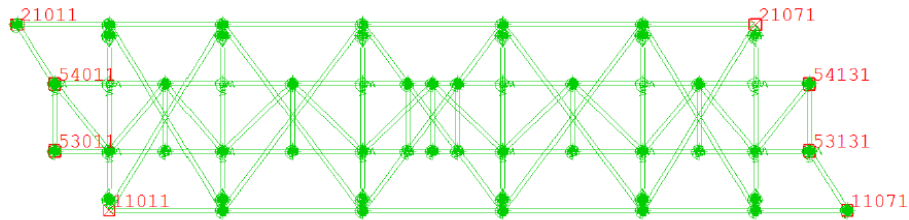


Figure 31 Johs Holt's FEM model

As for the boundary conditions, show in Figure 32, rotation in the joints is guaranteed in every direction.  
Concerning the translations:

- Support node 11011: zero translation
- Support node 21011: translation in the y-direction
- Support node 11071: translation in x-direction
- Support node 21071: translation in both y and x direction
- Support node 53011, 54011, 53131 and 54131: translation in both y and x direction



*Figure 32* Johs Holt's constraint definition

It should be underlined that Johs Holt Consultant Eng. has made different evaluations regarding the constraints. In particular, to the two ends of the stringers, it does not constrain the translation in the transverse direction. From the field inspections, however, it seems that the most appropriate way to define these constraints has been ours.

In the following sections it is shown, and in particular in the comparison between the influence lines, how such a difference in modeling can affect the results obtained.

## 3 Definition of railway trainsets

In the following chapters, it is intended to estimate the damage induced in correspondence of specific sections of the bridge following the single transit of a train.

Eight trains are evaluated and the determination of the most damaging of them is also of interest.

The load model, developed by third parties on *Python* [7], consists therefore of eight trains, passenger and freight trains. Each train corresponds to a specific time era, identified from 1900 to the present time.

Convoys are characterized by a total weight ranging from about 500 to 1300 *tons*.

The load acting on the rail tracks, due to the weight of the railway vehicle, is exchanged at the axles of each individual bogie which composes the train.

The load functions (*LF*), associated with the modeled trains, are described. *LF* consist of vertical loads, expressed in tons, distributed along a spatial coordinate. The distance between the various application points and the bogie extremities is specified.

Therefore, a spatial distribution of load, due to the stationing of a train on the bridge, is firstly defined. Afterwards, the wagon is simulated to drive along the bridge in order to examine the induced response.

Consequently, a static load condition is defined, moved then along the bridge tracks.

The static load condition is described by the following formula:

$$LF(x) = \sum_{i=1}^{n_p} p_i * \delta * (x - x_i) \quad (1)$$

Where:

- $\delta$ : Dirac's delta function
- $p_i$ : the load magnitude in the  $x_i$  position
- $n_p$ : number of train axles

Train type	Wagon types	Number of wagons	Total weight [tons]	Velocity [km/h]
1	BogieWagon	16	686.76	34
2	BogieWagon	17	774.00	63
3	BogieWagon	20	1071.56	71
4	BogieWagon	22	1279.36	110
5	TwoAxleWagon	27	543.00	5
6	TwoAxleWagon	30	730.50	12
7	BogieWagon, TwoAxleWagon	14	822.00	24
8	BogieWagon, TwoAxleWagon	19	1143.00	5

Table 4 Trains characteristics

As can be seen from Table 4, two types of wagons are used. They are defined as follows.

- Bogie wagon, Figure 33: is defined by axle loads  $p$  and geometry parameters  $a$ ,  $b$  and  $c$

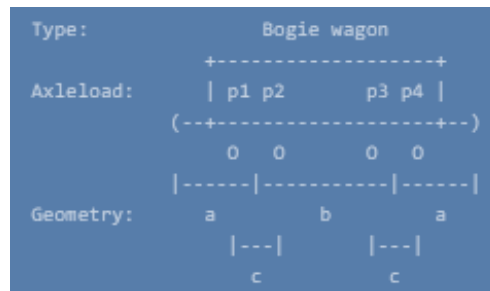


Figure 33 Bogie wagon

- Two axle wagon, Figure 34: is defined by axle loads  $p$  and geometry parameter  $a$  and  $b$

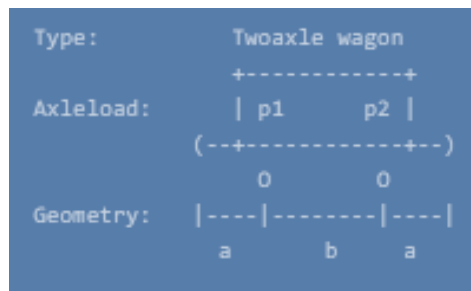


Figure 34 Two axle wagon

Load vectors are discretized in space every  $10\text{ cm}$  along the entire length of the train. For the main longitudinal beams, the same subdivision will be used in order to have a compatible discretization of the influence lines.

In the evaluation of the normal stress influence lines, in specific points of the structure, the convolution between the normal stress influence lines per unit load and the static load functions will be made.

In such way the static response of the structure, in terms of normal stress, is determined.

Has been plot, in Figure 35 - Figure 42, the load diagrams for each train to see how they are implemented.

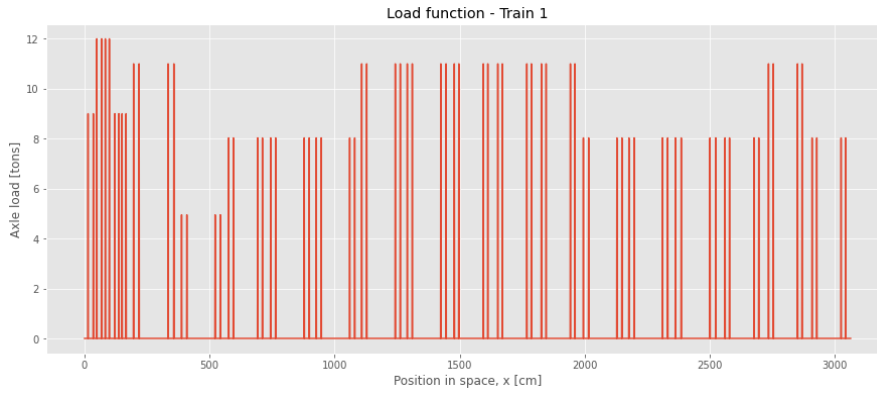


Figure 35 Load vector associated to Train1



Figure 36 Load vector associated to Train2



Figure 37 Load vector associated to Train3



Figure 38 Load vector associated to Train4

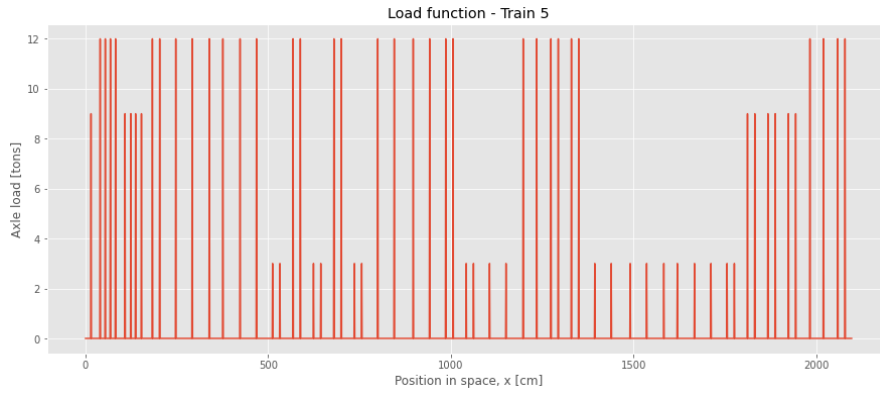


Figure 39 Load vector associated to Train5



Figure 40 Load vector associated to Train6



Figure 41 Load vector associated to Train7

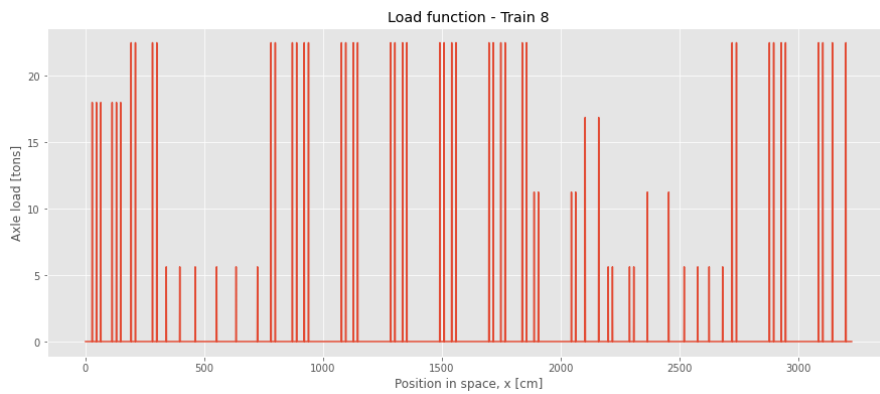


Figure 42 Load vector associated to Train8

# 4 Identification of disparities and similarities between models

## 4.1 Comparisons on the static behaviour of the bridge - Influence Line analysis

### 4.1.1 Theory

A static analysis is usually reasonable for fatigue assessment of existing railway bridges [2]. Static analysis by using the Influence Line (*IL*) approach, in particular, is most commonly used to predict the stress histories of such structures.

The influence line evaluated at a certain point of the structure  $IL(x)$  is equivalent to the response of the structure to a unit load moving along a predefined load path with spatial coordinate  $x$ .

In the present study, the stress *IL* are determined numerically for the three models analyzed and compared in order to evaluate the effect that different choices in modeling have entailed.

If the stress influence lines are determined for a structure that can be considered linear (the assumption made for the bridge considered), the principle of super position holds: as a consequence the static stress response in a structural detail can be determined by taking the convolution of the influence line and the load function.

The complete response in a structure generally consists of both a static and a dynamic part. The common approach to estimate the response in old steel railway bridges for the purpose of fatigue analysis is to estimate the static response with influence lines and the dynamic response by applying a dynamic amplification factor (*DAF*).

In this discussion the second part of the analysis is not carried out, so no *DAF* are considered.

In order to determine the influence lines, the action exerted by the wheels of the train on the rails, and therefore on the stringers, discretized in time (hence in space) is simulated.

As a result, two unit loads are applied in the center of gravity of the train which results in three different static load conditions. These loads are translated step by step along the two stringers with a spatial discretization of 10 *cm*.

Basically what is performed is a static analysis of the structure, repeated for a number of times resulting from the entity of the discretization. For each load step, the value of normal stress per unit load arisen at the sections considered most critical is observed. In such a way it is possible to have an idea of the evolution of the extent of stress present in a specific section when passing a traveling load.

The evaluated travelling loads, acting on the stringers, result from the assumption of applying a unit load, first in the vertical direction and then in the transverse one, at the center of gravity of the convoy, considered massless in this phase.

As a consequence of the fact that the study is conducted in the linear field, it will simply be sufficient to consider the actual load vector acting on the bridge at the passage of a train in order to identify the actual value of the stress in each individual element.

Afterwards the obtaining of the stress influence lines per unit length and those obtained operating the convolution with the load vectors, it is possible to make a comparison on the static behavior of the three models.

Another target in the determination of the stress influence lines per unit length is aimed at the consequent possibility of determining the actual stress arisen in the individual sections of the bridge and then evaluating their damage.

As mentioned, *IL* are evaluated in correspondence of elements of interest, considered critical for the evaluation of the residual life of the bridge.

Stringers and cross girders are known to be crucial components of the bridge deck and their connections in particular.

It is also intended to study elements lying on the subsystem, on the diagonals and on the lower and upper chords.

#### 4.1.2 Definition of the three loading conditions

In order to determine the influence lines, a unit axle load (1 *N*) is applied, distributed over two wheel loads of 0.5 *N* each, stepped through the bridge with an appropriate step length of 10 *cm*.

This step length is chosen on the basis of the geometry of the structure and the axle distances for the trains evaluated. The load distribution just described would be valid for bridges characterized by a straight rail track, where the axis line between the rail tracks coincides with that of the structure.

The bridge over the Sokna however has a horizontal curvature and consequently the center line of the track deviate from the center line of the bridge. This configuration involves a skewed distribution of the axle load acting on the stringers.

In addition to the existing vertical load, the horizontal curvature also provides a centrifugal force that will contribute to fatigue damaging on the bridge.

Such centrifugal force depends on two factors:

- The axles load
- The speed of the train squared

It should be emphasized that these two aspects depend on the type of convoy considered, whether this is a freight train or a passenger train, and on the epoch considered (trains of different weight and with different cruising speeds).

The centrifugal force is therefore defined in agreement with the consulting company, [8]:

$$Q_t = \frac{v^2}{g * r} * Q_v \quad (2)$$

Where:

- $Q_t$ : centrifugal force [N]
- $Q_v$ : vertical axle load [N]
- $v$ : train speed [ $\frac{m}{s}$ ]
- $g = 9.81 \frac{m}{s^2}$ : acceleration of gravity [ $\frac{m}{s^2}$ ]
- $r = 500$  m: curve radius [m]

The structure under consideration is therefore subject to two load conditions acting in unison: axle load and centrifugal force.

In order to properly consider the influence of centrifugal force on the bridge it is decided, such as Johs Holt Consultant Eng. has established, to divide the load exerted by the train into three components:

- Vertical axle load
- Vertical force pair to counteract the roll moment exerted by centrifugal force
- Horizontal load from the centrifugal force

On the basis of these three load conditions, three different influence lines are obtained.

For simplicity, it is assumed to calculate the influence lines starting from the application of a unit vertical load (shaft load) and a unit transverse load (centrifugal force) at the center of gravity of the train, as shown in Figure 43 and Figure 44.

- $Q_v = 1$  N -> shaft load
- $Q_t = 1$  N -> centrifugal load

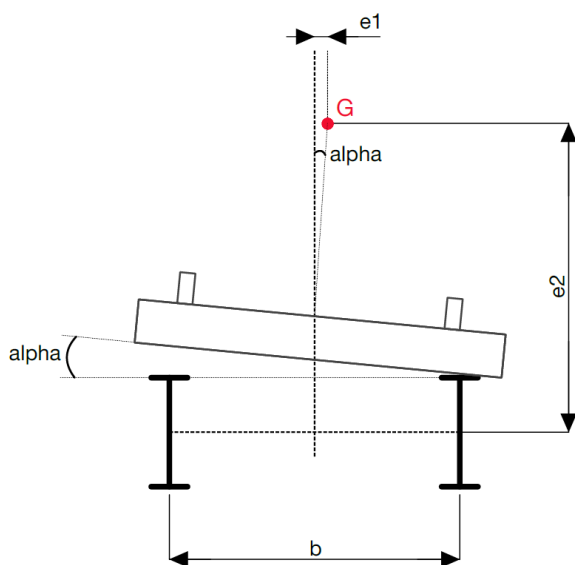


Figure 43 Inclination of the rail track plane with respect to the horizontal one

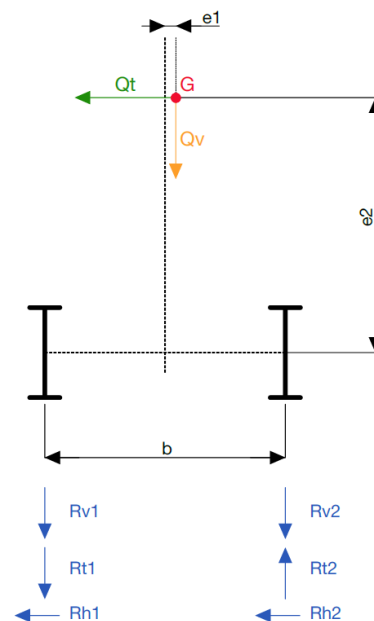


Figure 44 Application of unit loads and their distribution to the wheel-track contact

In which:

- $R_v$ : vertical axle loads
- $R_t$ : vertical pair of forces due to the centrifugal effect
- $R_h$ : horizontal pair of forces due to the centrifugal effect
- $b = 1800 \text{ mm}$ : center distance between the two stringers

By consulting the technical drawings can moreover be deducted the values of:

- $\alpha = 1.9956^\circ$ , look at Figure 43
- $e_1 = 29.3431 \text{ mm}$ : horizontal eccentricity of the action point of the vertical load with respect to the mid plane the two stringers
- $e_2 = 2539.786 \text{ mm}$ : vertical eccentricity of the action point of the transverse load with respect to the axis of the two stringers

The influence lines are therefore determined, for each load group, by stepping unit axle load of  $Q_v = 1 \text{ N}$  and a unit centrifugal force of  $Q_t = 1 \text{ N}$  through the bridge with a stepping distance of  $10 \text{ cm}$ .

The distribution of the axle loads and the centrifugal forces on the two main longitudinal beams depends on the geometry and is calculated imposing the balance of vertical forces and moments.

The following values are obtained:

- $R_{v1} = 0.4837 \text{ N}$
- $R_{v2} = 0.5163 \text{ N}$
- $R_{t1} = 1.411 \text{ N}$
- $R_{t2} = -1.411 \text{ N}$
- $R_{h1} = 0.5 \text{ N}$
- $R_{h2} = 0.5 \text{ N}$

### 4.1.3 Consulting company's IL calculation

The assumptions made by the consulting company and what were the simplifications made at the geometric level have already been illustrated previously. More details on the developed approach can be found in [8].

As already mentioned, the geometrical parameters of the analysed model are defined in *Excel* spreadsheets. Subsequently, the consulting company exploited the software *Sofistik* in order to perform simulations and evaluate the internal forces and moments arising in the single sections of the bridge.

The finite element model developed by the company sees the use of beam elements and springs in some connections, as displayed in Figure 45. Springs are assumed to be rigid in all connections with spring stiffnesses defined as  $C_x = C_y = C_z = 10^{12} \frac{kN}{m}$  and  $C_{Mx} = C_{My} = C_{Mz} = 10^{12} \frac{kN}{m}$ .

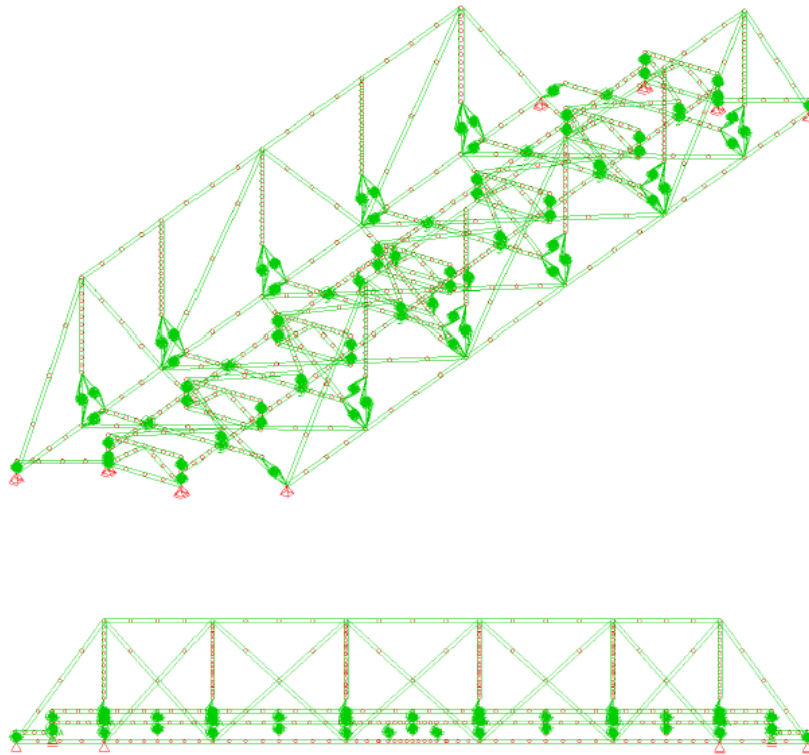


Figure 45. Johs Holt FEM model

The consulting company relied on a systematic numbering of nodes and elements in order to automatically and flexibly report results in the form of diagrams.

The results for post-processing (generation of influence lines, stress calculations, etc.) are presented in matrix form on *Excel*. For each beam element, forces and moments are presented in the start and end nodes for each load step.

In such a way, it has been easy to exploit the results obtained from the simulations performed by Johs Holt Consultant Eng., invoking them on *Python*. Those results have been used in order to obtain the stress *IL* (being in possession of the cross-sectional data) and the induced damages.

The entire calculation procedure followed by Johs Holt Consultant Eng., in order to assess the residual life of the bridge, can be summarized in the following points:

- Reading of data (forces, moments and geometric properties)
- Calculate normal stress influence lines
- Establish load time series for the trains

- Establish spectrum for stress ranges and damage summary per load train
- Weighting and summation of partial damages according to historical traffic
- Calculate residual life according to future traffic

The calculation of the influence lines is now considered.

As already explained, the live load groups to which the bridge is subjected are three.

The consulting company performed three different simulations by applying the moving loads as shown in the following figures, Figure 46 - Figure 48:

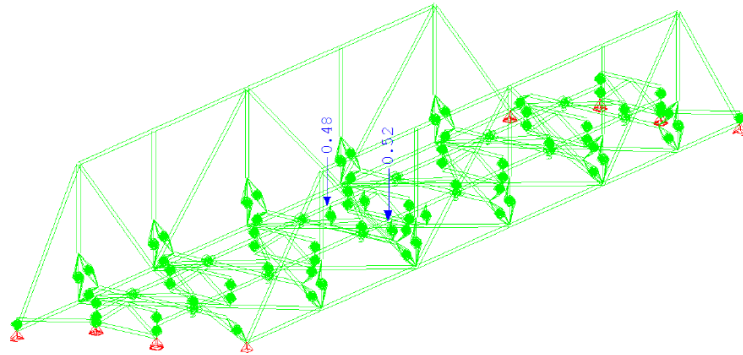


Figure 46 First company's load condition:  $R_v$

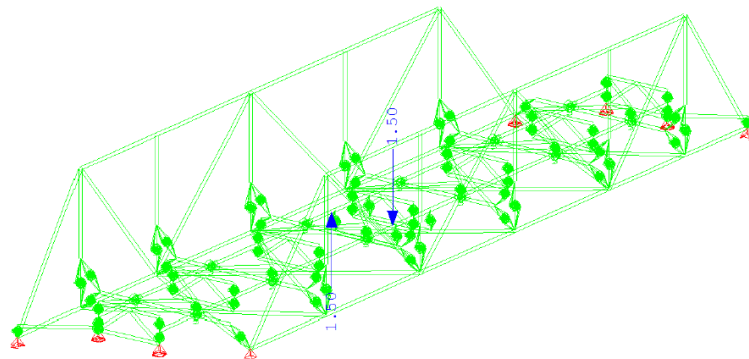


Figure 47 Second company's load condition:  $R_t$

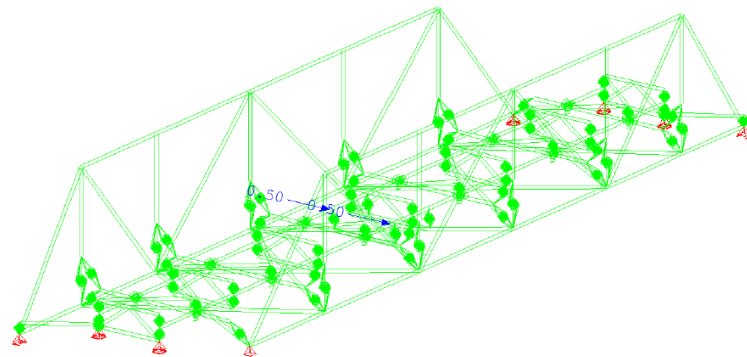


Figure 48 Third company's load condition:  $R_h$

In order to determine the normal stress  $IL$  per unit load, you start from forces/moments influence lines and the cross-sectional data.

The stress contribution coming from each load component is calculated by dividing the force/moment values by the respective resistor (section, second moment of inertia, etc.).

For each normal stress  $IL$  per unit load, three different contributions are summed together: the one coming from the axial internal forces and the ones arising from the internal flexural moments with respect to y and z axis.

As a result, are obtained:

- $R_a \left[ \frac{MPa}{N} \right]$ : normal stress  $IL$  per unit load due to the axle load
- $R_v \left[ \frac{MPa}{N} \right]$ : normal stress  $IL$  per unit load due to vertical forces coming from centrifugal effect
- $R_h \left[ \frac{MPa}{N} \right]$ : normal stress  $IL$  per unit load due to horizontal forces coming from centrifugal effect

These stress values are determined at four stress points for each section. In making comparisons with the results obtained from the self-made models, it has been decided to evaluate only the most stressed point of the section, the most critical. This choice has been made following a conservative approach.

In order to subsequently make comparisons between the influence lines, it is necessary to find a correspondence between the elements belonging to the three *FEM* models.

Once the position where to extract the  $IL$  has been decided (it is intended to carry out an analysis only at specific points of the structure), the corresponding number of the element is searched.

For the model created by Johs Holt Consultant Eng., [8] and *Excel*/spreadsheets are exploited.

The correspondence between nodes and elements is illustrated in the next chapter.

### 4.1.4 IL computation on self-made models

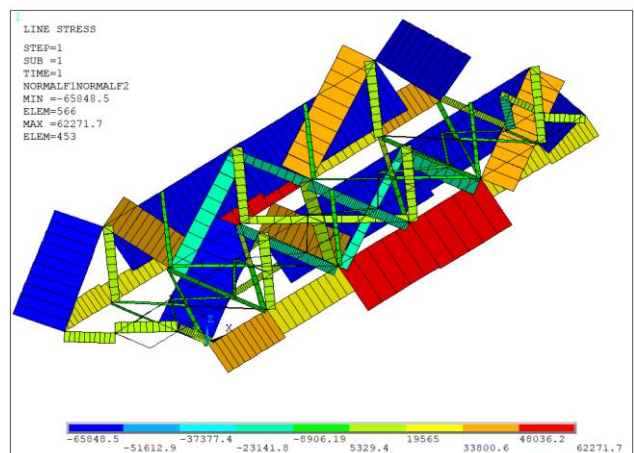
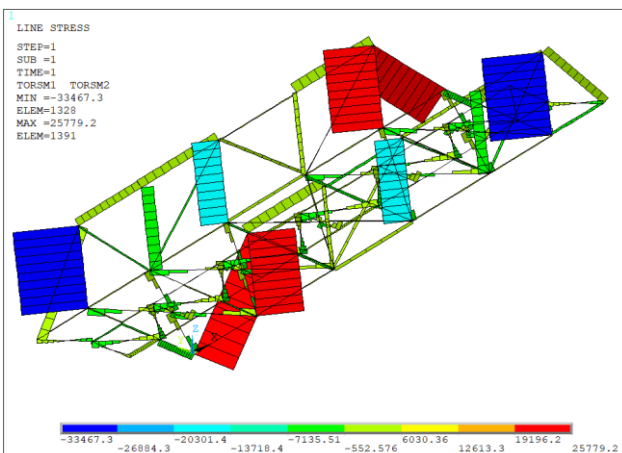
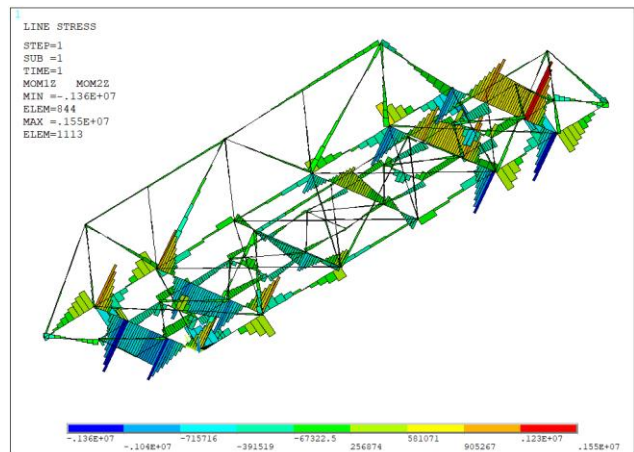
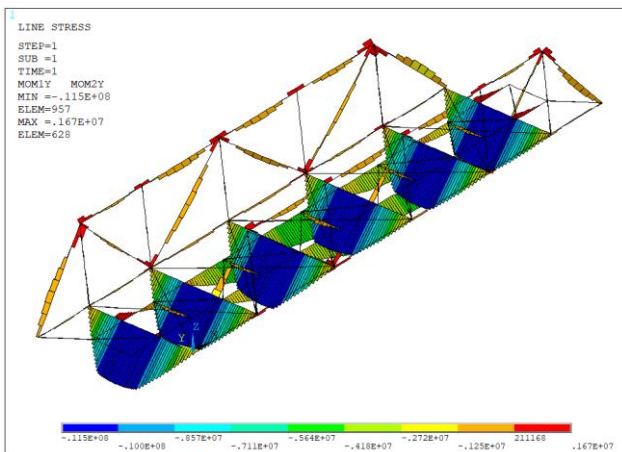
Taking into account the geometry of the structure and the load conditions, it is expected that the main responsible for the degradation of the bridge are the stresses arisen due to the axial and bending moments.

Thus the choice, already discussed, to calculate the normal stress  $\sigma$  in order to estimate the damage of the structure.

An analysis of the static behavior of the bridge, Figure 49, considering only its own weight, shows that stringers and cross girders are mainly subject to flexural loads with respect to the z and y axes.

The upper chords are subject to compression, hence the benefit of the vertical elements to counteract the phenomenon of buckling, while the lower chords are subjected to traction. The remaining components of the truss wall are all subject to extensional axial loads except for the outermost diagonals.

From this simple static analysis it is evident that the influence of torsional moments and shear forces is quite low. In the following, it will be shown that the contribution of torsional stress is lower and negligible compared to axial and flexural ones.



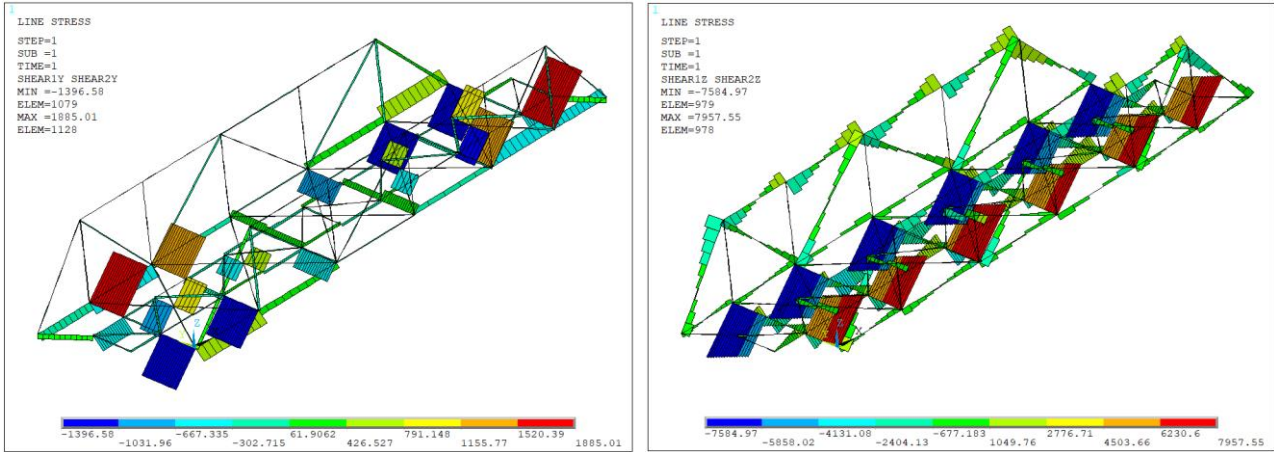


Figure 49 Internal forces and moments, for the simpler model, due to the self-weight of the structure

From the paper [3] it is deduced that for riveted components, on the basis of experimental observations, flexural and axial stresses are properly the main responsible for the appearance and propagation of fatigue cracks.

Even though the calculated  $\tau$  values are not, at each section, close to zero, a significant effect is not expected for the purposes of the fatigue behavior. As a result, you will totally neglect the shear stress contribution. No shear actions will be relevant on the crack occurrence since the beams considered are all slender.

The first step aimed at determining the *IL* sees the application of live loads on the structure. The approach followed is the same for both self-made models.

Simulations are performed on *Ansys Mechanical APDL*. Given the two developed *FEM* models, within the *Solution Processor*, a *\*DO loop* is defined aimed at applying a mobile unit load moved step by step on all the nodes constituting the two main longitudinal beams.

Unlike what the consulting company has done, it is preferred to perform four different simulations, applying once a unit load in a vertical direction and the other in a transverse direction, on one stringer at a time.

In order to get back to the load condition defined by Johs Holt Consultant Eng., the normal stress influence lines resulting from the four simulations are scaled and added algebraically in order to find the equivalent of the vectors  $R_a$ ,  $R_v$  and  $R_h$  previously defined.

For the self-made models, a unique name is given to these quantities, as highlighted in Table 5.

	Model type		
	Johs Holt's model	Simple model	Complete model
Component of normal stress per unit load	Ra	My_Ra	My_Ra_compl
	Rv	My_Rv	My_Rv_compl
	Rh	My_Rh	My_Rh_compl

Table 5 Normal stress *IL* per unit load univocal names

Not all the constituent elements of the three models are taken into account. The twelve potentially critical sections highlighted in Figure 50 have been selected, considered interesting for the purpose of studying their loss of structural capacity.

As already mentioned, it is necessary to find a correspondence between nodes and elements to make comparisons. The chosen sections for the three models has to be located as close as possible in the same point. Geometric differences between the models required approximations.

The result of this analysis are showed in Table 6.

Location	Simple model						Johs Holt's model					Complete model			
	My RF [mm]		My RF [mm]				Different RF's origin [mm]					My RF [mm]			
	Element	Node	x	y	z	Element	Node	x	y	z	Element	Node	x	y	z
Stinger	102	104	8750	1600	0	41144	5307	11250	-900	205	102	103	8750	1600	-50
Subsystem	1154	799	8750	2500	0	64074	9103	11250	0	0	1884	1857	8750	2500	-50
Cross girder (CG-vertical 9 junction)	829	412	0	5000	0	33014	2102	2500	2500	0	1049	1044	0	5000	0
Cross girder (CG-stringer junction)	844	207	0	3400	0	33011	3401	2500	900	500	1064	1061	0	3400	0
Cross girder (CG-diagonal 9/8 junction)	879	422	3050	5000	0	33024	3202	5550	1905	500	1618	867	3050	5000	-900
Vertical 9	1327	1296	0	5000	350	24011	2301	2500	2500	1245	2380	2326	0	5000	100
Vertical 1	1390	1351	14450	5000	350	28011	2305	16950	2500	1245	2696	2619	14450	5000	-800
Diagonal 1/0	620	622	17195	5000	350	23064	2107	20000	2500	0	817	822	16890	5000	-180
Diagonal 9/11	617	621	-2250	5000	350	23011	6101	0	2500	254	847	856	-2250	5000	-540
Upper chord	533	539	8750	5000	3500	22032	2204	13150	2500	3500	13766	12759	8370	5000	2700
Lower chord	426	431	9130	5000	0	21042	2105	13150	2500	0	13846	12828	8370	5000	-900
Cross girder (CG-vertical 5 junction)	929	428	6850	5000	0	33034	3203	9350	1905	500	1249	1248	6850	5000	0

Table 6 Elements and nodes correspondence

Correspondence between the 2 RF	
x_company	x_mine=x_company-2500 mm
y_company	y_mine=y_company+2500 mm
z_company	z_mine=z_company

Table 7 Correspondence between the position of the origin of the RFs for the self-made models and Johs Holt's one

Before proceeding with the calculation of normal stresses, it must be taken into account that the outputs provided by *Ansys*, in terms of forces and moments, are referred with respect to the nodal reference system (and therefore the global one). However, to calculate the various stress contributions and ensure that these are consistent for each evaluated model, it is necessary to evaluate the outputs with respect to the local reference frame (*RF*) of the individual elements.

It is therefore necessary to find the correspondence between the element local *RF* and the global *RF* in the two self-made models. (Table 8 - Table 9)

Simple model - Elements													
		102	1154	829	844	879	1327	1390	620	617	533	426	929
		Local											
Global	X	x	y	y	y	y	z	-z	$z \cdot \cos(41) - x \cdot \cos(49)$	$-z \cdot \cos(35.5) - x \cdot \cos(54.5)$	x	x	y
	Y	y	-x	-x	-x	-x	y	y	-y	-y	y	y	-x
	Z	z	z	z	z	z	-x	x	$z \cdot \cos(49) + x \cdot \cos(41)$	$z \cdot \cos(54.5) - x \cdot \cos(35.5)$	z	z	z

Table 8 Local and global RF correspondence - Simple model

Complete model - Elements													
		102	1884	1049	1064	1618	2380	2696	817	847	13766	13846	1249
		Local											
Global	X	x	y	y	y	-y	-z	-z	$-z \cdot \cos(40.3) + x \cdot \cos(49.7)$	$-z \cdot \cos(34.8) - x \cdot \cos(52.2)$	-x	x	y
	Y	y	-x	-x	-x	x	y	y	y	-y	-y	y	-x
	Z	z	z	z	z	z	x	x	$z \cdot \cos(49.7) + x \cdot \cos(40.3)$	$z \cdot \cos(52.2) - x \cdot \cos(34.8)$	z	z	z

Table 9 Local and global RF correspondence - Complete model

The angles that appear in the *sine* and *cosine* are those intercepted by the two external diagonals with respect to the horizontal plane in the two models.

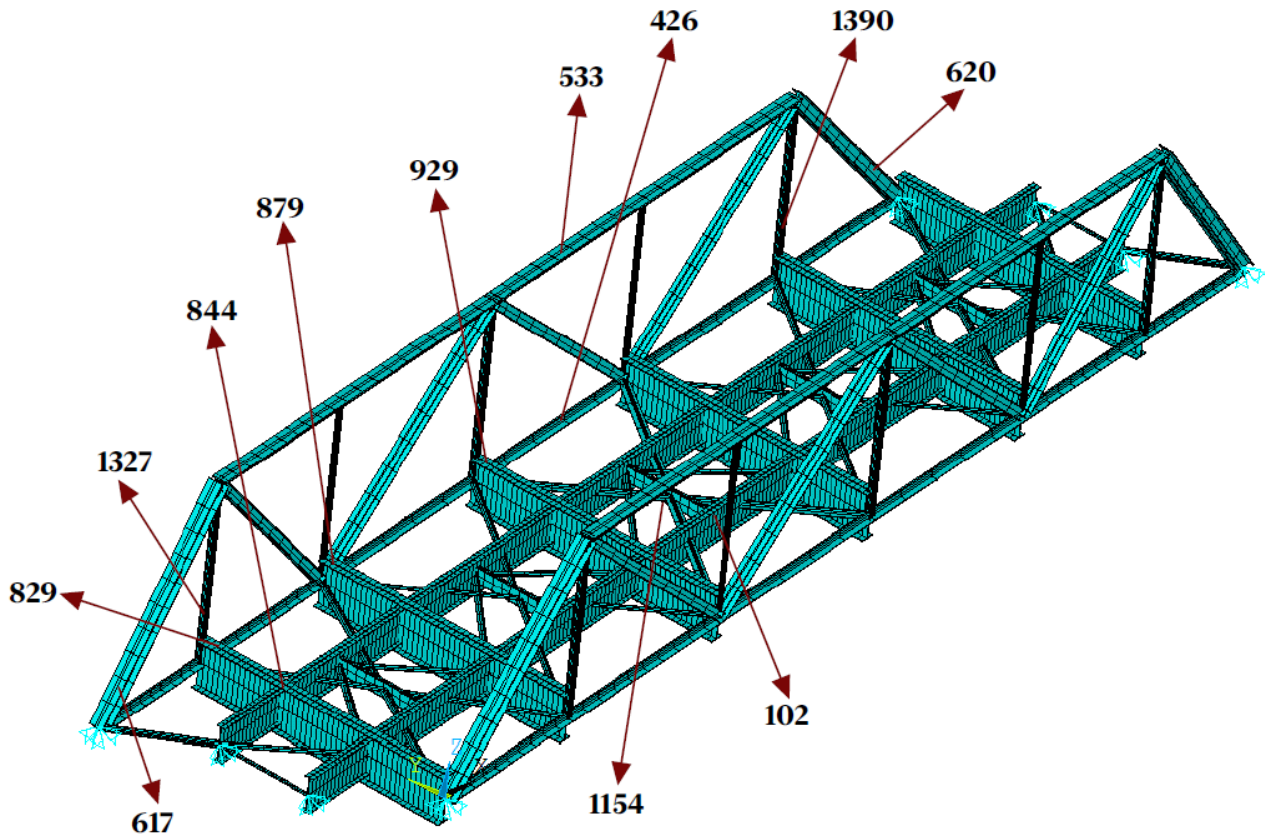


Figure 50 Considered elements position and number - Simple model

Obtained as output of the four simulations conducted, using *Ansys ESOL* command, the values of forces and moments in correspondence of the selected sections, the stresses are calculated.

The normal stress influence lines per unit of load are specifically determined starting from the internal forces and moments arisen at a specific section for each step of the simulation, therefore for each position of the load acting on the stringers.

The total normal stress and the equivalent Von Mises stress are calculated using the equations of material mechanics.

Normal stresses due to bending moments:

$$\sigma_{\text{fless,y}} = \frac{\text{Mom}_y \cdot TKZ}{I_{yy} \cdot 2} \quad (3)$$

$$\sigma_{\text{fless,z}} = \frac{\text{Mom}_z \cdot TKY}{I_{zz} \cdot 2} \quad (4)$$

Normal stresses due to axial forces:

$$\sigma_x = \frac{N}{\text{Area}} \quad (5)$$

As for the calculation of shear stress, a distinction must be made with respect to the type of section with which you are dealing.

- Closed thin-walled section: Bredt equation is exploited

$$\tau = \frac{\text{Mom}_x}{2\text{Area}_{\text{average}} \cdot s_{\min}} \quad (6)$$

- Opened thin-walled sections with uniform thickness

$$\tau = \frac{3 * M_t}{a * s^2} \quad (7)$$

- $a$ : mean section length
- $s$ : thickness of the section

- Opened thin-walled sections with uneven thickness

$$\tau = \frac{3 * s_{\max} * M_t}{\sum a * s^3} \quad (8)$$

- The summation is extended to all the rectangles that make up the section.
- $s_{\max}$  is the thickness of the thicker rectangle, at the edges of which the maximum tension is found.

The value of the total normal stress, here called  $\sigma_{tot}$ , is determined by making the sum, with sign, of the three  $\sigma$  contributions described.

Finally, for the determination of the equivalent Von Mises stress, aimed at demonstrating the small influence of the tangential stress on the determination of the total stress arisen, this formula is used:

$$\sigma_{VM} = \sqrt{(\sigma_{bend,tot} + \sigma_x)^2 + 3\tau^2} \quad (9)$$

As an example, are shown the values of the forces, moments and stresses for element 102, in the simple model, found following the application of a unit load in a vertical direction on the stringer closest to the origin of the reference system.

	Mom. y [N*m m]	Mom. z [N*m m]	Torsion [N*m m]	Axial [N]	Shear y [N]	Shear z [N]	$\sigma_{ben.}$ y [MPa/N]	$\sigma_{ben.}$ z [MPa/N]	$\sigma_{ben.}$ tot [MPa/N]	$\sigma_N$ [MPa/N]	$\tau$ [MPa/N]	$\sigma_{VM}$ [MPa/N]	$\sigma_{tot}$ [MPa/N]	$\tau$ effect %	$\tau$ effect > 10%?
TIME	102 MY	102 MZ	102 MX	102 FX	102 FY	102 FZ									
1	0	0.00E+00	0.00E+00	0.00E+00	0.00E+00	0.00E+00	0	0	0.00E+00	0	0	0	0.00E+00	0.00	
2	-2.93E-01	1.68E-01	-3.69E-04	-6.37E-03	-1.01E-04	1.82E-03	1.57E-07	-1.94E-06	-1.78E-06	-5.79E-07	-9.21E-09	2.36E-06	-2.36E-06	0.39	No
3	-6.15E-03	1.09E-02	4.41E-06	-2.85E-04	-6.60E-06	1.22E-04	3.30E-09	-1.26E-07	-1.23E-07	-2.59E-08	1.10E-10	1.49E-07	-1.49E-07	0.07	No
4	-1.27E-02	2.18E-02	8.03E-06	-5.74E-04	-1.32E-05	2.44E-04	6.80E-09	-2.52E-07	-2.46E-07	-5.21E-08	2.00E-10	2.98E-07	-2.98E-07	0.07	No
5	-1.99E-02	3.28E-02	1.01E-05	-8.70E-04	-1.98E-05	3.66E-04	1.07E-08	-3.79E-07	-3.68E-07	-7.91E-08	2.52E-10	4.47E-07	-4.47E-07	0.06	No
6	-2.82E-02	4.37E-02	9.85E-06	-1.18E-03	-2.65E-05	4.88E-04	1.51E-08	-5.05E-07	-4.90E-07	-1.07E-07	2.46E-10	5.97E-07	-5.97E-07	0.04	No
7	-3.79E-02	5.47E-02	6.49E-06	-1.50E-03	-3.31E-05	6.10E-04	2.04E-08	-6.33E-07	-6.12E-07	-1.36E-07	1.62E-10	7.48E-07	-7.48E-07	0.02	No
8	-4.94E-02	6.57E-02	-7.66E-07	-1.84E-03	-3.98E-05	7.32E-04	2.66E-08	-7.60E-07	-7.33E-07	-1.67E-07	-1.91E-11	9.01E-07	-9.01E-07	0.00	No
9	-6.31E-02	7.68E-02	-1.27E-05	-2.20E-03	-4.64E-05	8.53E-04	3.39E-08	-8.88E-07	-8.54E-07	-2.00E-07	-3.16E-10	1.05E-06	-1.05E-06	0.03	No
10	-7.93E-02	8.79E-02	-3.00E-05	-2.59E-03	-5.31E-05	9.75E-04	4.26E-08	-1.02E-06	-9.74E-07	-2.36E-07	-7.49E-10	1.21E-06	-1.21E-06	0.06	No
...															
166	-7.47E+00	-5.81E-01	-5.13E-03	-8.69E-02	4.33E-05	-8.06E-03	4.02E-06	6.71E-06	1.07E-05	-7.90E-06	-1.28E-07	2.84E-06	2.83E-06	4.50	No
167	-5.55E+00	-5.78E-01	-5.27E-03	-8.54E-02	4.54E-05	-6.96E-03	2.98E-06	6.68E-06	9.66E-06	-7.77E-06	-1.32E-07	1.91E-06	1.89E-06	6.90	No
168	-3.80E+00	-5.74E-01	-5.39E-03	-8.40E-02	4.75E-05	-5.97E-03	2.04E-06	6.64E-06	8.68E-06	-7.64E-06	-1.34E-07	1.07E-06	1.04E-06	12.59	Yes
169	-2.21E+00	-5.70E-01	-5.47E-03	-8.26E-02	4.94E-05	-5.07E-03	1.19E-06	6.60E-06	7.78E-06	-7.51E-06	-1.37E-07	3.66E-07	2.79E-07	37.33	Yes
170	-7.88E-01	-5.66E-01	-5.53E-03	-8.11E-02	5.13E-05	-4.26E-03	4.24E-07	6.55E-06	6.97E-06	-7.37E-06	-1.38E-07	4.66E-07	-4.00E-07	29.60	Yes
171	4.83E-01	-5.62E-01	-5.56E-03	-7.96E-02	5.31E-05	-3.53E-03	-2.60E-07	6.50E-06	6.24E-06	-7.24E-06	-1.39E-07	1.03E-06	-1.00E-06	13.50	Yes
172	1.61E+00	-5.57E-01	-5.57E-03	-7.81E-02	5.47E-05	-2.88E-03	-8.64E-07	6.44E-06	5.58E-06	-7.10E-06	-1.39E-07	1.54E-06	-1.52E-06	9.01	No
173	2.59E+00	-5.52E-01	-5.55E-03	-7.66E-02	5.63E-05	-2.31E-03	-1.39E-06	6.38E-06	4.99E-06	-6.96E-06	-1.38E-07	1.99E-06	-1.97E-06	6.96	No
174	3.44E+00	-5.46E-01	-5.51E-03	-7.50E-02	5.77E-05	-1.81E-03	-1.85E-06	6.32E-06	4.46E-06	-6.82E-06	-1.37E-07	2.37E-06	-2.36E-06	5.80	No
175	4.17E+00	-5.40E-01	-5.44E-03	-7.34E-02	5.91E-05	-1.38E-03	-2.24E-06	6.25E-06	4.00E-06	-6.68E-06	-1.36E-07	2.68E-06	-2.67E-06	5.06	No
176	4.78E+00	-5.34E-01	-5.36E-03	-7.18E-02	6.02E-05	-1.01E-03	-2.57E-06	6.17E-06	3.60E-06	-6.53E-06	-1.34E-07	2.94E-06	-2.93E-06	4.55	No
177	5.27E+00	-5.26E-01	-5.26E-03	-7.02E-02	6.13E-05	-7.05E-04	-2.84E-06	6.09E-06	3.25E-06	-6.38E-06	-1.31E-07	3.14E-06	-3.13E-06	4.18	No

178	5.66E+00	-5.19E-01	-5.14E-03	-6.85E-02	6.22E-05	-4.52E-04	-3.05E-06	6.00E-06	2.95E-06	-6.23E-06	-1.28E-07	3.28E-06	-3.28E-06	3.90	No
179	5.96E+00	-5.10E-01	-5.00E-03	-6.68E-02	6.29E-05	-2.50E-04	-3.20E-06	5.90E-06	2.70E-06	-6.07E-06	-1.25E-07	3.38E-06	-3.37E-06	3.69	No
180	6.16E+00	-5.02E-01	-4.85E-03	-6.50E-02	6.35E-05	-9.52E-05	-3.31E-06	5.80E-06	2.49E-06	-5.91E-06	-1.21E-07	3.43E-06	-3.42E-06	3.53	No
181	6.27E+00	-4.92E-01	-4.69E-03	-6.32E-02	6.39E-05	1.67E-05	-3.37E-06	5.69E-06	2.32E-06	-5.75E-06	-1.17E-07	3.44E-06	-3.43E-06	3.40	No
182	6.31E+00	-4.82E-01	-4.51E-03	-6.13E-02	6.41E-05	9.00E-05	-3.39E-06	5.57E-06	2.18E-06	-5.58E-06	-1.13E-07	3.40E-06	-3.40E-06	3.30	No
183	6.27E+00	-4.71E-01	-4.32E-03	-5.94E-02	6.41E-05	1.29E-04	-3.37E-06	5.44E-06	2.07E-06	-5.40E-06	-1.08E-07	3.34E-06	-3.33E-06	3.23	No
184	6.17E+00	-4.59E-01	-4.13E-03	-5.75E-02	6.39E-05	1.38E-04	-3.32E-06	5.31E-06	1.99E-06	-5.23E-06	-1.03E-07	3.24E-06	-3.24E-06	3.18	No
185	6.02E+00	-4.47E-01	-3.93E-03	-5.55E-02	6.36E-05	1.20E-04	-3.24E-06	5.17E-06	1.93E-06	-5.04E-06	-9.79E-08	3.12E-06	-3.11E-06	3.14	No
186	5.81E+00	-4.34E-01	-3.72E-03	-5.34E-02	6.29E-05	8.08E-05	-3.12E-06	5.02E-06	1.89E-06	-4.86E-06	-9.27E-08	2.97E-06	-2.97E-06	3.12	No
187	5.56E+00	-4.20E-01	-3.50E-03	-5.13E-02	6.21E-05	2.37E-05	-2.99E-06	4.86E-06	1.87E-06	-4.67E-06	-8.73E-08	2.80E-06	-2.80E-06	3.12	No
188	5.27E+00	-4.05E-01	-3.28E-03	-4.91E-02	6.11E-05	-4.69E-05	-2.83E-06	4.69E-06	1.85E-06	-4.47E-06	-8.19E-08	2.62E-06	-2.61E-06	3.13	No
189	4.95E+00	-3.90E-01	-3.06E-03	-4.69E-02	5.97E-05	-1.27E-04	-2.66E-06	4.51E-06	1.85E-06	-4.26E-06	-7.64E-08	2.42E-06	-2.42E-06	3.15	No
190	4.60E+00	-3.73E-01	-2.84E-03	-4.46E-02	5.82E-05	-2.12E-04	-2.47E-06	4.32E-06	1.84E-06	-4.05E-06	-7.09E-08	2.22E-06	-2.21E-06	3.20	No
191	0.00E+00	0.00E+00	0.00E+00	0.00E+00	0.00E+00	0.00E+00	0.00E+00	0.00E+00	0.00E+00	0.00E+00	0.00E+00	0.00E+00	0.00E+00	0.00	No
192	4.00E+00	-3.36E-01	-2.44E-03	-3.97E-02	5.38E-05	-2.91E-04	-2.15E-06	3.89E-06	1.74E-06	-3.61E-06	-6.08E-08	1.88E-06	-1.87E-06	3.24	No
193	3.75E+00	-3.16E-01	-2.26E-03	-3.72E-02	5.10E-05	-2.82E-04	-2.02E-06	3.65E-06	1.63E-06	-3.38E-06	-5.63E-08	1.75E-06	-1.74E-06	3.22	No
194	3.50E+00	-2.95E-01	-2.08E-03	-3.45E-02	4.80E-05	-2.70E-04	-1.88E-06	3.41E-06	1.53E-06	-3.14E-06	-5.18E-08	1.62E-06	-1.61E-06	3.21	No
195	3.23E+00	-2.73E-01	-1.90E-03	-3.18E-02	4.47E-05	-2.55E-04	-1.74E-06	3.15E-06	1.41E-06	-2.89E-06	-4.74E-08	1.48E-06	-1.48E-06	3.20	No
196	2.96E+00	-2.50E-01	-1.72E-03	-2.91E-02	4.13E-05	-2.39E-04	-1.59E-06	2.89E-06	1.30E-06	-2.65E-06	-4.30E-08	1.35E-06	-1.35E-06	3.18	No
197	2.68E+00	-2.27E-01	-1.55E-03	-2.63E-02	3.76E-05	-2.20E-04	-1.44E-06	2.62E-06	1.18E-06	-2.39E-06	-3.86E-08	1.22E-06	-1.22E-06	3.17	No
198	2.40E+00	-2.03E-01	-1.37E-03	-2.35E-02	3.38E-05	-2.00E-04	-1.29E-06	2.35E-06	1.05E-06	-2.14E-06	-3.43E-08	1.08E-06	-1.08E-06	3.16	No
199	2.11E+00	-1.79E-01	-1.20E-03	-2.06E-02	2.99E-05	-1.79E-04	-1.14E-06	2.06E-06	9.29E-07	-1.88E-06	-2.99E-08	9.49E-07	-9.48E-07	3.15	No
200	1.82E+00	-1.54E-01	-1.03E-03	-1.78E-02	2.59E-05	-1.55E-04	-9.78E-07	1.78E-06	8.01E-07	-1.61E-06	-2.56E-08	8.15E-07	-8.13E-07	3.14	No
201	1.52E+00	-1.29E-01	-8.55E-04	-1.48E-02	2.17E-05	-1.31E-04	-8.18E-07	1.49E-06	6.70E-07	-1.35E-06	-2.13E-08	6.80E-07	-6.79E-07	3.14	No
202	1.22E+00	-1.03E-01	-6.83E-04	-1.19E-02	1.75E-05	-1.06E-04	-6.57E-07	1.19E-06	5.38E-07	-1.08E-06	-1.70E-08	5.44E-07	-5.43E-07	3.13	No
203	9.18E-01	-7.77E-02	-5.12E-04	-8.94E-03	1.32E-05	-8.03E-05	-4.94E-07	8.98E-07	4.05E-07	-8.13E-07	-1.28E-08	4.09E-07	-4.08E-07	3.13	No
204	6.13E-01	-5.19E-02	-3.41E-04	-5.97E-03	8.81E-06	-5.38E-05	-3.30E-07	6.00E-07	2.70E-07	-5.42E-07	-8.51E-09	2.73E-07	-2.72E-07	3.12	No
205	3.07E-01	-2.60E-02	-1.70E-04	-2.99E-03	4.41E-06	-2.70E-05	-1.65E-07	3.00E-07	1.35E-07	-2.71E-07	-4.25E-09	1.36E-07	-1.36E-07	3.12	No

Table 10 Forces, moments and stresses for element 102, simple model, unit vertical load on a single stringer

As can be seen from Table 10, it has been calculated the effect that tangential stress has on the determination of the equivalent stress.

The  $\tau_{effect}$  parameter is calculated as follow:

$$\tau_{effect} = \left(1 - \frac{\sigma_{VM} - \tau}{\sigma_{VM}}\right) * 100 \quad (10)$$

It can be observed how the influence of  $\tau$  is modest, as expected. Only rarely  $\tau_{effect}$  exceeds 10%.

This demonstration can be carried out for all the sections evaluated in the analysis.

Consequently, as already mentioned, only normal stress influence lines will be evaluated for the purposes of the analysis.

Since it has been assumed to evaluate the normal stress  $\sigma$ , stress contributions can be summed (linear combination) and later superposition of influence lines will still be valid.

If you were to make combinations of Von Mises's equivalent stress, which is a non-linear combination of stress components, you must make all combinations per each stress component before finally making the Von Mises computation.

The stress at the end considered will therefore not be an equivalent tension, but a total normal stress deriving from the sum of the axial and flexural contributions.

To find the equivalent of the  $R_a$ ,  $R_v$  and  $R_h$  vectors, the normal stress  $IL$  per unit load, are reordered and a linear combination of them is carried out using *MATLAB* software. The normal stress  $IL$  per unit load has been determined for each section and for the four load conditions formerly explained

Before moving on the comparisons between the  $IL$  computed for the three models, one last aspect must be specified.

The original idea was to evaluate the most stressed points of each section, following a precautionary approach.

Indeed, cracks are expected to appear at a point at the extremity of the beam sections, where the maximum of the total normal tension is reached. For example, the point of interest could be the point *A* in Figure 51.

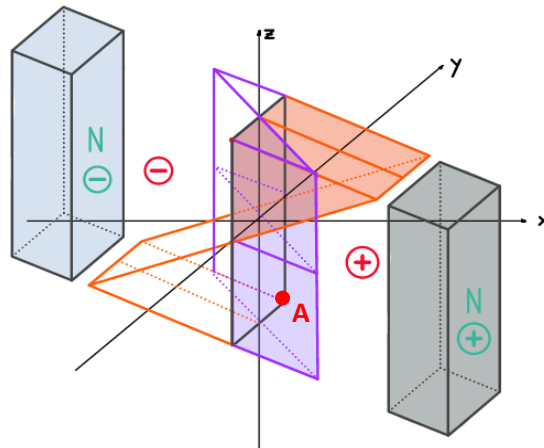


Figure 51 Most stressed point on the section

However, it has been found that the influence lines per unit of load and the damage assessed at the most stressed points of each section differ considerably from those calculated at the stress points chosen by Johs Holt Consultant Eng.

Specifically, there are damages that are much higher than what has been obtained by the consulting company. It is therefore pointless to continue the comparison using those points.

It has been hence decided, for the sole purpose of comparison, to adapt to the hypothesis formulated by the consulting company.

However, you are aware of the fact that the actual most stressed points will not be analyzed and that therefore the estimation of the stress and damages will be slightly non-conservative and underestimated.

The decision made by the company is considered questionable, but is believed it has been made in agreement with the railway infrastructure owner.

In the following chapters on comparisons, the disparity of the results obtained for different section points will be showed for a single component.

### 4.1.5 Shape equivalence

How to compare influence lines is a problem that needs to be addressed. Has to be evaluated the difference between the maximums of absolute values? Or the difference between the damage caused to the individual components? Or instead evaluate the differences in terms of the trend of the *IL* in a 2D graph?

It has been decided to follow all three of these paths.

First of all, it has been decided to start from the evaluation of the shape equivalence between the influence lines obtained.

In order to do this, two paths are chosen:

- Qualitative analysis, making a graphical comparison by plotting, overlapped, the *IL* with respect to the time step for the three models
- Quantitative analysis, calculating the linear correlation coefficient (*LCC*).

The *LCC* allows to evaluate how much two vectors "correspond" in their direction.

This parameter varies between -1 and 1.

- If  $LCC = 1$ : the two vectors have the same direction and the same toward
- If  $LCC = -1$ : the two vectors are characterized by the same direction but by opposite toward
- If  $LCC = 0$ : the two vectors are orthogonal to each other

For two-dimensional vectors, evaluating the *LCC* is equivalent to study the cosine of the angle that two vectors, represented on a plane, form between each other, as is done for complex numbers represented as vectors on the Argand Gauss plane.

In the same way, influence lines are here meant as vectors and not as signals or curves. Thereby, to analyze the similarity of the shape of the *IL* diagrams it will be sufficient to evaluate the direction that these vectors define in a n-dimensional space.

The *LCC* is therefore the benchmark for this analysis.

$$\cos\theta = LCC = \frac{\mathbf{a} \cdot \mathbf{b}}{|\mathbf{a}| * |\mathbf{b}|} \quad (11)$$

where  $\mathbf{a}$  and  $\mathbf{b}$  are two *IL* represented as n-dimensional vectors.

IL shape equivalence							
Simple model				Complete model			
LCC							
Elem.	My_Ra	My_Rv	My_Rh	Elem.	My_Ra_compl	My_Rv_compl	My_Rh_compl
102	0.999	0.994	0.967	102	0.996	0.996	0.948
1154	-0.147	-0.103	0.234	1884	0.655	0.023	0.825
829	0.978	0.962	0.122	1049	0.996	0.998	0.349
844	0.999	0.999	-0.854	1064	0.998	0.998	-0.081
879	0.993	0.996	-0.028	1618	0.996	0.966	-0.422
1327	0.997	0.991	0.290	2380	0.970	0.993	0.433
1390	0.953	0.993	-0.184	2696	0.982	0.972	-0.219
620	0.844	0.970	-0.232	817	0.989	0.963	0.517
617	1.000	0.999	0.498	847	1.000	0.997	0.538
533	0.995	0.998	-0.136	13766	0.995	0.993	-0.469
426	0.999	0.999	-0.020	13846	0.997	0.999	0.377
929	0.948	0.988	-0.144	1249	0.990	0.996	0.030

Table 11 Normal stress *IL* shape equivalence

It is recalled that:

- $R_a, MyR_a, MyR_{a,compl} [\frac{MPa}{N}]$ : normal stress  $IL$  per unit load due to the axle load
- $R_v, MyR_v, MyR_{v,compl} [\frac{MPa}{N}]$ : normal stress  $IL$  per unit load due to vertical forces coming from centrifugal effect
- $R_h, MyR_h, MyR_{h,compl} [\frac{MPa}{N}]$ : normal stress  $IL$  per unit load due to horizontal forces coming from centrifugal effect

A value of  $LCC$  as close as possible to the unit means that the correspondence in terms of shape of the influence lines is good. (Table 11)

From the analysis of the correlation coefficients, it is clear that all the sections analyzed see the  $IL$  per unit load due to the axle load characterized by a rather similar trend, as illustrated in Figure 52 - Figure 63.

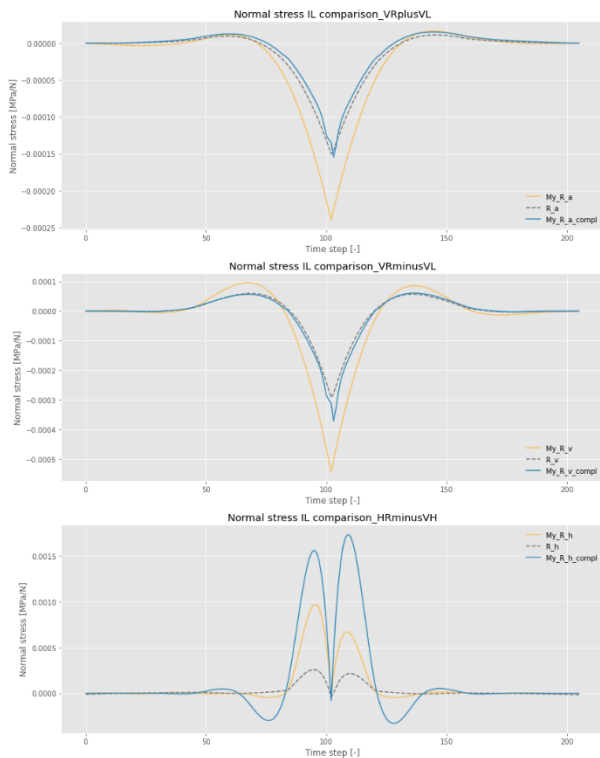


Figure 52 Normal stress  $IL$  per unit load comparison - Stringer: elem. 102 simple, elem. 102 complete

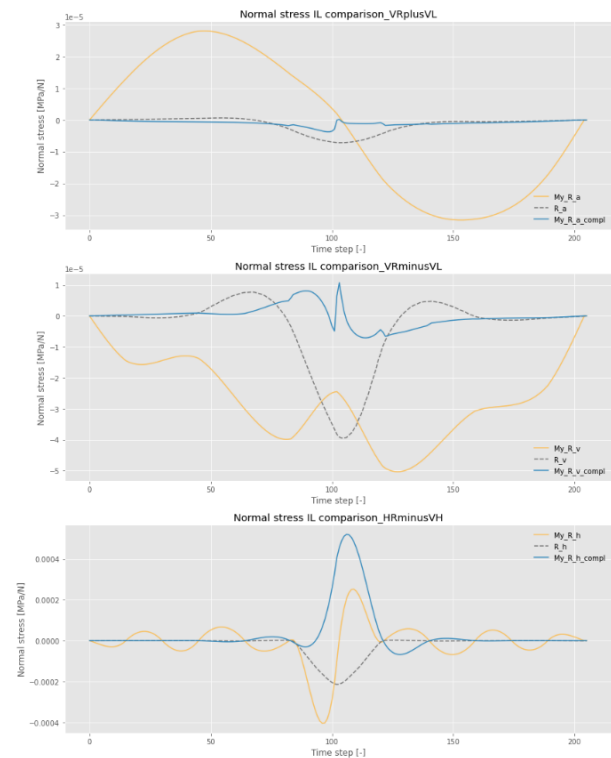


Figure 53 Normal stress  $IL$  per unit load comparison - Subsystem: elem. 1154 simple, elem. 1884 complete

The element on the subsystem, has by far the worst coherence. It is evident looking at Figure 53. The modeling of this element is very different in the three models. This explains why the values of the correlation coefficient are so distant from the unitary value, thus complete dissimilarity in terms of vector direction.

Table 12 and Figure 55 show the comparison made for the element 844, belonging to the simple model, when the most stressed section point and the one chosen by Johs Holt Consultant Eng. are evaluated.

IL shape equivalence			
Simple model			
LCC			
Elem.	My_Ra	My_Rv	My_Rh
844	0.999	0.999	-0.854
844 most damaged, at the section extremity	0.841	0.951	-0.032

Table 12 Normal stress  $IL$  shape equivalence - Different section points evaluation

It can be seen that generally the shape equivalence is worse for the most stressed point of the section, in particular for a load applied transversely. The *LCC* highlights this.

Such a conclusion can be made for all the elements in the *FEM* models considered.

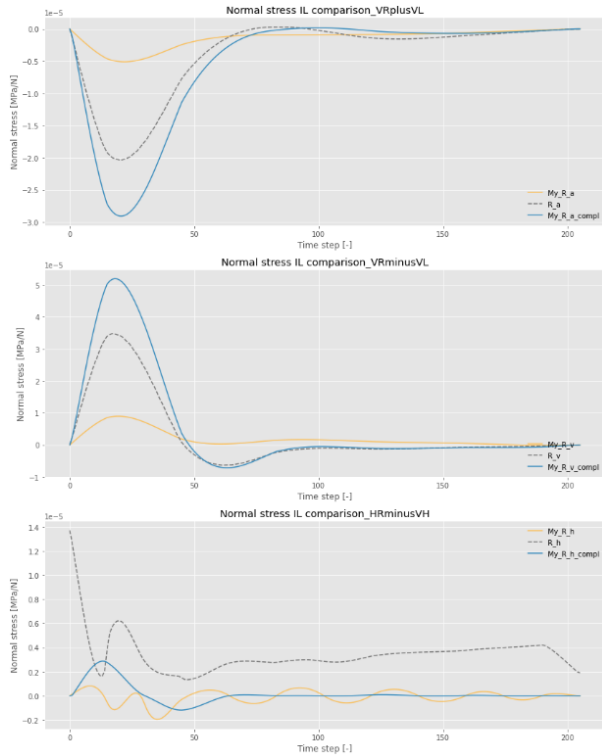


Figure 54 Normal stress *IL* per unit load comparison – Cross girder: elem. 829 simple, elem. 1049 complete

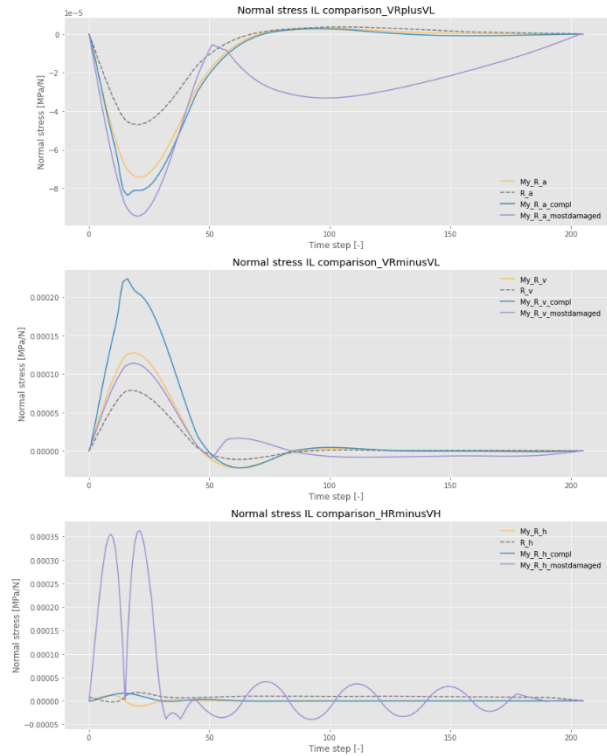


Figure 55 Normal stress *IL* per unit load comparison – Cross girder: elem. 844 simple, elem. 1064 complete

When a transversal load is applied, it is noticed that the self-made models *IL* are really far from the one computed by the consulting company in terms of shape and magnitude. The reason why has to be found in the different constraints defined at the extremities of the stringers.

As already pointed out, Johs Holt Consultant Eng. decided to model the constraints at the ends of the stringers by constraining only the vertical translation, allowing instead a translational movement both in the longitudinal and transverse direction.

Self-made models, see on the other hand a translation in a transverse direction forbidden in these points.

Consequently, as confirmed by the stress *IL* per unit load diagrams, it is expected that the value of the stress at the extremities of the stringers is zero.

Differently, the curves related to the model made by the consulting company show a value of stress in the constraints, when the load is applied transversely, not equal to zero.

In addition to this, this difference in modeling has meant that the entire trend of the *IL* with respect to the time step differs strongly between the various models.

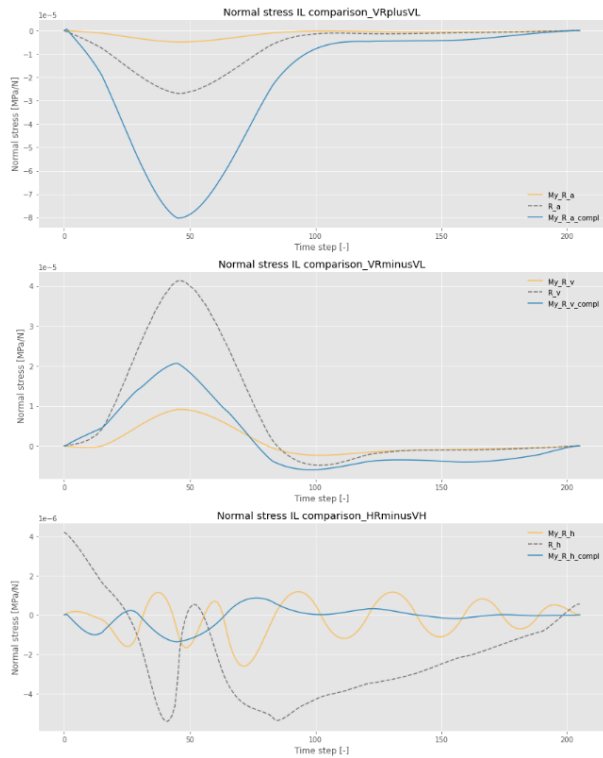


Figure 56 Normal stress IL per unit load comparison - Cross girder: elem. 879 simple, elem. 1618 complete

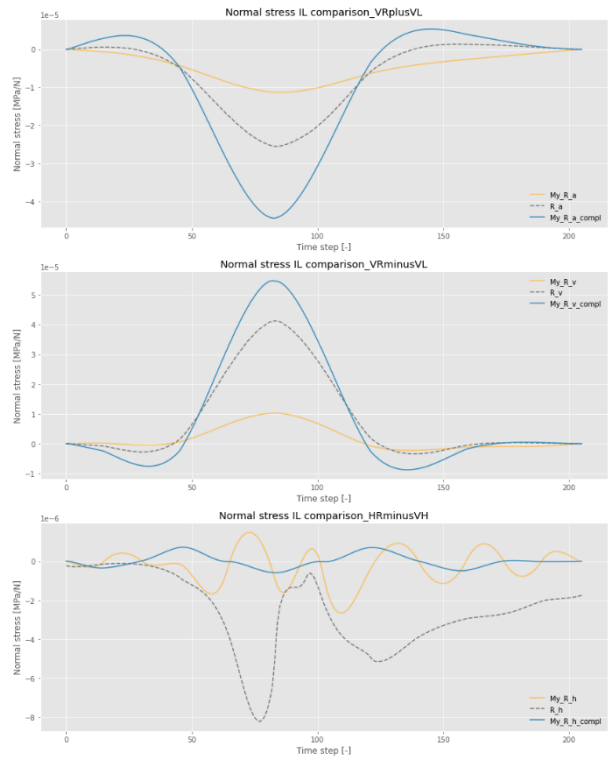


Figure 57 Normal stress IL per unit load comparison - Cross girder: elem. 929 simple, elem. 1249 complete

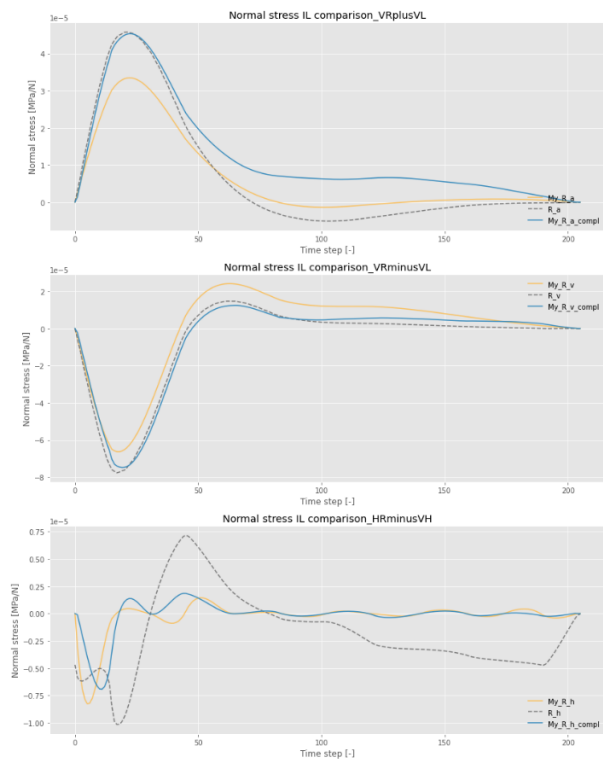


Figure 58 Normal stress IL per unit load comparison - Vertical 9: elem. 1327 simple, elem. 2380 complete

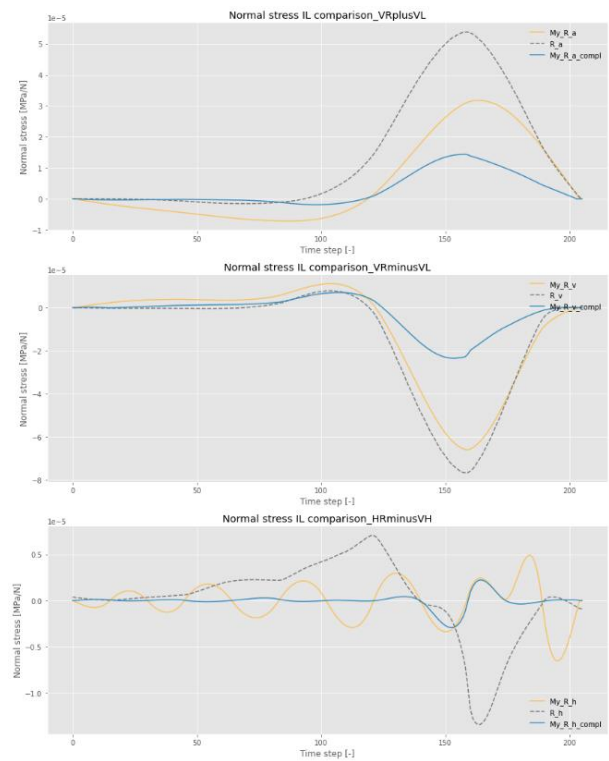


Figure 59 Normal stress IL per unit load comparison - Vertical 1: elem. 1390 simple, elem. 2696 complete

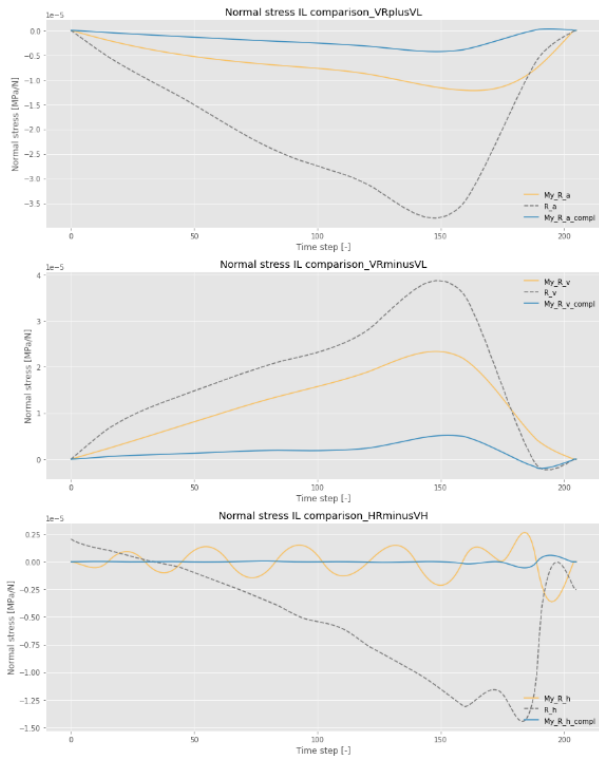


Figure 60 Normal stress IL per unit load comparison - Diagonal 1/0: elem. 620 simple, elem. 817 complete

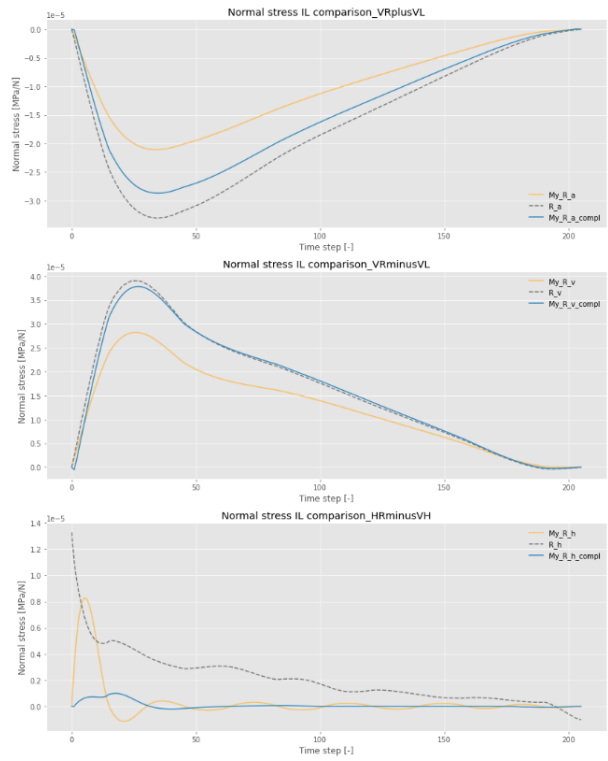


Figure 61 Normal stress IL per unit load comparison - Diagonal 9/11: elem. 617 simple, elem. 847 complete

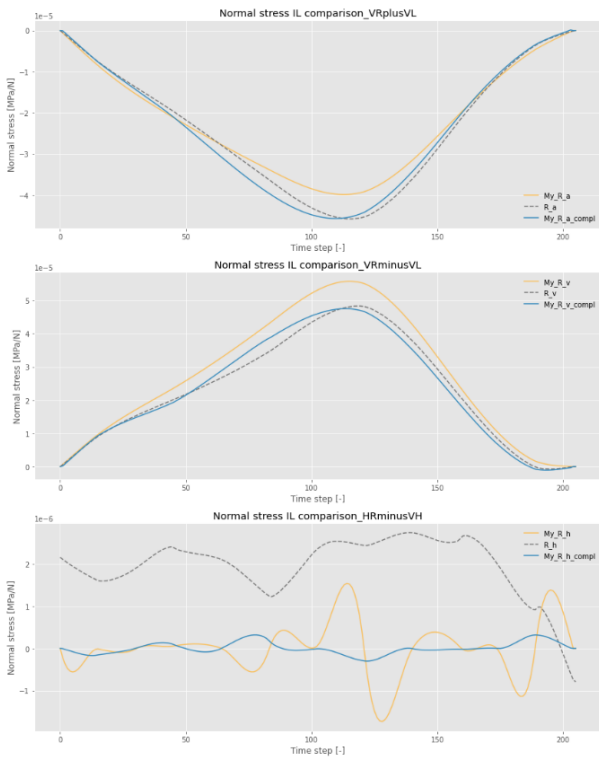


Figure 62 Normal stress IL per unit load comparison- Upper chord: elem. 533 simple, elem. 13766 complete

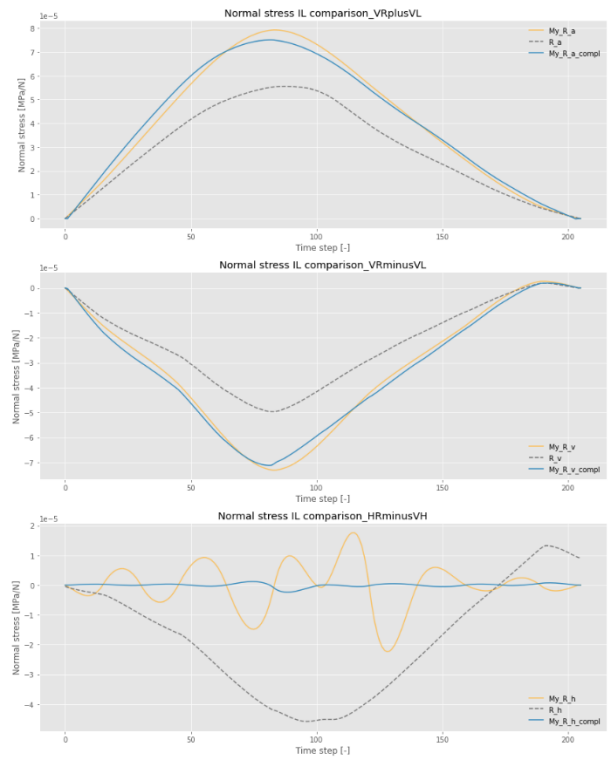


Figure 63 Normal stress IL per unit load comparison - Lower chord: elem. 426 simple, elem. 13846 complete

### 4.1.6 Stresses magnitude comparative

It has been shown that from the point of view of the congruence of  $IL$ 's shapes, quite satisfactory results have been obtained. However, differences in terms of intensities have been highlighted.

Rather than comparing the amplitude of the influence lines per unit load, it is already decided to consider the action that each train exerts on the structure and then make a comparison directly on the stresses that actually arise at the sections. Hence the need to consider the load vectors associated to the modelled trains and apply the convolution in order to calculate stresses.

The convolution between two signals, in this case the influence line ( $IL$ ) and the load function relative to a single train ( $LF$ ), consists in integrating the product between the first and second translated by a certain value, as shown in *eq. 12*.

The two signals under consideration are both functions of the same variable, time.

$$(IL * LF)(t) := \int_{-\infty}^{\infty} IL(\tau) LF(t - \tau) d\tau = \int_{-\infty}^{\infty} IL(t - \tau) LF(\tau) d\tau \quad (12)$$

- “\*” is the convolution operator
- “t” is the *shift* variable: interpreted as time distance (it can also be understood as spatial distance) that the train has moved along the load path of the influence line.

The calculated integral is a defined integral in the set of real numbers. Consequently, the result of this operation is a real number as well, i.e. the actual stress arisen at the point considered, in the time step considered.

Invoked in *Python* the script in which the  $LF$  for the eight trains are defined, the convolution operation is performed for the three components of the normal stress  $IL$  per unit load vector  $R_a$ ,  $R_v$  and  $R_h$ .

In such a way, the three effective normal stress components  $z_a$ ,  $z_v$  and  $z_h$  are computed. These three components contribute to the definition of the total stress acting on the analyzed point,  $z$ .

	Model type		
	Johs Holt's model	Simple model	Complete model
Component of normal stress	$z_a$	My_za	My_za_compl
	$z_v$	My_zv	My_zv_compl
	$z_h$	My_zh	My_zh_compl

Table 13 Normal stress  $IL$  univocal names

The final stress response, which also takes into account the effect of centrifugal force is  $z$ .

$$\begin{aligned} z_a &= \text{train.apply}(R_a) * 9.81 * 10^3 \\ z_v &= \text{train.apply}(R_v) * 9.81 * 10^3 \\ z_h &= \text{train.apply}(R_h) * 9.81 * 10^3 \end{aligned}$$

$$z = (z_a + z_v * Q + z_h * Q) \quad (13)$$

Through the *train.apply* command, convolution has been applied.

It should be noted that the length of the convoluted vector is a result of the length of the two vectors involved (*LF* and *IL*).

Attention has been paid to the units of measurement.

- Stress influence lines per unit load are expressed in  $[\frac{MPa}{N}]$
- The load function is expressed in [tons]

Consequently, it is necessary to multiply *z* by  $10^3$  in order to have loads in [kg] and multiply by the acceleration of gravity in order to obtain a final stress response in [MPa].

$$z = \left[ \frac{MPa}{N} * \text{tons} * \frac{m}{s^2} * 10^3 \right] = [MPa]$$

Once the three stress influence lines for the three different load configurations are obtained, these are added together in order to obtain the stress *IL* inclusive of all the actions acting on the structure. (eq. 13)

Two of these contributions,  $z_v$  and  $z_h$ , are multiplied by a factor *Q*, which considers the action of centrifugal force resulting from the curvature of the bridge rail tracks.

In order to explain the meaning of *Q* and its value, a parameter called *cant deficiency (CD)* is defined.

The cant deficiency is defined in the scenario of travel of a rail vehicle at constant speed on a constant radius curve.

Cant is a synonym for the superelevation of the curve, i.e. the elevation of the outside rail minus the elevation of the inside rail. Rail tracks indeed, in correspondence of a curve, do not lie in the same plane: the outermost rail is in an elevated position, as shown in Figure 64.

Cant deficiency is present when the vehicle's speed on a curve is greater than the speed at which the components of wheel-to-rail force are normal to the plane of the track.

In this case, the resultant force (as a vector sum between the gravitational force and the centrifugal force) insists on the outside rail more than the inside rails. A lateral acceleration is created toward the outside of the curve.

In order to reduce cant deficiency, the speed has to be decreased or the superelevation has to be increased. The amount of cant deficiency is expressed in term of required superelevation to be added in order to bring the resultant force into balance between the two rails.

On the contrary, the *cant excess* can be defined if the resultant force insists more against the inside rail than the outside rail.

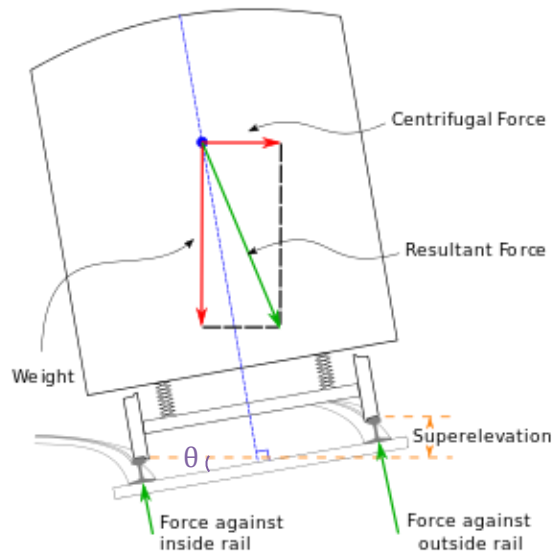


Figure 64 Resultant force exerts more against the outside rail than the inside rail

The *equilibrium cant*  $C$  (or *superelevation*), necessary for any speed, is calculated from the formula:

$$C = \frac{G * v^2}{127 * R} \quad (14)$$

Where:

- $C$  is in [ $mm$ ]
- $G$  (track gauge, the distance between the two rails of a railway track) in [ $mm$ ]
- $R$  (curve radius) in [ $m$ ]
- $v$  (train speed) in [ $\frac{km}{h}$ ], different for each train considered

Then the parameter  $Q$  is defined as follows:

$$Q = \frac{C}{G} = \text{sen}\theta = \frac{v^2}{127 * R} \quad (15)$$

To make it clear, the number “127” comes from the conversion of acceleration of gravity in  $\frac{km}{h^2}$  in order to express the velocity in  $\frac{km}{h}$ , in fact:

$$127 = 9.81 * (3.6)^2 \quad (16)$$

To conclude the discussion on  $z$  calculation, it is added that the analysis conducted is only static and not dynamic, therefore the presence of any dynamic effect is not considered. No dynamic amplification factor (*DAF*) is considered in the calculation of normal stresses.

It is now possible to make another quantitative comparison between the influence lines, this time between the actual normal stress influence lines. It is chosen to examine the difference between the maximum of the absolute values. This comparison shall be made for each of the eight trains.

Table 14 - Table 21 summarize the results obtained. The differences between the maximum absolute values of stress influence lines are expressed in MPa.

<b>Train1</b>	<b>Company</b>		<b>Simple model</b>			
Location	Elem	Elem	Max_zaDiff	Max_zvDiff	Max_zhDiff	Max_zDiff
Stringer	41144	102	0.938	7.980	5.850	1.030
Subsyst	64074	1154	1.950	0.002	31.800	2.730
CG-vert 9	33014	829	3.760	4.310	5.180	3.660
CG-str	33011	844	0.896	0.263	10.400	1.050
CG-diag 9/8	33024	879	7.790	9.360	2.920	7.650
Vertical 9	24011	1327	2.650	8.620	3.120	2.580
Vertical 1	28011	1390	11.100	4.830	1.840	11.000
Diagonal 1/0	23064	620	16.700	8.380	7.150	16.600
Diagonal 9/11	23011	617	7.640	4.990	3.320	7.510
Upper chord	22032	533	2.160	0.029	2.360	2.210
Lower chord	21042	426	0.012	0.023	25.900	0.025
CG-vert 5	33034	929	3.930	9.470	3.420	3.800
	<b>Company</b>		<b>Complete model</b>			
Location	Elem	Elem	Max_zaDiff	Max_zvDiff	Max_zhDiff	Max_zDiff
Stringer	41144	102	5.720	3.310	5.820	10.500
Subsyst	64074	1884	1.180	6.180	15.900	2.710
CG-vert 9	33014	1049	0.277	0.516	5.140	0.230
CG-str	33011	1064	1.150	0.745	10.100	1.260
CG-diag 9/8	33024	1618	0.023	6.910	2.880	0.017
Vertical 9	24011	2380	0.213	2.150	3.230	0.204
Vertical 1	28011	2696	15.200	16.400	1.990	14.900
Diagonal 1/0	23064	817	22.700	21.000	7.170	22.500
Diagonal 9/11	23011	847	2.680	0.666	3.280	2.630
Upper chord	22032	13766	0.452	0.760	2.420	0.422
Lower chord	21042	13846	0.073	0.047	26.300	0.070
CG-vert 5	33034	1249	0.946	0.895	3.470	0.961

Table 14 Maximum difference between the absolute values of normal stress IL - Train 1

<b>Train2</b>	<b>Company</b>		<b>Simple model</b>			
Location	Elem	Elem	Max_zaDiff	Max_zvDiff	Max_zhDiff	Max_zDiff
Stringer	41144	102	0.951	6.390	6.110	1.300
Subsyst	64074	1154	1.950	0.001	31.800	4.460
CG-vert 9	33014	829	3.760	4.530	4.660	3.420
CG-str	33011	844	0.840	0.350	9.990	1.250
CG-diag 9/8	33024	879	7.790	9.360	2.920	7.290
Vertical 9	24011	1327	2.700	8.620	2.870	2.410
Vertical 1	28011	1390	11.000	4.830	2.010	10.700
Diagonal 1/0	23064	620	16.600	8.380	7.120	16.500
Diagonal 9/11	23011	617	7.640	4.990	3.320	7.200
Upper chord	22032	533	2.160	0.021	2.330	2.350
Lower chord	21042	426	0.009	0.020	25.900	0.046
CG-vert 5	33034	929	3.930	9.470	3.390	3.480
	<b>Company</b>		<b>Complete model</b>			
Location	Elem	Elem	Max_zaDiff	Max_zvDiff	Max_zhDiff	Max_zDiff
Stringer	41144	102	5.720	3.290	7.280	19.300
Subsyst	64074	1884	1.300	6.180	17.400	3.340
CG-vert 9	33014	1049	0.302	0.495	4.620	0.203
CG-str	33011	1064	1.050	0.825	9.660	1.380
CG-diag 9/8	33024	1618	0.023	6.910	2.880	0.023
Vertical 9	24011	2380	0.213	2.050	2.960	0.181
Vertical 1	28011	2696	15.200	16.300	1.990	14.100

Diagonal 1/0	23064	817	22.600	20.800	7.270	21.600
Diagonal 9/11	23011	847	2.680	0.666	3.280	2.510
Upper chord	22032	13766	0.501	0.875	2.370	0.382
Lower chord	21042	13846	0.073	0.047	26.300	0.063
CG-vert 5	33034	1249	0.886	0.934	3.470	0.926

 Table 15 Maximum difference between the absolute values of normal stress  $IL$  - Train 2

<b>Train3</b>	<b>Company</b>		<b>Simple model</b>			
Location	Elem	Elem	Max_zaDiff	Max_zvDiff	Max_zhDiff	Max_zDiff
Stringer	41144	102	1.290	9.960	7.980	3.250
Subsyst	64074	1154	1.130	0.003	44.100	6.260
CG-vert 9	33014	829	5.280	7.010	5.430	4.660
CG-str	33011	844	0.919	0.640	11.100	1.470
CG-diag 9/8	33024	879	9.630	12.500	3.560	8.840
Vertical 9	24011	1327	4.200	10.000	3.580	3.800
Vertical 1	28011	1390	13.000	6.420	2.600	12.400
Diagonal 1/0	23064	620	19.000	10.400	8.380	18.700
Diagonal 9/11	23011	617	8.950	6.330	4.580	8.230
Upper chord	22032	533	2.380	0.046	2.480	2.600
Lower chord	21042	426	0.019	0.043	26.600	0.126
CG-vert 5	33034	929	5.560	12.600	3.960	4.740
	<b>Company</b>		<b>Complete model</b>			
Location	Elem	Elem	Max_zaDiff	Max_zvDiff	Max_zhDiff	Max_zDiff
Stringer	41144	102	6.560	3.600	9.010	28.100
Subsyst	64074	1884	2.020	10.400	20.600	4.210
CG-vert 9	33014	1049	0.295	0.780	5.430	0.192
CG-str	33011	1064	1.110	1.230	11.300	1.610
CG-diag 9/8	33024	1618	0.045	9.830	3.440	0.059
Vertical 9	24011	2380	0.464	2.210	3.620	0.346
Vertical 1	28011	2696	17.200	21.400	2.610	15.500
Diagonal 1/0	23064	817	25.300	23.900	8.470	24.000
Diagonal 9/11	23011	847	3.130	0.974	4.510	2.900
Upper chord	22032	13766	0.469	0.891	2.540	0.334
Lower chord	21042	13846	0.147	0.094	26.700	0.146
CG-vert 5	33034	1249	1.030	2.030	3.990	1.060

 Table 16 Maximum difference between the absolute values of normal stress  $IL$  - Train 3

<b>Train4</b>	<b>Company</b>		<b>Simple model</b>			
Location	Elem	Elem	Max_zaDiff	Max_zvDiff	Max_zhDiff	Max_zDiff
Stringer	41144	102	1.820	8.200	6.590	7.310
Subsyst	64074	1154	2.670	0.003	46.100	12.900
CG-vert 9	33014	829	5.730	7.400	5.420	4.040
CG-str	33011	844	0.799	0.562	10.600	2.030
CG-diag 9/8	33024	879	9.710	12.700	2.900	7.670
Vertical 9	24011	1327	4.150	9.250	3.840	3.320
Vertical 1	28011	1390	12.300	6.150	2.560	10.800
Diagonal 1/0	23064	620	16.000	9.700	7.370	15.300
Diagonal 9/11	23011	617	7.990	5.680	4.440	6.400
Upper chord	22032	533	2.690	0.050	2.550	3.210
Lower chord	21042	426	0.020	0.047	24.100	0.342
CG-vert 5	33034	929	5.960	13.000	3.180	3.850
	<b>Company</b>		<b>Complete model</b>			
Location	Elem	Elem	Max_zaDiff	Max_zvDiff	Max_zhDiff	Max_zDiff
Stringer	41144	102	6.060	3.660	4.910	31.000
Subsyst	64074	1884	2.160	10.200	22.200	6.710

CG-vert 9	33014	1049	0.263	0.772	5.660	0.488
CG-str	33011	1064	0.914	1.050	9.210	1.990
CG-diag 9/8	33024	1618	0.048	10.200	2.710	0.149
Vertical 9	24011	2380	0.490	2.630	3.910	0.247
Vertical 1	28011	2696	17.700	22.100	2.610	13.400
Diagonal 1/0	23064	817	21.600	21.300	7.570	18.800
Diagonal 9/11	23011	847	2.880	0.957	4.360	2.320
<b>Upper chord</b>	22032	13766	0.596	1.500	2.500	0.232
<b>Lower chord</b>	21042	13846	0.155	0.099	24.100	0.307
<b>CG-vert 5</b>	33034	1249	2.210	2.150	3.360	2.250

Table 17 Maximum difference between the absolute values of normal stress IL - Train 4

<b>Train5</b>	<b>Company</b>		<b>Simple model</b>			
Location	Elem	Elem	Max_zDiff	Max_zvDiff	Max_zhDiff	Max_zDiff
Stringer	41144	102	0.986	9.720	7.470	0.986
Subsyst	64074	1154	1.900	0.002	34.000	1.900
CG-vert 9	33014	829	4.330	5.290	5.200	4.320
CG-str	33011	844	0.609	0.385	10.600	0.612
CG-diag 9/8	33024	879	8.200	10.500	2.770	8.200
Vertical 9	24011	1327	3.250	8.350	2.980	3.250
Vertical 1	28011	1390	11.600	5.280	2.050	11.600
Diagonal 1/0	23064	620	16.800	8.700	7.470	16.800
Diagonal 9/11	23011	617	7.330	4.860	3.310	7.330
Upper chord	22032	533	2.270	0.043	2.340	2.270
Lower chord	21042	426	0.017	0.049	25.600	0.018
CG-vert 5	33034	929	4.480	10.300	3.300	4.480
	<b>Company</b>		<b>Complete model</b>			
Location	Elem	Elem	Max_zDiff	Max_zvDiff	Max_zhDiff	Max_zDiff
Stringer	41144	102	5.660	3.690	8.120	5.770
Subsyst	64074	1884	1.350	7.460	17.800	1.400
CG-vert 9	33014	1049	0.252	0.565	5.130	0.251
CG-str	33011	1064	0.820	0.390	9.900	0.821
CG-diag 9/8	33024	1618	0.023	7.450	2.960	0.023
Vertical 9	24011	2380	0.213	2.120	3.130	0.213
Vertical 1	28011	2696	15.800	18.400	2.080	15.800
Diagonal 1/0	23064	817	22.800	21.300	7.450	22.800
Diagonal 9/11	23011	847	2.550	0.745	3.370	2.550
Upper chord	22032	13766	0.409	0.667	2.410	0.409
Lower chord	21042	13846	0.073	0.064	25.600	0.073
CG-vert 5	33034	1249	0.782	1.230	3.350	0.782

Table 18 Maximum difference between the absolute values of normal stress IL - Train 5

<b>Train6</b>	<b>Company</b>		<b>Simple model</b>			
Location	Elem	Elem	Max_zDiff	Max_zvDiff	Max_zhDiff	Max_zDiff
Stringer	41144	102	0.986	9.690	6.820	0.989
Subsyst	64074	1154	1.900	0.003	34.000	2.030
CG-vert 9	33014	829	4.330	5.290	5.130	4.310
CG-str	33011	844	0.774	0.396	10.100	0.783
CG-diag 9/8	33024	879	8.200	10.500	2.740	8.180
Vertical 9	24011	1327	3.250	8.200	2.700	3.240
Vertical 1	28011	1390	11.600	5.190	2.050	11.500
Diagonal 1/0	23064	620	16.900	8.660	7.260	16.900
Diagonal 9/11	23011	617	7.330	4.860	3.610	7.320
Upper chord	22032	533	2.280	0.054	2.410	2.280
Lower chord	21042	426	0.022	0.050	25.600	0.025

CG-vert 5	33034	929	4.480	10.300	3.340	4.460
Company		Complete model				
Location	Elem	Elem	Max_zaDiff	Max_zvDiff	Max_zhDiff	Max_zDiff
Stringer	41144	102	5.660	3.690	9.250	6.280
Subsyst	64074	1884	1.350	7.460	24.300	1.620
CG-vert 9	33014	1049	0.236	0.434	5.340	0.233
CG-str	33011	1064	1.030	0.460	10.300	1.030
CG-diag 9/8	33024	1618	0.023	7.450	2.770	0.022
Vertical 9	24011	2380	0.213	2.440	2.800	0.212
Vertical 1	28011	2696	15.800	18.400	2.080	15.700
Diagonal 1/0	23064	817	22.800	21.200	7.340	22.700
Diagonal 9/11	23011	847	2.550	0.745	3.610	2.540
Upper chord	22032	13766	0.443	0.709	2.400	0.440
Lower chord	21042	13846	0.073	0.076	25.600	0.073
CG-vert 5	33034	1249	0.691	1.120	3.410	0.695

 Table 19 Maximum difference between the absolute values of normal stress  $IL$  - Train 6

Train7	Company		Simple model			
Location	Elem	Elem	Max_zaDiff	Max_zvDiff	Max_zhDiff	Max_zDiff
Stringer	41144	102	1.860	11.300	9.010	1.860
Subsyst	64074	1154	2.130	0.004	43.900	2.630
CG-vert 9	33014	829	4.790	6.810	6.040	4.710
CG-str	33011	844	1.070	0.518	10.600	1.130
CG-diag 9/8	33024	879	8.120	10.100	2.910	8.050
Vertical 9	24011	1327	3.660	8.720	4.120	3.610
Vertical 1	28011	1390	11.300	5.550	2.610	11.300
Diagonal 1/0	23064	620	16.500	8.740	6.990	16.400
Diagonal 9/11	23011	617	7.920	5.690	4.400	7.840
Upper chord	22032	533	2.750	0.064	2.580	2.770
Lower chord	21042	426	0.026	0.060	25.400	0.041
CG-vert 5	33034	929	4.470	10.000	3.380	4.390
Company		Complete model				
Location	Elem	Elem	Max_zaDiff	Max_zvDiff	Max_zhDiff	Max_zDiff
Stringer	41144	102	6.000	5.010	5.190	9.820
Subsyst	64074	1884	1.740	9.950	26.300	2.670
CG-vert 9	33014	1049	0.418	0.786	6.040	0.395
CG-str	33011	1064	1.400	1.250	10.100	1.480
CG-diag 9/8	33024	1618	0.030	8.040	3.080	0.026
Vertical 9	24011	2380	0.284	2.760	4.380	0.278
Vertical 1	28011	2696	16.200	17.400	2.770	16.100
Diagonal 1/0	23064	817	21.600	20.500	7.450	21.400
Diagonal 9/11	23011	847	2.810	0.859	4.420	2.780
Upper chord	22032	13766	0.706	1.390	2.590	0.683
Lower chord	21042	13846	0.098	0.091	25.700	0.096
CG-vert 5	33034	1249	1.940	2.170	3.740	1.940

 Table 20 Maximum difference between the absolute values of normal stress  $IL$  - Train 7

Train8	Company		Simple model			
Location	Elem	Elem	Max_zaDiff	Max_zvDiff	Max_zhDiff	Max_zDiff
Stringer	41144	102	2.240	14.100	14.400	2.240
Subsyst	64074	1154	2.670	0.004	55.300	2.730
CG-vert 9	33014	829	5.990	8.540	7.590	5.990
CG-str	33011	844	1.340	0.903	13.400	1.340
CG-diag 9/8	33024	879	10.100	12.600	3.730	10.100
Vertical 9	24011	1327	4.560	11.000	5.770	4.550

Vertical 1	28011	1390	14.200	6.960	3.260	14.200
Diagonal 1/0	23064	620	20.600	10.900	8.740	20.600
Diagonal 9/11	23011	617	9.900	7.110	5.440	9.890
Upper chord	22032	533	3.430	0.080	2.990	3.430
Lower chord	21042	426	0.032	0.075	31.700	0.033
CG-vert 5	33034	929	5.590	12.500	4.500	5.580
<b>Company</b>			<b>Complete model</b>			
Location	Elem	Elem	Max_zzDiff	Max_zvDiff	Max_zhDiff	Max_zDiff
Stringer	41144	102	7.510	6.260	11.600	7.490
Subsyst	64074	1884	2.340	12.600	32.900	2.400
CG-vert 9	33014	1049	0.522	0.983	7.380	0.521
CG-str	33011	1064	1.750	1.570	12.300	1.750
CG-diag 9/8	33024	1618	0.045	10.100	3.850	0.045
Vertical 9	24011	2380	0.464	3.740	6.090	0.463
Vertical 1	28011	2696	20.300	21.800	3.470	20.300
Diagonal 1/0	23064	817	27.000	25.700	9.310	26.900
Diagonal 9/11	23011	847	3.480	1.070	5.430	3.480
Upper chord	22032	13766	0.882	1.710	3.000	0.881
Lower chord	21042	13846	0.147	0.113	32.100	0.147
CG-vert 5	33034	1249	2.430	2.710	4.710	2.430

Table 21 Maximum difference between the absolute values of normal stress  $IL$  - Train 8

As for the simple model, the element that sees a greater difference between the maxima of the stress absolute values is the number 620, which lies on the diagonal 1/0.

The maximum stress difference observed with respect to the value obtained by John Holt Consultant Eng. is approximately equal to **20 MPa**, due the passage of the train number 8. This difference is remarkable considering that the  $z$  absolute maximum value is about **30 MPa**.

Considering the complete model, the element that sees the biggest difference is the 817, which lies again on the 1/0 diagonal. The difference in terms of  $z$  amounts to approximately **26 MPa**, so even larger. This is evident by looking at Figure 65.

The stress value arisen in this section has been strongly underestimated by the two self-made models. Related to this, it will be seen afterwards that this element is one of those characterized by the greatest relative difference in terms of damage, but it will not be among the most damaged elements.

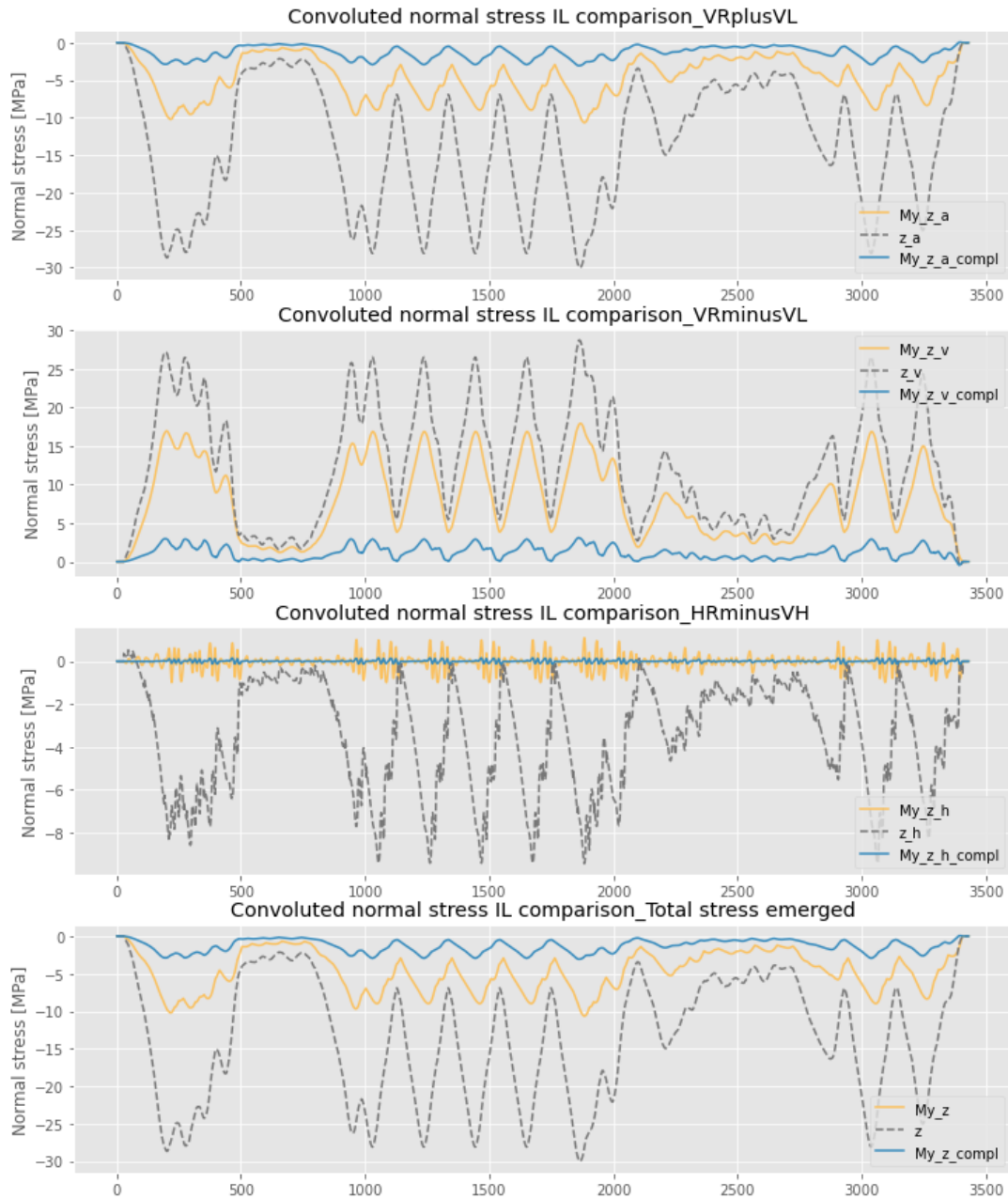


Figure 65 Normal stress IL comparison - Diagonal 1/0: elem. 620 simple, elem. 817 complete. T8

Finally, Figure 66 - Figure 68 report the normal stress *IL* comparison between three specific sections of the bridge. These sections will be chosen for the model updating since are considered among the most critical.

It is noted that the section evaluated on the stringer is the one that has a greater disparity in terms of total normal stress between the three models. Both the shapes and the intensities of the total normal stress influence lines for the other two sections are more consistent.

In Figure 66 - Figure 68 the train under consideration is again the number 8, which will be discovered in the next chapter to be the most damaging.

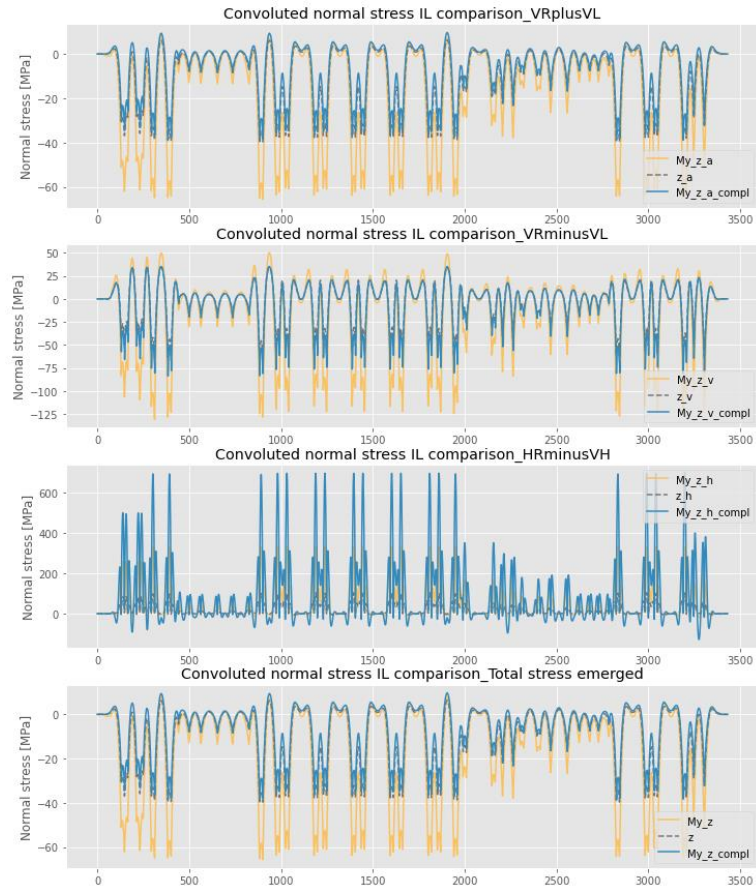


Figure 66 Normal stress IL comparison - Stringer: elem. 102 simple, elem. 102 complete. T8

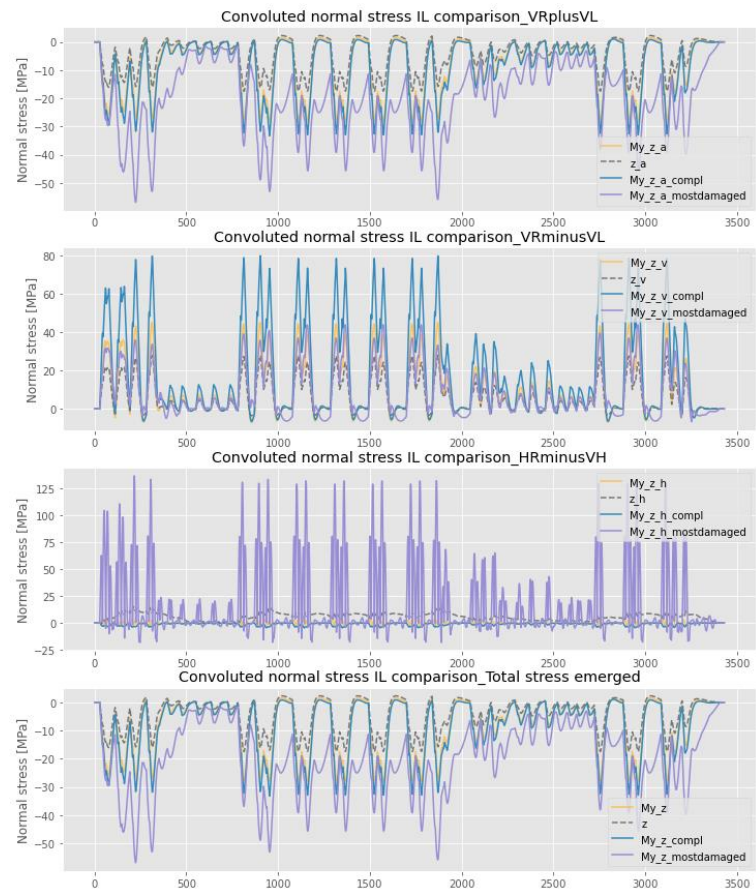


Figure 67 Normal stress IL comparison - Cross girder: elem. 844 simple, elem. 1064 complete. T8

For the element 844, belonging to the simple model, the difference in terms of stress response between the most stressed point of the section and the one evaluated by the consulting company is shown in Figure 67.

As expected, the intensity of the normal stress  $IL$  for the point lying at the edge of the section  $Myz_{most\,damaged}$ , is considerably higher than that calculated for the other point,  $Myz$ . The estimated damage at the most stressed point is therefore expected to be greater.

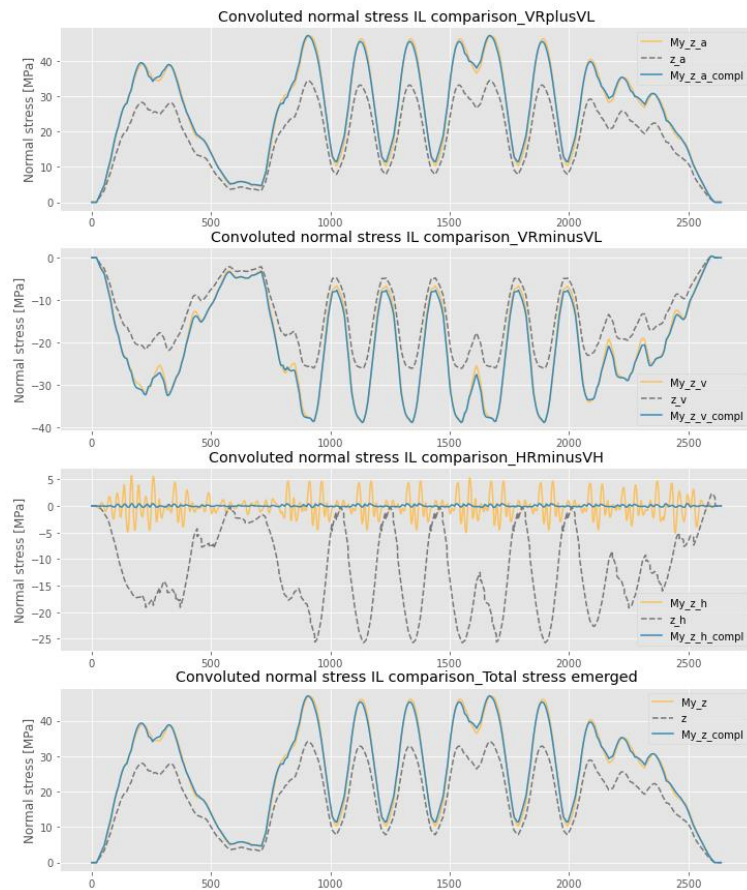


Figure 68 Normal stress  $IL$  comparison – Lower chord: elem. 426 simple, elem. 13846 complete. T8

In the following chapter, a further comparison will be made, this time between the damages induced in the single elements analyzed. The intention will be to understand which sections are most at risk for fatigue degradation. These subsequent analyses are still carried out taking into account the eight different convoys. Identifying the most damaging train is another goal.

## 4.2 Comparisons on the dynamic behaviour of the bridge - Modal Assurance Criterion

Although the analysis conducted so far is a static analysis, a method to compare the dynamic behavior of the two self-made models is considered [9]. With the *IL* analysis the two models have been compared in terms of static response, now is intended to compare the dynamic one.

Specifically, it is meant to make a comparison in terms of mode shapes, determined by performing a modal analysis.

Thereafter, the Modal Assurance Criterion (*MAC*) method is implemented in order to compare the modal characteristics of the two self-made models. The goal is to validate the two models with respect to each other, evaluating their compatibility in modal terms.

### 4.2.1 Theory

It is recalled that in the modal analysis you study the free vibrations of the structure, therefore in the absence of external forcing. It is also assumed that the model is not damped. Hence, this analysis allows us to understand the intrinsic dynamic behavior of the bridge.

The output of the modal analysis, at the end of the resolution of the so-called *eigenvalue problem*, consists in the determination of the eigenfrequencies and the mode shapes of the system under examination.

The evaluation of natural frequencies and mode shapes is carried out on the constrained structure, thus excluding rigid body motions with zero frequency. The bridge could also have been considered not constrained.

The Modal Assurance Criterion allows to assess the degree of correlation between two vectors, in this case the mode shapes vectors. The *MAC* is defined as follows:

$$MAC_{ij} = \frac{|V_i V_j^*|^2}{(|V_i|^2 |V_j|^2)} \quad (17)$$

In which:

- $0 < i, j < N$ , where  $N$  is the number of degrees of freedom at which the mode shapes are evaluated in the comparison
- $V_i$  and  $V_j$  are the modal vectors containing a set of modes
- $V_j^*$  is the complex and conjugate of the vector  $V_j$
- $|\cdot|$  is the symbol of absolute value

The definition of the *MAC*, evaluated between two vectors, follows the definition of coherence, between two signals.

The *MAC* value is between 0 and 1.

- If the two mode shape vectors are equal, the value of the *MAC* is unitary
- If the two mode shape vectors are orthogonal to each other, the *MAC* value is 0

Since the mode shapes are orthogonal only with respect to the mass matrix and stiffness matrix (they are therefore base vectors with respect to the matrices that generated them) and are not orthogonal to each other, the *MAC* cannot reach the value 0.

What has been said follows therefore what has been seen for the *LCC* definition.

A rule that is generally adopted is that with a value of  $MAC > 0.9$  the mode shapes can be considered equal, if  $MAC < 0.15$  then the mode shape vectors are considered orthogonal to each other and there is no modal compatibility. It should be noted that the modal assurance criterion can only indicate consistency, not validity or orthogonality.

## 4.2.2 Applying the model

The *Ansys* software implements a command to calculate the *MAC*, called *RSTMAC*.

It starts from the execution of the modal analysis on *Ansys*. Compared to the static analyses previously conducted on the two self-made models, it is now necessary to specify the characteristics of the material of which the structure is made of. A *material property* to be associated to the finite elements has to be defined, so that the mass matrix can be computed.

After developing the discretized model and defining the constraint conditions, you enter in the modal solution environment with the *antype,modal* command.

It is decided to consider a number of mode shapes equal to 187, so that the cumulative mass fraction reaches a percentage close to 90%, at least for the modes that evaluate the translations in the three directions in space. You are thus sure that almost all the mass of the model, which can move because it is un-constrained, is effectively moving. If not, it is like the structure had lost mass just due to the fact of having evaluated a reduced number of mode shapes.

Once the modal analysis for both the simple and the refined model is performed, you enter in the */post1* postprocessing environment and the *RSTMAC* command is invoked. It is necessary to give as input the result files (*.rst* or *.rstp*) of the modal analysis previously conducted.

The result of the Modal Assurance Criterion is a  $187 \times 187$  matrix, called *MAC* matrix, which summarizes the values of the *MAC* coefficient. In such a way it is possible to determine the degree of correlation that exists between all the considered modes of the two models. This matrix, deprived of some rows and columns because they are not significant, is depicted in Figure 69.

It is deduced that there is a perfect correspondence in modal terms only for three pairs of mode shapes, illustrated in Table 22.

Matched solutions					
	Complete model	Simple model	MAC value	Frequency difference (kHz)	Frequency error %
Mode	7	9	0.953	3.30E-03	29%
shape	9	9	0.95	5.30E-04	7%
number	15	10	0.956	3.60E-04	2%

Table 22 Matched mode shapes

# Identification of disparities and similarities between models

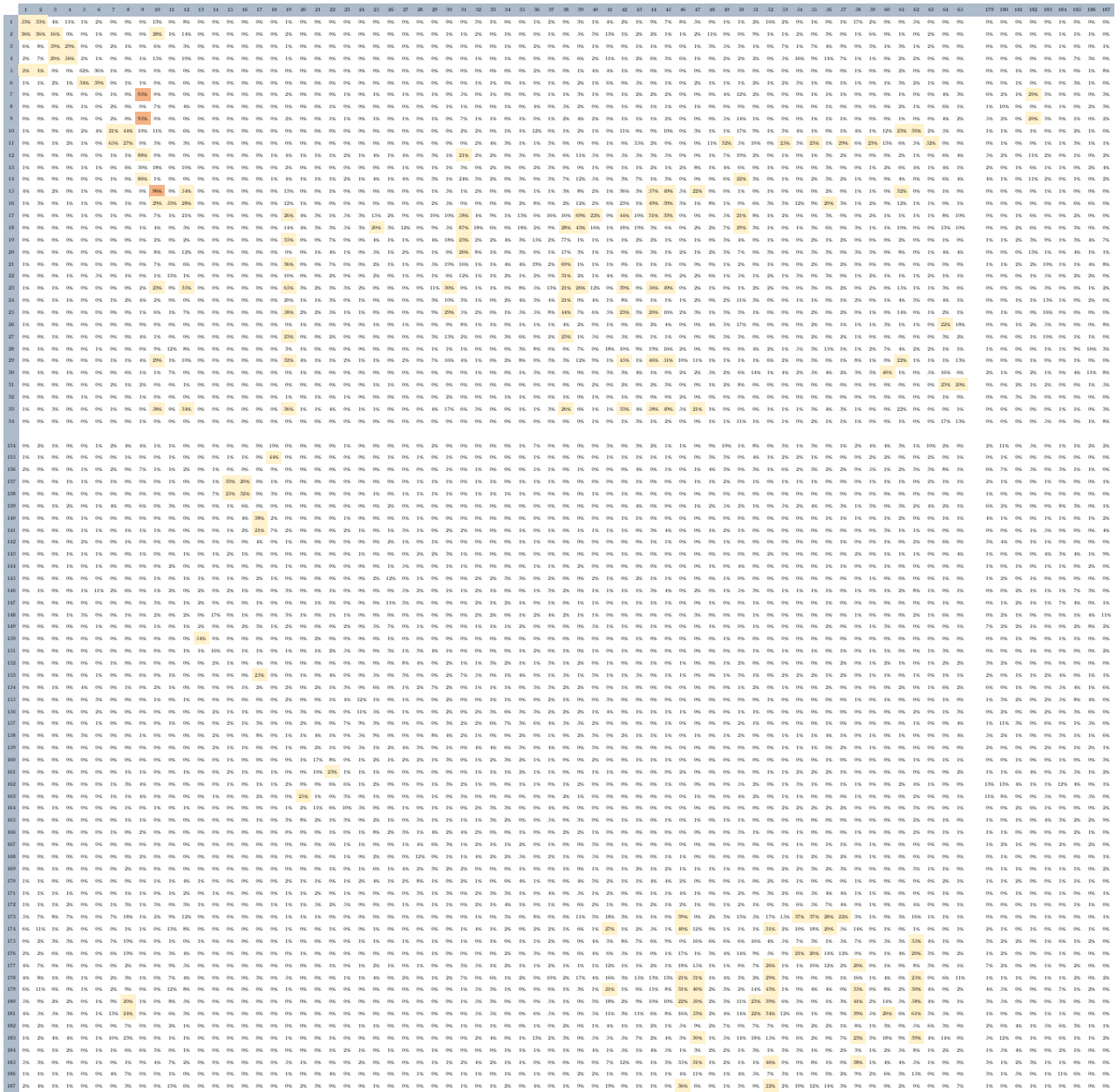


Figure 69 MAC matrix

In the *MAC* matrix the color legend represents:

- Orange box:  $MAC \geq 90\%$
- Yellow box:  $20 < MAC < 90\%$
- White box:  $0 < MAC \leq 20\%$

Looking at the matrix, it is clear that there is not a great correspondence between the two models in terms of mode shapes and therefore in terms of the intrinsic dynamic behavior of the system.

A more accurate analysis aimed at understanding the reason why of such a difference would have to be performed. Since, however, the intent of the discussion is to evaluate the fatigue behavior of the bridge, it is decided not to deepen this aspect.

# 5 Damage evaluation on critical components

## 5.1 Miner's linear damage summation rule

The present chapter is aimed at the evaluation of the damage induced, in the sections examined, by the single passage of a train on the bridge.

In order to determine the arisen damage, it is necessary to be aware of the load history to which the component was subjected and the material data (the Whöler  $S - N$  curve for example).

First of all, damage is defined according to Miner's hypothesis. The damage induced by fatigue phenomena is to be linked to microscopic effects acting on the material: dislocations, slip bands, microcracks. Damage can be defined as the used life fraction of the component.

More specifically, in the case of linear damage hypothesis, the damage fraction  $D_i$  at the specific load level  $S_i$  is defined as:

$$D_i = \frac{n_i}{N_i} \quad \text{at load level } S_i \quad (18)$$

The basic aspect on which Miner's theory is based on consist of the assumption that there is no sequence effect in the application of load levels: a certain load causes the same damage regardless of its position in the load history.

The component will collapse when:

$$\sum_{i=1}^k D_i \geq \text{Constant } C \quad (19)$$

According to Miner, the constant  $C$  value varies between 0.5 and 2, based on experimental evidence.  $C = 1$  for pseudo-random load histories.

It is therefore decided to refer in this discussion to Miner's linear damage rule. Although simple, it has greater validity for random load histories. The loading history resulting from the passages of different convoys types on the bridge over the years can be meant as random loading history, where the sequence effect does not have any influence.

The fatigue damage is therefore computed exploiting a linear fatigue/endurance curve with detail category or characteristic stress  $S_c$ . Endurance curves are a set of log-log curves giving the relationship between stress ranges  $\Delta\sigma$  and number of cycles until failure  $N$ .

The explanation for using a linear and non-bi/trilinear fatigue curve lies in the fact that the results obtained would be too markedly affected by the fatigue limit of the material.

For riveting structures, the use of linear fatigue curves, as explained in [3], is suitable.

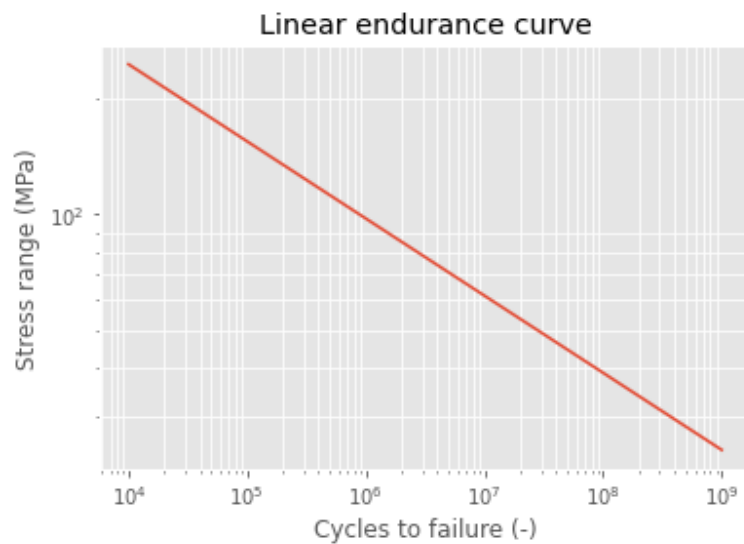


Figure 70 Linear endurance curve

The fatigue endurance model defines the fatigue life when the component is subjected to repeated application of a single and constant stress range. The response in a railway bridge generally consists of a combination of different stress ranges. A damage accumulation model must be introduced to find the total damage.

It is also necessary to recognize the damage event in a variable load history and then extract constant amplitude events from the real load history. It is therefore necessary to define a cycles counting method.

Being aware of stress time series, it is now necessary to obtain a spectrum of stress ranges. The stress time series generated by a certain train can consist of a number of cycles with varying amplitude.

It is intended to lead back these load cycles to a series of events with constant amplitude: the load block is then reorganized into cycles with constant amplitude, such as to reproduce the actual damage induced on the real component. It is therefore chosen to use a *rainflow* counting method to establish the spectrum and extract the stress cycles. Counted stress ranges and the corresponding number of cycles are determined.

In order to do this, the *Python* package "*fatpack*" [10] is exploited, which automatically calculates load cycles starting from the stress time series.

Subsequently, the damage is calculated according to the Miner sum theory from the stress ranges with the endurance curve. This is done accordingly to a linear  $S - N$  curve (fatigue curve 71 from Eurocode 3 part 1-9, represented in Figure 70) with  $\Delta\sigma_c = S_c = 85 \text{ MPa}$  and a slope  $m = 5$ , which gives significantly better fatigue strength for stress ranges between  $20 \text{ MPa}$  and  $80 \text{ MPa}$ . The characteristic endurance  $N_c$  is assumed equal to  $2 * 10^6$ .

The fatigue endurance model defines the number of cycles  $N$  from a uncracked and perfect material to fatigue failure for a component subjected to repeated application of stress range  $S$ .

A prerequisite for being able to use the chosen linear  $S - N$  curve is that the shear forces in the rivets do not exceeds a slip resistance limit. For rivets with unknown manufacturing method, this limit value is 12 kN per nail. It is considered in this study that the effect of shear forces is negligible, therefore no verifications are carried out.

Partial damage for each stress range can now be calculated and summed. This process is repeated for each of the eight trains analyzed.

## 5.2 Discrepancies between the three models

The damage that occurred in each of the twelve sections analyzed due to the single passage of all eight trains has now been calculated. You want to estimate the value of these damages and evaluate how much they differ between one model and another. It is also intended to evaluate which is the train that produces the greatest damage.

Table 23 summarizes the maximum occurred damage values for each component and due to the passage of which train they were induced.

It is immediately noticeable that train number 8 is the most damaging. This could have been predicted by looking at the load function associated with that train. Train 8 is indeed the second heaviest train (after train 4), but shorter than the train number 4, so then the load is less distributed.

<b>Most damaged elements and most damaging trains</b>									
	Company	Train	D	Simple	Train	D	Complete	Train	D
1°	Stringer	8	3.18E-06	Stringer	8	3.68E-05	Stringer	4	6.63E-05
2°	Lower chord	8	7.27E-07	Lower chord	8	3.79E-06	Lower chord	8	3.42E-06
3°	Upper chord	8	2.27E-07	Subsyst	8	6.96E-07	CG-diag 9/8	8	9.49E-07
4°	Vertical 1	8	1.67E-07	CG-str	8	4.26E-07	CG-str	8	8.54E-07
5°	Diagonal 1/0	8	1.10E-07	Upper chord	8	1.28E-07	Upper chord	8	2.52E-07
6°	Diagonal 9/11	8	6.47E-08	Vertical 1	8	2.93E-08	CG-vert 5	8	5.57E-08
7°	Vertical 9	8	6.03E-08	Vertical 9	8	9.98E-09	Vertical 9	8	5.16E-08
8°	CG-str	8	5.19E-08	Diagonal 9/11	8	6.53E-09	Diagonal 9/11	8	3.20E-08
9°	CG-vert 5	8	4.57E-09	Diagonal 1/0	8	4.85E-10	Subsyst	4	1.39E-08
10°	CG-diag 9/8	8	3.44E-09	CG-vert 5	8	1.26E-10	CG-vert 9	8	3.90E-09
11°	Subsyst	4	7.23E-10	CG-vert 9	8	8.76E-13	Vertical 1	8	2.18E-10
12°	CG-vert 9	8	5.86E-10	CG-diag 9/8	8	5.67E-13	Diagonal 1/0	8	1.68E-12

Table 23 Most damaged elements and most damaging trains

As for the components subject to a greater loss of structural capacity, stringer and lower chord are certainly the worst, with damage values even one or two orders of magnitude higher than what happens for the other elements. It was expected that the stringers were the most stressed components of the structure, subject in fact to a high bending moment with respect to the y-axis when a train passes.

This condition of repeated load over time for a very large number of cycles can lead to the structural failure of the component, more likely at the junctions with other components of the structure (cross girder in particular). For the second part of the study, in fact, it is intended to understand what may be critical points of the structure, in which a failure may occur. For such components, a correct estimate of the remaining structural capacities is necessary. Hence the need to optimize the model with a model updating procedure, which will be discussed in the following chapter.

For the optimization procedure, the focus will be put on the study of three specific components of the bridge, highlighted in yellow in Table 23, considered critical for their function and for the levels of damage highlighted.

As a final observation, differences of the damage induced in the three models are evaluated.

The damage relative error is defined to have an estimation of the relative difference between the damages arising in the self-made models and in the one developed by Johs Holt Consultant Eng.

$$\text{DamageRelErr} = \frac{|D - My\_D|}{D} * 100 \% \quad (20)$$

It is pointed out in Table 24 - Table 31 that the values of the *DamageRelErr* are quite high for all the elements and for all the trains analyzed, for both self-made models. Damage values often deviate by at least an order of magnitude between models. This difference in the results is attributable to the different modelling choices and the different hypotheses made.

A damage estimation closest to the Johs Holt Consultant Eng. model is generally found for the complete model, where for some components the *DamageRelErr* does not exceed 50%.

Consequently, if the model developed by the consulting company were taken as a reference, the complete model would seem more accurate in estimating the damage.

As explained in the next chapter, for the purposes of the study, it is not believed that the complete model can give strongly more accurate results than the simple one. It will therefore be the latter to be used in the optimization process.

The difference in terms of damage is an aspect that will be deepened on in the model updating procedure.

<b>Train1</b>	<b>Company</b>		<b>Simple model</b>			
Location	Elem	Damage	Elem	Damage	DamageDiff	DamageRelErr
Stringer	41144	3.95E-08	102	4.46E-07	4.07E-07	91.14%
Subsyst	64074	3.45E-13	1154	9.26E-09	9.26E-09	100.00%
CG-vert 9	33014	6.61E-12	829	1.15E-14	6.60E-12	99.83%
CG-str	33011	5.91E-10	844	4.92E-09	4.33E-09	87.99%
CG-diag 9/8	33024	6.92E-11	879	1.16E-14	6.92E-11	99.98%
Vertical 9	24011	7.29E-10	1327	1.31E-10	5.98E-10	82.03%
Vertical 1	28011	3.10E-09	1390	3.66E-10	2.73E-09	88.19%
Diagonal 1/0	23064	6.35E-09	620	2.78E-11	6.32E-09	99.56%
Diagonal 9/11	23011	1.97E-09	617	1.78E-10	1.79E-09	90.96%
Upper chord	22032	1.42E-08	533	9.43E-09	4.77E-09	33.59%
Lower chord	21042	3.71E-08	426	2.03E-07	1.66E-07	81.72%
CG-vert 5	33034	8.43E-11	929	4.54E-12	7.98E-11	94.61%
	<b>Company</b>		<b>Complete model</b>			
Location	Elem	Damage	Elem	Damage	DamageDiff	DamageRelErr
Stringer	41144	3.95E-08	102	3.55E-08	4.00E-09	10.13%
Subsyst	64074	3.45E-13	1884	5.32E-14	2.92E-13	84.58%
CG-vert 9	33014	6.61E-12	1049	4.37E-11	3.71E-11	84.87%
CG-str	33011	5.91E-10	1064	8.54E-09	7.95E-09	93.08%
CG-diag 9/8	33024	6.92E-11	1618	2.09E-08	2.08E-08	99.67%
Vertical 9	24011	7.29E-10	2380	6.52E-10	7.70E-11	10.56%
Vertical 1	28011	3.10E-09	2696	3.14E-12	3.10E-09	99.90%
Diagonal 1/0	23064	6.35E-09	817	6.27E-14	6.35E-09	100.00%
Diagonal 9/11	23011	1.97E-09	847	9.65E-10	1.01E-09	51.02%
Upper chord	22032	1.42E-08	13766	1.55E-08	1.30E-09	9.15%
Lower chord	21042	3.71E-08	13846	2.00E-07	1.63E-07	81.45%
CG-vert 5	33034	8.43E-11	1249	1.09E-09	1.01E-09	92.27%

Table 24 Damages and damage differences - Train 1

<b>Train2</b>	<b>Company</b>		<b>Simple model</b>			
Location	Elem	Damage	Elem	Damage	DamageDiff	DamageRelErr
Stringer	41144	8.65E-08	102	1.01E-06	9.24E-07	91.44%
Subsyst	64074	8.02E-12	1154	2.70E-08	2.70E-08	99.97%
CG-vert 9	33014	6.74E-12	829	9.95E-15	6.73E-12	99.85%
CG-str	33011	7.03E-10	844	5.48E-09	4.78E-09	87.17%
CG-diag 9/8	33024	7.29E-11	879	1.05E-14	7.29E-11	99.99%
Vertical 9	24011	9.07E-10	1327	1.29E-10	7.78E-10	85.78%
Vertical 1	28011	3.38E-09	1390	4.52E-10	2.93E-09	86.63%
Diagonal 1/0	23064	5.23E-09	620	1.65E-11	5.21E-09	99.68%
Diagonal 9/11	23011	1.67E-09	617	1.47E-10	1.52E-09	91.20%
Upper chord	22032	1.13E-08	533	6.94E-09	4.36E-09	38.58%
Lower chord	21042	2.67E-08	426	1.77E-07	1.50E-07	84.92%
CG-vert 5	33034	9.38E-11	929	4.79E-12	8.90E-11	94.89%
	<b>Company</b>		<b>Complete model</b>			
Location	Elem	Damage	Elem	Damage	DamageDiff	DamageRelErr
Stringer	41144	8.65E-08	102	2.32E-07	1.46E-07	62.72%
Subsyst	64074	8.02E-12	1884	2.38E-11	1.58E-11	66.30%
CG-vert 9	33014	6.74E-12	1049	4.33E-11	3.66E-11	84.43%
CG-str	33011	7.03E-10	1064	7.38E-09	6.68E-09	90.47%
CG-diag 9/8	33024	7.29E-11	1618	2.79E-08	2.78E-08	99.74%
Vertical 9	24011	9.07E-10	2380	6.57E-10	2.50E-10	27.56%
Vertical 1	28011	3.38E-09	2696	3.37E-12	3.38E-09	99.90%
Diagonal 1/0	23064	5.23E-09	817	5.07E-14	5.23E-09	100.00%
Diagonal 9/11	23011	1.67E-09	847	8.04E-10	8.66E-10	51.86%
Upper chord	22032	1.13E-08	13766	1.26E-08	1.30E-09	11.50%
Lower chord	21042	2.67E-08	13846	1.69E-07	1.42E-07	84.20%
CG-vert 5	33034	9.38E-11	1249	1.29E-09	1.20E-09	92.73%

Table 25 Damages and damage differences - Train 2

<b>Train3</b>	<b>Company</b>		<b>Simple model</b>			
Location	Elem	Damage	Elem	Damage	DamageDiff	DamageRelErr
Stringer	41144	1.68E-07	102	1.86E-06	1.69E-06	90.97%
Subsyst	64074	1.42E-11	1154	2.46E-08	2.46E-08	99.94%
CG-vert 9	33014	8.03E-12	829	1.36E-14	8.02E-12	99.83%
CG-str	33011	5.34E-10	844	4.31E-09	3.78E-09	87.61%
CG-diag 9/8	33024	5.92E-11	879	1.48E-14	5.92E-11	99.98%
Vertical 9	24011	6.26E-10	1327	9.70E-11	5.29E-10	84.50%
Vertical 1	28011	1.80E-09	1390	2.58E-10	1.54E-09	85.67%
Diagonal 1/0	23064	3.77E-09	620	1.17E-11	3.76E-09	99.69%
Diagonal 9/11	23011	1.38E-09	617	1.19E-10	1.26E-09	91.38%
Upper chord	22032	5.71E-09	533	3.65E-09	2.06E-09	36.08%
Lower chord	21042	1.27E-08	426	9.05E-08	7.78E-08	85.97%
CG-vert 5	33034	4.32E-11	929	2.97E-12	4.02E-11	93.13%
	<b>Company</b>		<b>Complete model</b>			
Location	Elem	Damage	Elem	Damage	DamageDiff	DamageRelErr
Stringer	41144	1.68E-07	102	7.92E-07	6.24E-07	78.79%
Subsyst	64074	1.42E-11	1884	1.31E-10	1.17E-10	89.16%
CG-vert 9	33014	8.03E-12	1049	3.63E-11	2.83E-11	77.88%
CG-str	33011	5.34E-10	1064	5.69E-09	5.16E-09	90.62%
CG-diag 9/8	33024	5.92E-11	1618	2.27E-08	2.26E-08	99.74%
Vertical 9	24011	6.26E-10	2380	9.12E-10	2.86E-10	45.69%
Vertical 1	28011	1.80E-09	2696	2.40E-12	1.80E-09	99.87%

Diagonal 1/0	23064	3.77E-09	817	3.93E-14	3.77E-09	100.00%
Diagonal 9/11	23011	1.38E-09	847	6.44E-10	7.36E-10	53.33%
Upper chord	22032	5.71E-09	13766	6.24E-09	5.30E-10	9.28%
Lower chord	21042	1.27E-08	13846	9.52E-08	8.25E-08	86.66%
CG-vert 5	33034	4.32E-11	1249	8.24E-10	7.81E-10	94.76%

Table 26 Damages and damage differences - Train 3

Train4		Company		Simple model		
Location	Elem	Damage	Elem	Damage	DamageDiff	DamageRelErr
Stringer	41144	8.67E-07	102	1.25E-05	1.16E-05	93.06%
Subsyst	64074	7.23E-10	1154	2.07E-07	2.06E-07	99.65%
CG-vert 9	33014	7.71E-12	829	9.30E-15	7.70E-12	99.88%
CG-str	33011	5.33E-10	844	3.75E-09	3.22E-09	85.79%
CG-diag 9/8	33024	4.84E-11	879	1.39E-14	4.84E-11	99.97%
Vertical 9	24011	6.87E-10	1327	1.05E-10	5.82E-10	84.72%
Vertical 1	28011	1.27E-09	1390	1.67E-10	1.10E-09	86.85%
Diagonal 1/0	23064	1.92E-09	620	4.19E-12	1.92E-09	99.78%
Diagonal 9/11	23011	7.14E-10	617	5.35E-11	6.61E-10	92.51%
Upper chord	22032	2.04E-09	533	8.56E-10	1.18E-09	58.04%
Lower chord	21042	3.59E-09	426	3.89E-08	3.53E-08	90.77%
CG-vert 5	33034	3.71E-11	929	2.00E-12	3.51E-11	94.61%

		Company		Complete model		
Location	Elem	Damage	Elem	Damage	DamageDiff	DamageRelErr
Stringer	41144	8.67E-07	102	6.63E-05	6.54E-05	98.69%
Subsyst	64074	7.23E-10	1884	1.39E-08	1.32E-08	94.80%
CG-vert 9	33014	7.71E-12	1049	2.83E-11	2.06E-11	72.76%
CG-str	33011	5.33E-10	1064	2.06E-09	1.53E-09	74.13%
CG-diag 9/8	33024	4.84E-11	1618	3.60E-08	3.60E-08	99.87%
Vertical 9	24011	6.87E-10	2380	7.69E-10	8.20E-11	11.94%
Vertical 1	28011	1.27E-09	2696	1.79E-12	1.27E-09	99.86%
Diagonal 1/0	23064	1.92E-09	817	1.83E-14	1.92E-09	100.00%
Diagonal 9/11	23011	7.14E-10	847	2.88E-10	4.26E-10	59.66%
Upper chord	22032	2.04E-09	13766	2.25E-09	2.10E-10	10.29%
Lower chord	21042	3.59E-09	13846	3.73E-08	3.37E-08	90.38%
CG-vert 5	33034	3.71E-11	1249	8.68E-10	8.31E-10	95.73%

Table 27 Damages and damage differences - Train 4

Train5		Company		Simple model		
Location	Elem	Damage	Elem	Damage	DamageDiff	DamageRelErr
Stringer	41144	4.96E-08	102	5.89E-07	5.39E-07	91.58%
Subsyst	64074	1.04E-13	1154	5.87E-09	5.87E-09	100.00%
CG-vert 9	33014	1.44E-11	829	2.55E-14	1.44E-11	99.82%
CG-str	33011	1.07E-09	844	9.61E-09	8.54E-09	88.87%
CG-diag 9/8	33024	1.35E-10	879	2.66E-14	1.35E-10	99.98%
Vertical 9	24011	1.34E-09	1327	2.47E-10	1.09E-09	81.57%
Vertical 1	28011	5.15E-09	1390	4.84E-10	4.67E-09	90.60%
Diagonal 1/0	23064	1.30E-08	620	6.36E-11	1.29E-08	99.51%
Diagonal 9/11	23011	3.66E-09	617	3.33E-10	3.33E-09	90.90%
Upper chord	22032	2.65E-08	533	1.79E-08	8.60E-09	32.45%
Lower chord	21042	6.86E-08	426	3.50E-07	2.81E-07	80.40%
CG-vert 5	33034	1.41E-10	929	7.42E-12	1.34E-10	94.74%

		Company		Complete model		
Location	Elem	Damage	Elem	Damage	DamageDiff	DamageRelErr
Stringer	41144	4.96E-08	102	5.02E-08	6.00E-10	1.21%

Subsyst	64074	1.04E-13	1884	6.13E-15	9.79E-14	94.11%
CG-vert 9	33014	1.44E-11	1049	8.72E-11	7.28E-11	83.49%
CG-str	33011	1.07E-09	1064	1.63E-08	1.52E-08	93.44%
CG-diag 9/8	33024	1.35E-10	1618	3.63E-08	3.62E-08	99.63%
Vertical 9	24011	1.34E-09	2380	1.53E-09	1.90E-10	14.18%
Vertical 1	28011	5.15E-09	2696	4.63E-12	5.15E-09	99.91%
Diagonal 1/0	23064	1.30E-08	817	1.38E-13	1.30E-08	100.00%
Diagonal 9/11	23011	3.66E-09	847	1.81E-09	1.85E-09	50.55%
Upper chord	22032	2.65E-08	13766	2.80E-08	1.50E-09	5.66%
Lower chord	21042	6.86E-08	13846	3.44E-07	2.75E-07	80.06%
CG-vert 5	33034	1.41E-10	1249	1.57E-09	1.43E-09	91.02%

Table 28 Damages and damage differences - Train 5

<b>Train6</b>	<b>Company</b>		<b>Simple model</b>			
Location	Elem	Damage	Elem	Damage	DamageDiff	DamageRelErr
Stringer	41144	1.16E-07	102	1.26E-06	1.14E-06	90.79%
Subsyst	64074	1.15E-13	1154	6.82E-09	6.82E-09	100.00%
CG-vert 9	33014	1.34E-11	829	2.25E-14	1.34E-11	99.83%
CG-str	33011	1.10E-09	844	9.20E-09	8.10E-09	88.04%
CG-diag 9/8	33024	1.27E-10	879	2.41E-14	1.27E-10	99.98%
Vertical 9	24011	1.32E-09	1327	2.37E-10	1.08E-09	82.05%
Vertical 1	28011	4.95E-09	1390	4.71E-10	4.48E-09	90.48%
Diagonal 1/0	23064	1.21E-08	620	5.89E-11	1.20E-08	99.51%
Diagonal 9/11	23011	3.52E-09	617	3.16E-10	3.20E-09	91.02%
Upper chord	22032	2.52E-08	533	1.68E-08	8.40E-09	33.33%
Lower chord	21042	6.41E-08	426	3.33E-07	2.69E-07	80.75%
CG-vert 5	33034	1.36E-10	929	7.14E-12	1.29E-10	94.75%

	<b>Company</b>		<b>Complete model</b>			
Location	Elem	Damage	Elem	Damage	DamageDiff	DamageRelErr
Stringer	41144	1.16E-07	102	1.37E-07	2.10E-08	18.10%
Subsyst	64074	1.15E-13	1884	1.33E-14	1.02E-13	88.43%
CG-vert 9	33014	1.34E-11	1049	8.58E-11	7.24E-11	84.38%
CG-str	33011	1.10E-09	1064	1.61E-08	1.50E-08	93.17%
CG-diag 9/8	33024	1.27E-10	1618	3.44E-08	3.43E-08	99.63%
Vertical 9	24011	1.32E-09	2380	1.39E-09	7.00E-11	5.30%
Vertical 1	28011	4.95E-09	2696	4.42E-12	4.95E-09	99.91%
Diagonal 1/0	23064	1.21E-08	817	1.32E-13	1.21E-08	100.00%
Diagonal 9/11	23011	3.52E-09	847	1.74E-09	1.78E-09	50.57%
Upper chord	22032	2.52E-08	13766	2.64E-08	1.20E-09	4.76%
Lower chord	21042	6.41E-08	13846	3.23E-07	2.59E-07	80.15%
CG-vert 5	33034	1.36E-10	1249	1.43E-09	1.29E-09	90.49%

Table 29 Damages and damage differences - Train 6

<b>Train7</b>	<b>Company</b>		<b>Simple model</b>			
Location	Elem	Damage	Elem	Damage	DamageDiff	DamageRelErr
Stringer	41144	1.30E-06	102	1.55E-05	1.42E-05	91.61%
Subsyst	64074	4.85E-12	1154	2.73E-07	2.73E-07	100.00%
CG-vert 9	33014	1.96E-10	829	3.08E-13	1.96E-10	99.84%
CG-str	33011	1.95E-08	844	1.56E-07	1.37E-07	87.50%
CG-diag 9/8	33024	1.21E-09	879	2.08E-13	1.21E-09	99.98%
Vertical 9	24011	2.25E-08	1327	3.65E-09	1.89E-08	83.78%
Vertical 1	28011	6.13E-08	1390	1.07E-08	5.06E-08	82.54%

Diagonal 1/0	23064	3.58E-08	620	1.50E-10	3.57E-08	99.58%
Diagonal 9/11	23011	2.28E-08	617	2.28E-09	2.05E-08	90.00%
Upper chord	22032	6.95E-08	533	3.68E-08	3.27E-08	47.05%
Lower chord	21042	2.31E-07	426	1.24E-06	1.01E-06	81.37%
CG-vert 5	33034	1.65E-09	929	4.36E-11	1.61E-09	97.36%
<b>Company</b>			<b>Complete model</b>			
Location	Elem	Damage	Elem	Damage	DamageDiff	DamageRelErr
Stringer	41144	1.30E-06	102	1.39E-06	9.00E-08	6.92%
Subsyst	64074	4.85E-12	1884	3.17E-13	4.53E-12	93.46%
CG-vert 9	33014	1.96E-10	1049	1.36E-09	1.16E-09	85.59%
CG-str	33011	1.95E-08	1064	2.90E-07	2.71E-07	93.28%
CG-diag 9/8	33024	1.21E-09	1618	3.61E-07	3.60E-07	99.66%
Vertical 9	24011	2.25E-08	2380	1.88E-08	3.70E-09	16.44%
Vertical 1	28011	6.13E-08	2696	7.84E-11	6.12E-08	99.87%
Diagonal 1/0	23064	3.58E-08	817	5.60E-13	3.58E-08	100.00%
Diagonal 9/11	23011	2.28E-08	847	1.12E-08	1.16E-08	50.88%
Upper chord	22032	6.95E-08	13766	7.76E-08	8.10E-09	11.65%
Lower chord	21042	2.31E-07	13846	1.11E-06	8.79E-07	79.19%
CG-vert 5	33034	1.65E-09	1249	2.02E-08	1.86E-08	91.83%

Table 30 Damages and damage differences - Train 7

<b>Train8</b>	<b>Company</b>		<b>Simple model</b>			
Location	Elem	Damage	Elem	Damage	DamageDiff	DamageRelErr
Stringer	41144	3.18E-06	102	3.68E-05	3.36E-05	91.36%
Subsyst	64074	5.35E-12	1154	6.96E-07	6.96E-07	100.00%
CG-vert 9	33014	5.86E-10	829	8.76E-13	5.85E-10	99.85%
CG-str	33011	5.19E-08	844	4.26E-07	3.74E-07	87.82%
CG-diag 9/8	33024	3.44E-09	879	5.67E-13	3.44E-09	99.98%
Vertical 9	24011	6.03E-08	1327	9.98E-09	5.03E-08	83.45%
Vertical 1	28011	1.67E-07	1390	2.93E-08	1.38E-07	82.46%
Diagonal 1/0	23064	1.10E-07	620	4.85E-10	1.10E-07	99.56%
Diagonal 9/11	23011	6.47E-08	617	6.53E-09	5.82E-08	89.91%
Upper chord	22032	2.27E-07	533	1.28E-07	9.90E-08	43.61%
Lower chord	21042	7.27E-07	426	3.79E-06	3.06E-06	80.82%
CG-vert 5	33034	4.57E-09	929	1.26E-10	4.44E-09	97.24%
<b>Company</b>			<b>Complete model</b>			
Location	Elem	Damage	Elem	Damage	DamageDiff	DamageRelErr
Stringer	41144	3.18E-06	102	3.83E-06	6.50E-07	20.44%
Subsyst	64074	5.35E-12	1884	1.47E-13	5.20E-12	97.25%
CG-vert 9	33014	5.86E-10	1049	3.90E-09	3.31E-09	84.97%
CG-str	33011	5.19E-08	1064	8.54E-07	8.02E-07	93.92%
CG-diag 9/8	33024	3.44E-09	1618	9.49E-07	9.46E-07	99.64%
Vertical 9	24011	6.03E-08	2380	5.16E-08	8.70E-09	14.43%
Vertical 1	28011	1.67E-07	2696	2.18E-10	1.67E-07	99.87%
Diagonal 1/0	23064	1.10E-07	817	1.68E-12	1.10E-07	100.00%
Diagonal 9/11	23011	6.47E-08	847	3.20E-08	3.27E-08	50.54%
Upper chord	22032	2.27E-07	13766	2.52E-07	2.50E-08	11.01%
Lower chord	21042	7.27E-07	13846	3.42E-06	2.69E-06	78.74%
CG-vert 5	33034	4.57E-09	1249	5.57E-08	5.11E-08	91.80%

Table 31 Damages and damage differences - Train 8

Lastly, is shown in Table 32 the damage values comparison for the element 844 belonging to the simple model, at the transit of the train number 8.

As expected from the observation of the normal stress values, the most stressed point of the section presents a significantly higher estimated damage. It sees a damage one order of magnitude higher than that of the point of the section evaluated by the consulting company. The damage value is two orders of magnitude higher than the damage calculated from the model developed by the consulting company.

This conclusion, which can be made for all the sections analysed, explains why, in conducting the comparisons, it was preferred to stick to the assumption made by Johs Holt Consultant Eng. in terms of selection of the analysis point.

Train8	Company		Simple model			Simple model - most damaged point				
	Location	Elem	Damage	Elem	Damage	Damage Diff	Damage RelErr	Elem	Damage	Damage Diff
CG-str	33011	5.19E-08	844	4.26E-07	3.74E-07	87.82%	844	2.70E-06	2.65E-06	98.08%

*Table 32 Damages and damage differences - Train 8 - elem. 844*

## 6 Model Updating

In order to make the most accurate estimation of the remaining useful life of a structure or structural component, it is necessary to be able to correctly simulate its behavior under the action of external loads and to evaluate the load history that has characterized its entire period of activity.

When there is no possibility to carry out periodical on-site measurements and structural checks, the challenge becomes even more difficult. In this situation you can only rely on numerical models made through the use of *FEM* software, simulating in a virtual environment the scenario in which the structure stands.

Hence the need to work with models that are reliable, whose outputs of the simulations are consistent and in line with what happens in reality.

Afterwards the realization of the first numerical models, it is therefore necessary to update and optimize them in order to make the stress and strain responses more accurate, especially in correspondence of the elements considered most critical. The most correct approach to follow would be to carry out an optimization procedure based on measurements made in the field and therefore on the actual response of the structure. In this way, the *FEM* models created would be calibrated in an appropriate manner, for the purpose of reproducing the performance of the structure in a digital environment.

Given that, as already pointed out, there is no experimental data, the model created by Johs Holt Consultant Eng. is taken as a reference. This approach therefore has a purely academic validity, aimed at demonstrating the effectiveness of an optimization algorithm rather than improving the reliability of the model in describing the real behavior of the structure and predicting the loss of its structural capabilities.

The model created by the consulting company presents also, as highlighted, inaccuracies (a questionable modeling of the constraints at the ends of the stringers for example) and simplifications.

It is already mentioned that the optimization procedure will focus on the analysis of the behavior of three specific sections of the bridge, considered critical for structural purposes. It has already been seen in the previous chapter how these sections are also among the most damaged. The damage is the chosen parameter to compare the performance between the model to be optimized and the one taken as a reference.

## 6.1 FE model modification

It has been seen that the two self-made models have shown to deviate from the Johs Holt Consultant Eng. model in relation to some aspects. The influence lines analysis showed a good correspondence in terms of shape equivalence, except for the  $IL$  arising from the application of a load in the transverse direction. A less good compatibility has been observed in terms of stress intensity. As regards the determination of the damage arisen in the sections analyzed, there were major differences.

For most components, the complete model showed better consistency in terms of damage. Despite this, both self-made models showed values of the induced damage often similar and most of the time of a lower magnitude (therefore underestimated damage) than what is assessed by the consulting company.

For the implemented optimization procedure it is decided to use only the simple model for the subsequent analysis. This choice follows from what has been highlighted (not great disparity in terms of results between the self-made models) and for reasons of convenience. If the two models provide fairly similar outputs, you prefer to work with the model that is easier to treat and lighter in terms of computational cost.

The refined model, in fact, consisting of both one-dimensional and bi-dimensional elements, is characterized by a simulation execution times approximately twice as long as simulations carried out on the simple model.

### 6.1.1 Evaluation of the parameters that influence fatigue behaviour: model uncertainties

It is necessary to identify the parameters whose values were uncertain during the modeling of the simple model. These parameters with an uncertain value may have led to an incorrect representation of the structure from which the disparities highlighted could have come from.

Model uncertainties are therefore the aspects to focus on to evaluate where to intervene in order to optimize the model. A sensitivity approach must be followed.

Since the damage induced in the chosen components is the main benchmark that guides in the optimization, it is necessary to evaluate the parameters that influence its determination.

In the formulas used for the calculation of normal stresses, the area moments of inertia with respect to the local  $x$  and  $y$  axes and the area of the sections appear.

In constructing the profiles of the beams constituting the bridge, some geometric simplifications have been made. Equivalent sections has been defined, however second moments of inertia and areas values of each element were similar to what was defined by Johs Holt Consultant Eng.

A difference in modeling, compared to what the consulting company have done, consists in the different definition of the constraints at the ends of the stringers. One-dimensional springs capable of deforming only in the  $y$ -direction could have been added in these points. The springs stiffness could have been used as a parameter to be tuned in order to improve the response of the system.

Intervening on this parameter, however, would probably have led to an improvement only with regard to the shape equivalence and not to the damage.

A very important aspect to take into account are the stiffnesses in correspondence of the connections. Specifically, for torsional stiffnesses at the joints between stringers and cross girders, it is difficult to establish a value. Johs Holt Consultant Eng. has modeled these connections through the use of springs, while the self-made models see fully fixed connections. This difference in modeling may have affected the results. It should also be noted that these connections are critical for the structural stability of the bridge and for the degradation to which they are subjected. With the subsequent application of load cycles, such joints are expected to become less rigid.

It is therefore decided to take the torsional stiffness with respect to the y and z axes at the intersections between cross girders and stringers as parameters to be tuned in the model updating process.

### 6.1.2 Modification of the connections between critical components

As pointed out, the components considered critical are the stringers and the cross girders and in particular their connections. An incorrect estimation of the stiffness in the joints would lead to an incorrect assessment of the stress risen in these points and therefore of the degradation to which they are subjected.

It is therefore intended to modify the *FEM* model from which the study has started by inserting one-dimensional spring elements at the junctions considered.

The following changes are made to the simple model.

- Definition of three torsional stiffnesses and three linear stiffnesses to be associated with the six spring elements created at the aforementioned junctions.

With regard to the stiffness values on which it is not intended to intervene in the optimization, the following common sense values are attributed:

$$kt_x = 1 * 10^5 \frac{N}{mm * rad}$$

$$kl_x = kl_y = kl_z = 1 * 10^4 \frac{N}{mm}$$

- Determination of six *real constants*, to which the stiffnesses are associated, to be assigned to the new finite elements created.
- Definition and creation of six two-node spring-damper 1D *COMBIN14*, Figure 71, finite elements.

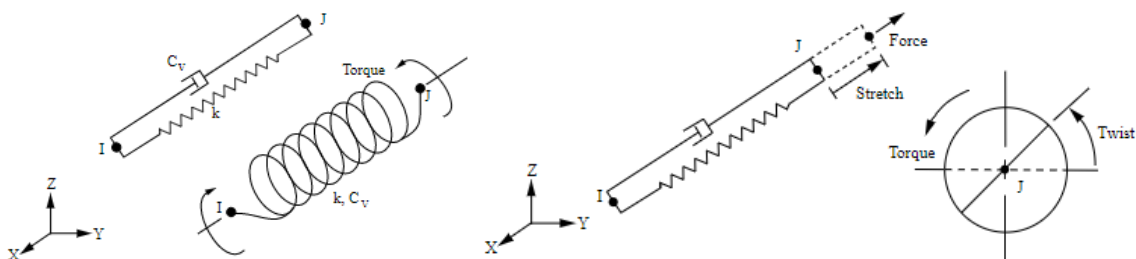


Figure 71 Element COMBIN14 Ansys

The elements created have no dimension at rest and they join the nodes of the stringer element and the cross girder element that meet and overlap at the created joint.

Through the declaration of the *KEYOPT(2)*, with values from 1 to 6, the *COMBIN14* element is defined as a one-dimensional element with longitudinal or torsional capabilities.

---

With this option the element operates in the nodal coordinate system, which by default follows the global coordinate system. Attention has therefore been paid to the direction of the nodal reference frame in the attribution of the correct rigidities.

The 1D longitudinal spring element is a tension-compression element with 1 translational *DOF* per node. No bending or torsion are in this case considered.

The 1D torsional spring element is a purely rotational element with 1 rotational *DOF* per node. No bending or axial loads are considered.

The longitudinal spring element stiffness acts only along its length. The torsion spring element stiffness acts only about its length, as in a torsion bar.

The *COMBIN14* element is massless. In this discussion no damping capacity of this element is considered.

In correspondence of the stringer-cross girder joint are now located elements without mass and dimension at rest, joining two-node elements with coincident nodes.

Since, at these intersections, the nodes are no longer fully fixed, you perform merge and compress operations, using the *NUMMRG* and *NUMCMP* commands, on all but these nodes.

The only parameters not defined at the moment are therefore the torsional stiffnesses with respect to the y and z axes. Afterwards the definition of their first attempt value, their values will be tuned in order to obtain a match in terms of damage between the models under consideration.

## 6.2 Late Acceptance Hill Climbing algorithm

There are several optimization algorithms that can be exploited in order to perform an automatic optimization. One of them is called *Random search*: simulations are performed by attributing random values to the variables to be tuned until an acceptable match is reached on the set target.

In this discussion, it is chosen to use the so-called *Late Acceptance Hill Climbing (LAHC)* method. The *Python* “*lahc*” package [11] has been exploited.

### 6.2.1 How the algorithm works

To understand how the algorithm works, a simple example is showed.

The so called move and energy functions must be implemented before the algorithm is applied.

- Through the move function, you intervene by changing the state of the system, in this discussion the stiffnesses to be tuned.
- The energy function instead returns the energy of the state. The new state of the system is reassigned to the unknown stiffnesses. The energy function returns the objective function.

The goal is trying to minimize the objective function, which is the damage difference in this study, and minimize the energy of the system.

The initial state of the system, thus the initial values of the torsional stiffness  $kt_y$  and  $kt_z$ , must be provided as input in order to define a starting point.

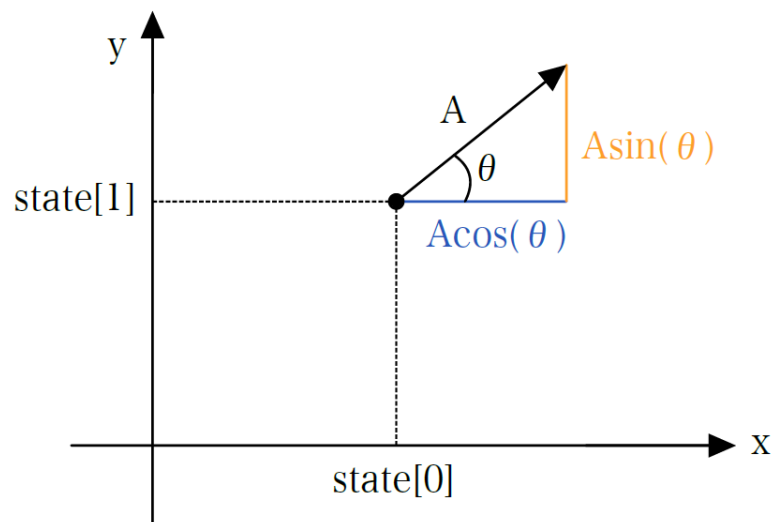


Figure 72 LAHC example

At each iteration the new state of the system is calculated:

$$\begin{aligned} self.state[0] &= self.state[0] + A\cos\theta \\ self.state[1] &= self.state[1] + A\sin\theta \end{aligned}$$

In this example, Figure 72, it is decided to change the state of the system by moving by an amount resulting from  $A$  and  $\theta$  variable values.

The state variables,  $state[0]$  and  $state[1]$ , must be modified in order to minimize the objective function. The move functions are two as well, so it is like you are moving in a two-dimensional space. The fundamental aspect of this algorithm is that you always move from the last state reached by the system, not randomly.

Figure 73 shows graphically the meaning of this. In the example showed, the goal is to identify the maximum of the curve.

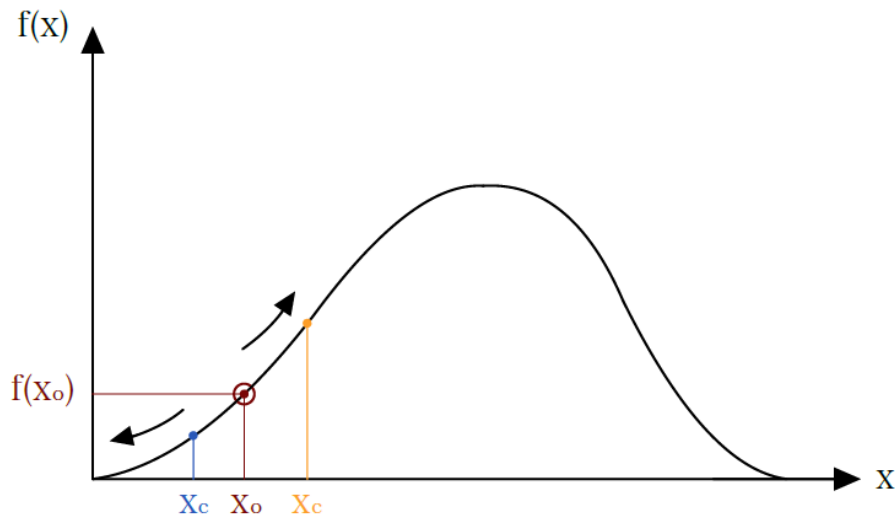


Figure 73 Hill climbing functioning

If the curve to be studied is the one represented in Figure 73, the Hill Climbing (*HC*) method would be sufficient. You can start from a randomly chosen point lying on the curve. Then you take a step in the domain: from  $x_0$  you move to  $x_c$  ( $x_{\text{candidate}}$ ).

If  $f(x_c)$  is greater than  $f(x_0)$ , you accept the new state of the system, otherwise it is rejected. This procedure shall be repeated iteratively until the target has been achieved. As the name of the method itself says, in this case you are "climbing the hill", moving towards the  $x$  that leads to an higher value of the  $f(x)$  until the peak is reached.

But what happens if the considered function had not only an absolute maximum, but also a relative maximum as shown in Figure 74?

The first relative maximum is not what you want since the goal is to find the absolute maximum of the function. If the Hill Climbing method were applied, the solution to the problem would depend on the choice of the first randomly chosen starting point and therefore on the initial state of the system. This is not acceptable for the optimization algorithm it is intended to be implemented.

The *LAHC* method, on the other hand, creates a memory of the direction in which you are moving. Each new value of the function,  $f(x_i)$ , for example, is compared with the value that the function had assumed  $n$  points before, that is,  $f(x_{i-n})$ .

Consequently, the objective function will be compared with the value that it has assumed  $n$ -steps previously. In this way you avoid incurring incorrect results as the Hill Climbing method could do.

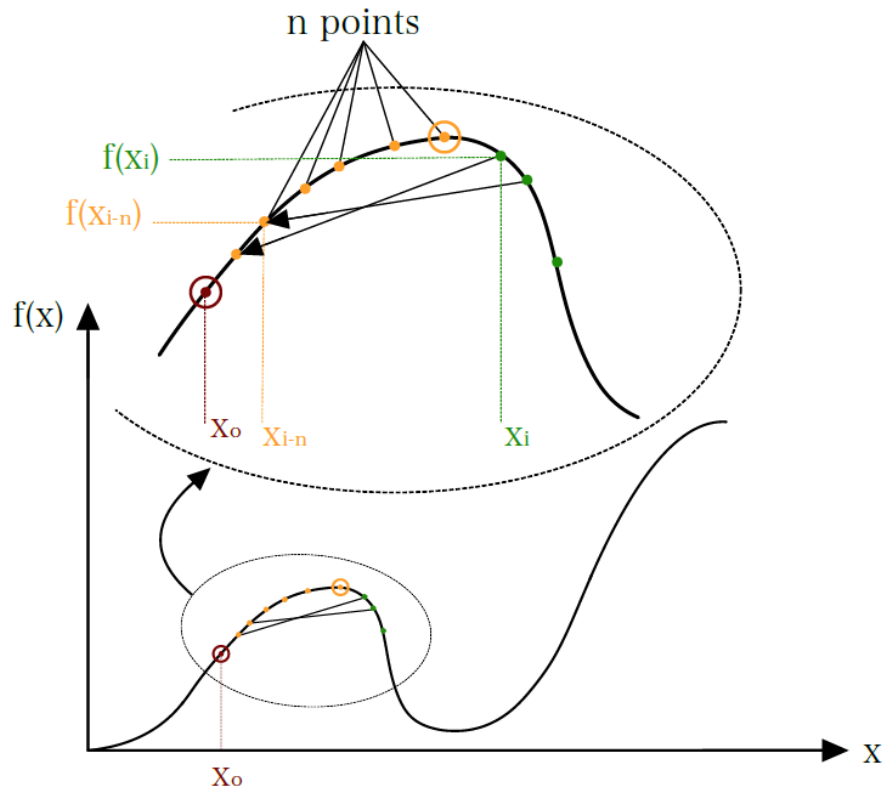


Figure 74 Late acceptance hill climbing functioning

Defined the energy and move functions, it is possible to intervene on some other parameter of the problem.

- The history length: it is the most important parameter on which to intervene. It establishes the number of steps back in time with which to compare the objective function.

If the history length is equal to 1, *LAHC* is equivalent to the Hill Climbing method

Increasing this parameter you improve the quality of the solution but on the other hand the time needed to achieve convergence increases.

Selection of the history length should therefore be based on requirements related to the quality of the solution and time available for the analysis. It will be seen later how the time available for analysis will be a critical factor.

- Minimum number of steps
- Maximum number of steps
- Maximum number of steps that do not lead to an improvement of the solution
- The termination criteria is set so that the algorithm is terminated when a minimum number of attempts has been made and the algorithm has not been able to improve the solution for a certain number of steps.

The termination criterion has been modified by defining a maximum number of iterations that can be performed.

- The initial state of the problem. Updated each time a simulation is finished based on stiffness values obtained from the previous simulation.

## 6.2.2 Definition of move and objective functions

The target set is to minimize the distance, in terms of response, between the self-made model and the one made by Johs Holt Consultant Eng.

The parameters that are intended to be analyzed are the torsional stiffnesses with respect to the y and z axes. Due to the degradation resulting from fatigue phenomena, in fact, it is expected that the conjunctions between critical elements lose in stiffness. Their modeling as fully fixed joints is not adequate anymore. Consequently, a softening can be made at the junctions between cross and longitudinal elements in order to obtain a more realistic clamping and thus lower internal moments.

Defining the move function, therefore, you assign a new state to the system and consequently a new value of the variables  $kt_y$  and  $kt_z$ . Compared to the value assumed by them in the previous step, these variables are modified by means of a stiffness delta ( $dk$ ), whose value is selected randomly in the range between  $-5 * 10^{-2}$  and  $5 * 10^2$  at each step.

It is necessary to define a comparison parameter between the two models, the objective function or cost function, returned by the energy function. This objective function must be brought to convergence during the execution of the optimization process.

In choosing the cost function, different possibilities were evaluated, including linear correlation coefficients, the maximum difference in the absolute values of the stress influence lines or the difference between the damages induced in specific components.

Since the aim of the study is being able to estimate the useful residual life of the structure as accurately as possible, it is intended to evaluate damages occurred. In particular, rather than assessing the difference between the induced damages, the relative error between the damages is taken into account.

The intent of model updating is to minimize this cost function and consequently minimize the energy of the system.

Another objective function that could have been analyzed is the *LCC* in the transverse direction, since the shape equivalence between the *IL* in this direction has shown unsatisfactory results.

Consequently, the parameter to be taken into account and tuned to each iteration could have been the linear stiffness in the transverse direction at the stringers supports.

In fact, it has been highlighted how these have been modeled differently in the three models used and how Johs Holt Consultant Eng. has considered it more appropriate not to constrain the translation of these supports in the y direction.

It was considered, however, that going to improve the value of this *LCC*, bringing it as close as possible to the unit value, could not bring benefits in the estimation of the damage. Therefore, this aspect is neglected in the optimization procedure.

Within the moving function appear:

- Attribution of the two unknown stiffnesses.
- Editing of the *.txt* files to be provided in input to *Ansys* by assigning the updated values of  $kt_y$  and  $kt_z$ .
- Invocation of *Ansys* from *Python* and execution in succession of the three input files related to the three load conditions to which the structure is subject.
- Upload to *Python* the outputs, in terms of internal forces and moments, provided by the simulations launched in *Ansys*.

- Determination, for the three selected components, of the normal stress influence lines per unit load, of the normal stress influence lines and of the damages induced using the load function associated to the most damaging train (the number 8).
- Calculation of the cost function to be minimized: relative error on the damage.

### 6.2.3 Identification of the three most damaged components to be analysed

As already discussed, Table 33 highlights the three components chosen for the optimization procedure. Elements 102 and 426, lying on a stringer and a lower chord, were the most damaged elements by far. In particular as a result of the passage of train 8.

The 844 element is also one of the most damaged but has been considered critical in particular for its position: lying on a cross girder, at the intersection with a main longitudinal beam.

Train8		Company			Simple model					
Location	Elem	Damage	Elem	Damage	Max_z aDiff [MPa]	Max_zv Diff [MPa]	Max_zh Diff [MPa]	Max_z Diff [MPa]	Damage Diff	Damage RelErr
Stringer	41144	3.18E-06	102	3.68E-05	2.240	14.100	14.400	2.240	3.36E-05	91.36%
Subsyst	64074	5.35E-12	1154	6.96E-07	2.670	0.004	55.300	2.730	6.96E-07	100.00%
CG-vert 9	33014	5.86E-10	829	8.76E-13	5.990	8.540	7.590	5.990	5.85E-10	99.85%
CG-str	33011	5.19E-08	844	4.26E-07	1.340	0.903	13.400	1.340	3.74E-07	87.82%
CG-diag 9/8	33024	3.44E-09	879	5.67E-13	10.100	12.600	3.730	10.100	3.44E-09	99.98%
Vertical 9	24011	6.03E-08	1327	9.98E-09	4.560	11.000	5.770	4.550	5.03E-08	83.45%
Vertical 1	28011	1.67E-07	1390	2.93E-08	14.200	6.960	3.260	14.200	1.38E-07	82.46%
Diagonal 1/0	23064	1.10E-07	620	4.85E-10	20.600	10.900	8.740	20.600	1.10E-07	99.56%
Diagonal 9/11	23011	6.47E-08	617	6.53E-09	9.900	7.110	5.440	9.890	5.82E-08	89.91%
Upper chord	22032	2.27E-07	533	1.28E-07	3.430	0.080	2.990	3.430	9.90E-08	43.61%
Lower chord	21042	7.27E-07	426	3.79E-06	0.032	0.075	31.700	0.033	3.06E-06	80.82%
CG-vert 5	33034	4.57E-09	929	1.26E-10	5.590	12.500	4.500	5.580	4.44E-09	97.24%

Table 33 Normal stress differences, damages and damage differences - Train 8

## 6.2.4 Optimal values of the considered parameters

The results of the model updating procedure are presented in this section. It should be noted that the same values of the three torsional stiffnesses and of the three linear ones are attributed, for each joint considered.

In Table 34 are summarized the chosen parameters and the results of the optimization problem.

The first three simulations are conducted by imposing a maximum number of steps allowed equal to 150 and a history length equal to 1 (then a Hill Climbing is performed).

An initial stiffness value of  $1.5 * 10^4$  for  $kt_z$  and  $1 * 10^4$  for  $kt_y$  is set. The first three simulations are launched in succession choosing, at the beginning of each iterative loop, a stiffness value closer to the final value obtained from the previous simulation.

The second simulation provides better *DamageRelErr* values than the first and better than the original case, based on the simple starting model, for elements 844 and 426 but not for element 102.

The third simulation, slightly varying the initial state of the system compared to the second simulation, provides quite different results compared to the first two.

The final stiffness values of the second simulation had therefore led to the discovery of a relative minimum of the objective function, since, slightly changing the initial state of the system, quite different results were found.

Regarding the fourth simulation, in fact, a small modification the initial state of the iterative loop provides still different results, more similar to what was seen for the first two simulations.

All four of the first simulations end due to the achievement of the maximum number of steps that did not lead to an improvement in the result. It is therefore probably far from finding the absolute minimum of the objective function.

For the fifth simulation it is decided to impose an initial state of the system a little more different from the first simulations and a history length of 2 is selected, consequently the *LAHC* is implemented.

The duration of the simulation is longer than simulations 2, 3 and 4 but not that much. The process is interrupted again because the maximum of idle steps has been reached. The values of *DamageRelErr* are among the lowest found, in particular for elements 102 and 426, but there has not been a noticeable improvement in the comparison between damages.

The sixth simulation sees a history length further increased: the objective function is compared, at each iteration, with its value obtained 5 previous steps. In this way you try to avoid the discovery of relative minimums. The final values of the stiffnesses, however, do not differ much from the starting ones and the simulation ends because the maximum number of steps that do not lead to an improvement in the result has been achieved.

As a result, the final values of the *DamageRelErr* do not differ much from what was found in the previous case and the simulation, which this time took longer, did not lead to improvements.

Trying to obtain an estimation of the damage more in line with the reference model, it is decided to launch a seventh simulation. The maximum number of iterative steps that can be performed is increased and a value of 10 is attributed to the history length. A much longer simulation execution time is expected than in previous cases. So it is in fact. The iterative loop lasted for over 11 *hours*. The final values of  $kt_z$  and  $kt_y$  are believed to be the optimal ones for this problem.

$$kt_{z,optimal} = 3.28E + 03 \frac{N}{mm * rad}$$

$$kt_{y,optimal} = 1.22E + 04 \frac{N}{mm * rad}$$

The values of the *DamageRelDiff* are the lowest recorded among the seven simulations and the difference in terms of damage is very small except for element 102, whose estimated damage remains an order of magnitude higher than what emerges from the reference model.

However, the results obtained are considered satisfactory. Having to balance between quality of results and simulation execution times, it is not intended to perform longer iterations.

Despite the increase in length history, therefore, the method still seems to depend heavily on the initial state of the system. This problem is related to the relatively high cost in terms of time required to run this iterative loop. If it were admitted to further increase the history length, and consequently the length of the simulation, the algorithm would have more time to look for the absolute minimum of the objective function and better results would be obtained.

		Attempt number							
		1	2	3	4	5	6	7	
Original state	102	D				3.18E-06			
		My_D				3.68E-05			
		DamageDiff				3.36E-05			
		DamageRelErr				91.36%			
	844	D				5.19E-08			
		My_D				4.26E-07			
		DamageDiff				3.74E-07			
		DamageRelErr				87.82%			
	426	D				7.27E-07			
		My_D				3.79E-06			
		DamageDiff				3.06E-06			
		DamageRelErr				80.82%			
Input values	ktz initial [N/mm*rad]	1.50E+04	1.20E+04	1.00E+04	9.00E+03	9.00E+04	5.00E+04	5.00E+03	
	kty initial [N/mm*rad]	1.00E+04	1.20E+04	1.50E+04	5.00E+04	9.50E+04	9.50E+04	8.00E+03	
	Steps minimum	50	50	50	50	50	50	50	
	Steps idle fraction	0.08	0.08	0.08	0.08	0.08	0.1	0.12	
	Max step	150	150	150	200	200	200	300	
	Max step idle	12	12	12	16	16	20	36	
	History length	1	1	1	1	2	5	10	
Output values	Process time [min]	170	83	90	54	102	178	674	
	N° of steps	75	35	39	22	41	71	262	
	N° of steps idle	13	13	13	17	17	21	37	
Final state	ktz final [N/mm*rad]	1.34E+04	1.16E+04	9.40E+03	9.07E+03	8.88E+04	4.86E+04	3.28E+03	
	kty final [N/mm*rad]	1.23E+04	1.28E+04	1.50E+04	5.05E+04	9.63E+04	9.58E+04	1.22E+04	
	102	My_D	3.17E-04	3.05E-04	4.98E-05	2.94E-04	6.25E-05	2.77E-04	3.59E-05
		DamageDiff	3.14E-04	3.02E-04	4.67E-05	2.91E-04	5.93E-05	2.74E-04	3.27E-05
		DamageRelErr	99.00%	98.96%	93.62%	98.92%	94.91%	98.85%	91.13%
	844	My_D	7.54E-08	7.17E-08	2.86E-07	7.07E-08	8.05E-08	7.37E-08	6.54E-08
		DamageDiff	2.35E-08	1.98E-08	2.34E-07	1.88E-08	2.86E-08	2.18E-08	1.35E-08
		DamageRelErr	31.14%	27.60%	81.87%	26.55%	35.57%	29.55%	20.66%
	426	My_D	4.00E-06	3.48E-06	4.18E-06	3.27E-06	2.62E-06	2.87E-06	1.59E-06
		DamageDiff	3.27E-06	2.75E-06	3.45E-06	2.54E-06	1.89E-06	2.14E-06	8.63E-07
		DamageRelErr	81.80%	79.10%	82.60%	77.74%	72.27%	74.63%	54.28%

Table 34 Results of the model updating procedure

The model updating procedure aimed at narrowing the gap in terms of response between the two models in consideration, the simple one and the one implemented by the consulting company, has therefore been completed. Despite the limitations deriving from the computational cost required and the length of the simulations conducted, the result achieved are considered adequate.

The optimized model can now be used for subsequent analysis, which will not be covered in this discussion, such as estimating the remaining fatigue life of the components demonstrated to be the most critical.

## 6.2.5 LAHC efficiency and effectiveness

The *LAHC* method has a lot of potential and nowadays new more and more complex algorithms are continuously released that implement it.

The algorithm used needs a large number of iteration steps to provide satisfactory results if the initial state of the system is far away from the optimal one. The problem analyzed in this discussion, however, requires the execution of three simulations at a time for a total duration of about five minutes for each iterative step.

Consequently, a large number of hours would be necessary if the search for the optimal value was not truncated once the maximum number of steps or the maximum number of idle steps have been reached.

The efficiency of the *LAHC* method consequently depends on the number of steps that can be performed.

The time factor in this case is limiting and binding. Not being able to afford to perform an optimization simulation tens of hours long, it is admitted, in this discussion, to find less satisfactory results.

So, higher the number of steps back in time (and consequently the history length), higher is the accuracy, but at the same time higher is the computational power required. A compromise solution has to be found, a trade-off.

The model updating problem discussed here has as its main objective to describe the *LAHC* algorithm and implement it, rather than finding an optimal solution. Consequently, it is admitted to limit the computational power used and be satisfied with the results obtained.

To get an idea of the effectiveness of this algorithm, it is possible to observe the graphs (Figure 75 - Figure 81) that represent the energy of the system with respect to the number of iterative steps performed.

You should analyze the gradient of that curve to see how effective is the iterative process. A quick decrease of that energy, followed by a less strong descent and therefore a lower gradient means that the algorithm works effectively.

For attempts 1, 5, 6 and 7, for example, it is noted that the decrease in system energy (one of the objectives of the optimization method) is more gradual than in other cases. So the state of the system is moving more slowly and gradually towards a solution considered optimal.

Although the reduction of energy is more gradual in these cases, the curves are far from being soft and regular, but show steps. This is again due to the limited number of iteration steps performed. A longer duration of the optimization simulation would certainly have led to better results and energy-number of steps curves that reach convergence more gradually.

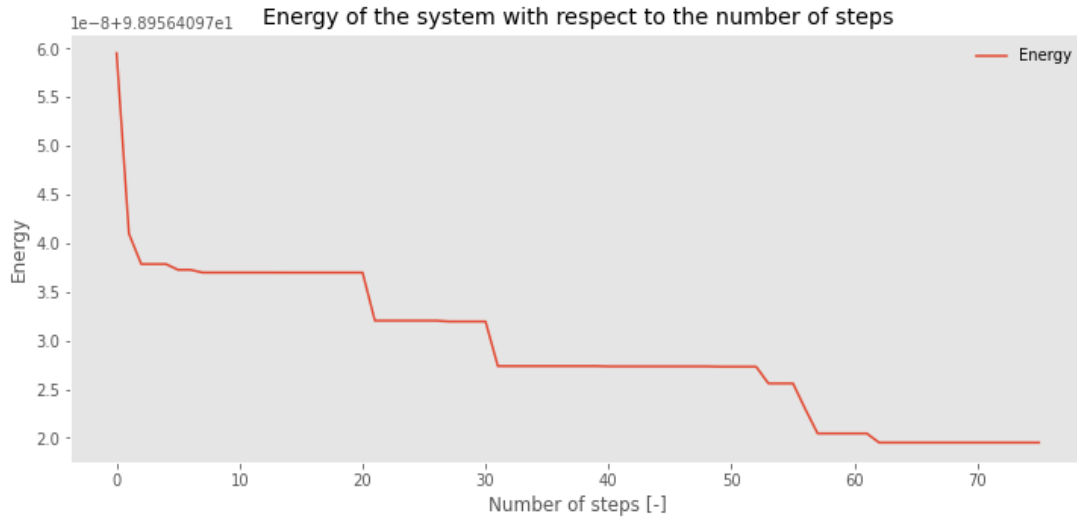


Figure 75 Energy vs number of steps - Attempt 1

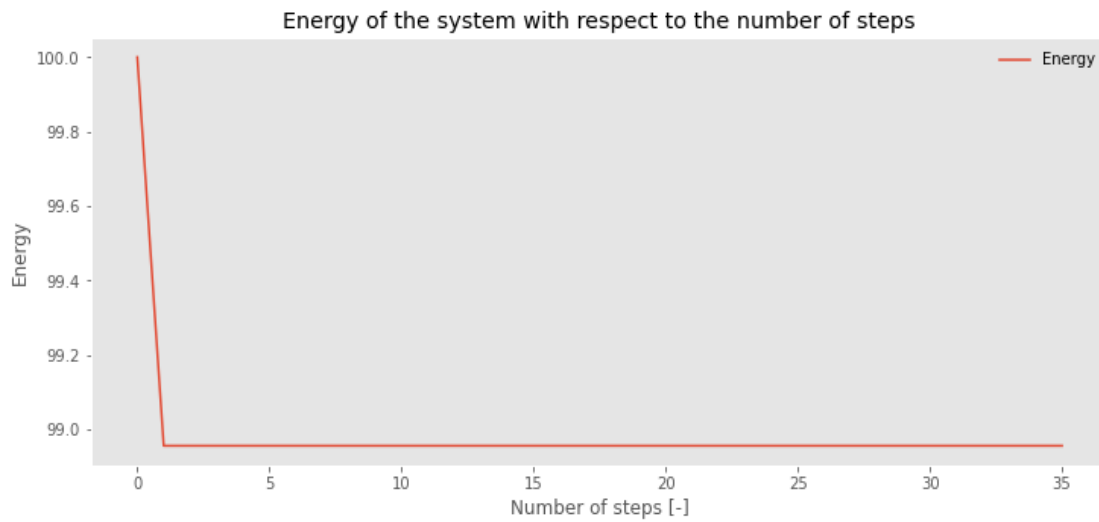


Figure 76 Energy vs number of steps - Attempt 2

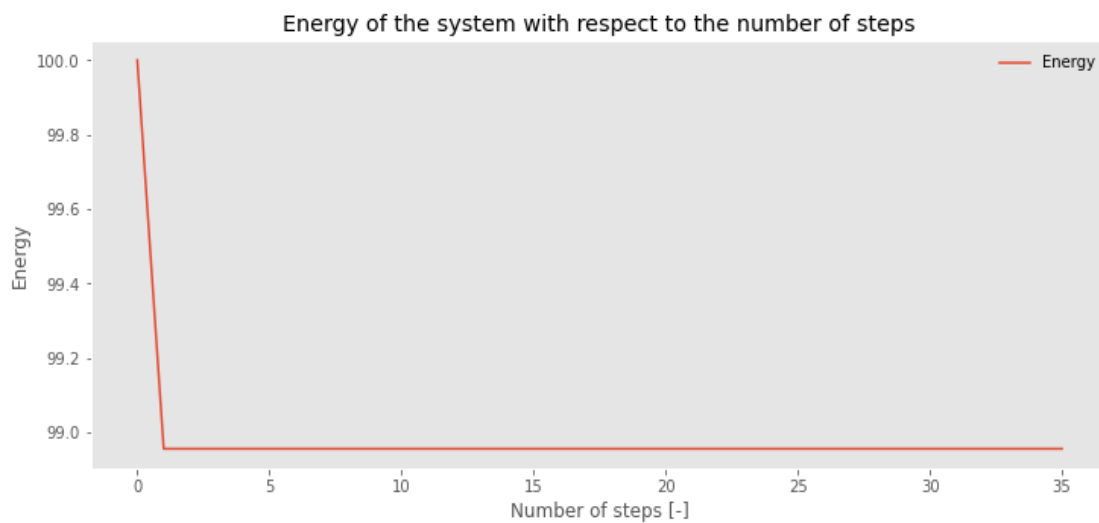


Figure 77 Energy vs number of steps - Attempt 3

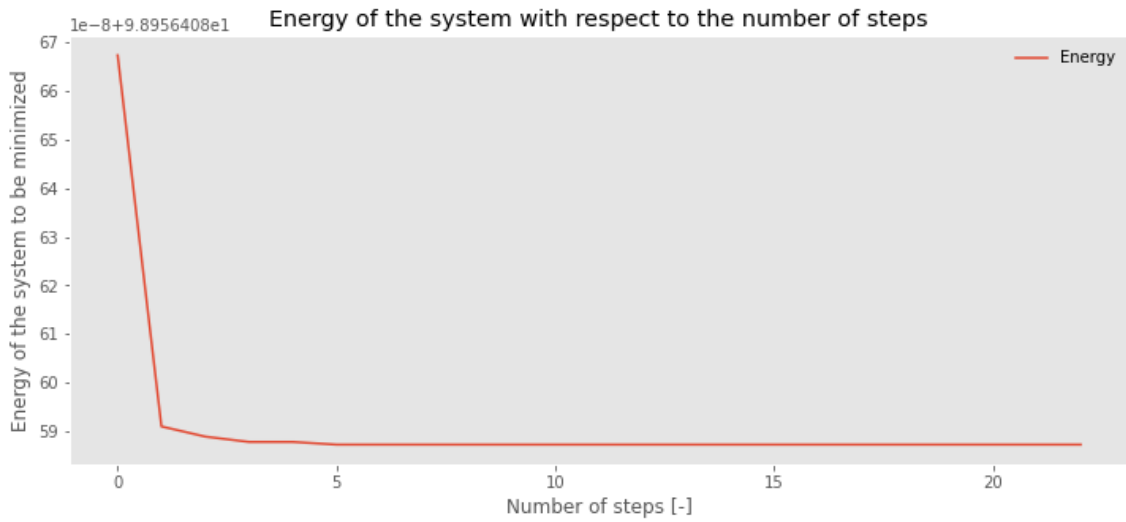


Figure 78 Energy vs number of steps - Attempt 4

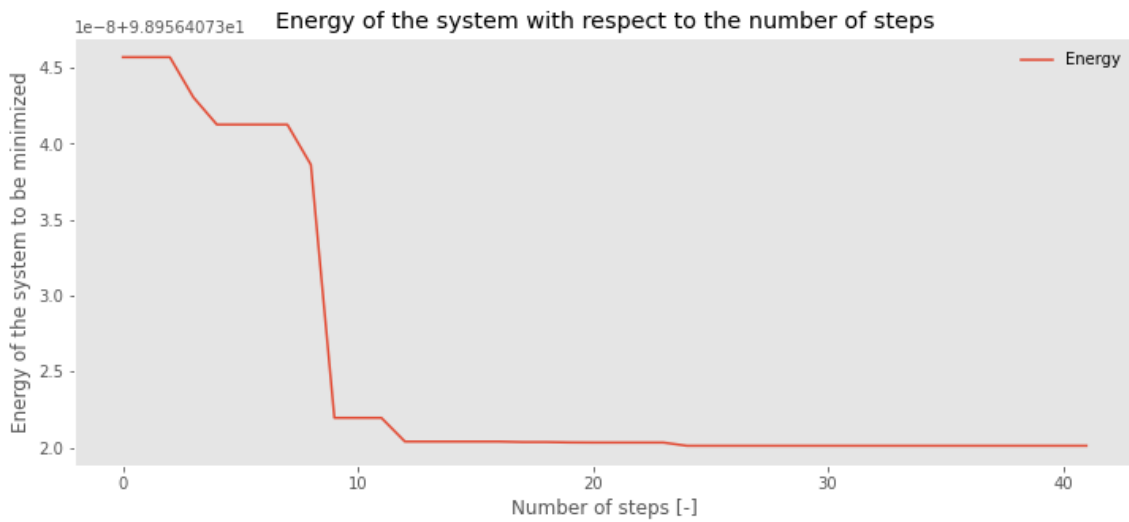


Figure 79 Energy vs number of steps - Attempt 5

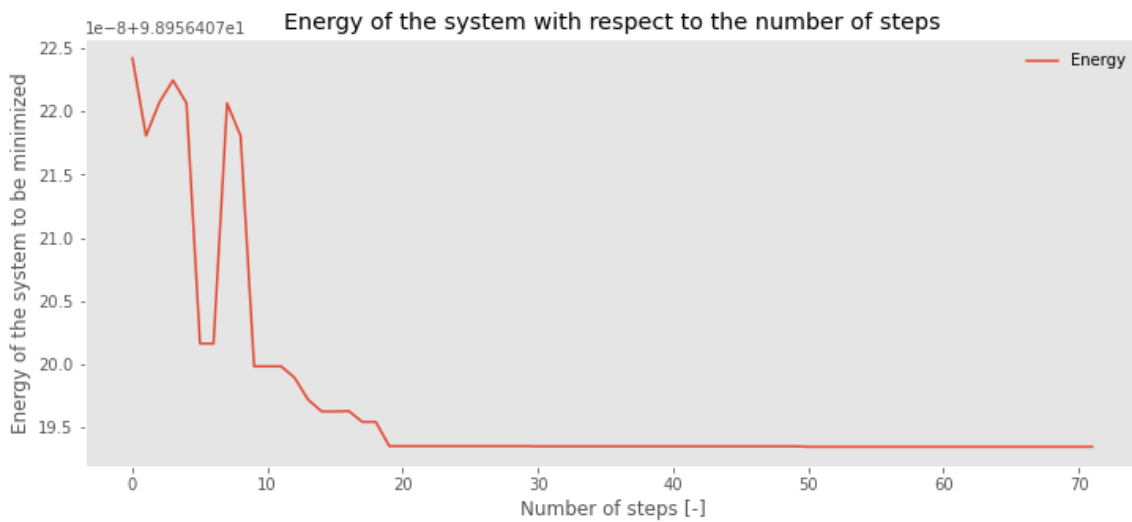


Figure 80 Energy vs number of steps - Attempt 6

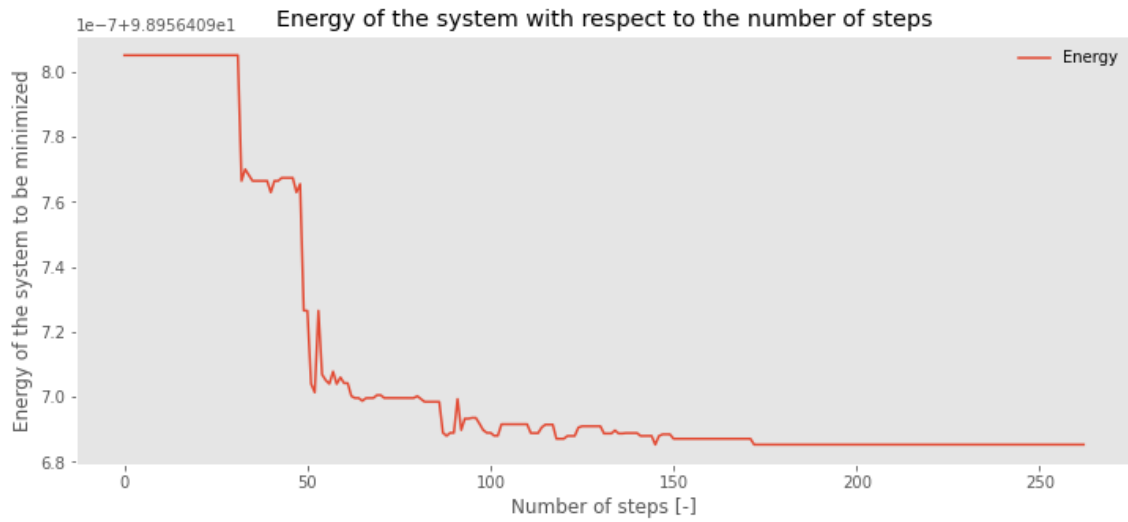


Figure 81 Energy vs number of steps - Attempt 7

The process of model optimization aimed at improving its response is therefore concluded. Specifically, the goal was to reduce the gap, in terms of damage induced in the individual components analyzed, with the Johs Holt Consultant Eng. model taken as a reference. The efficiency and effectiveness of the method were evaluated and it was concluded that if the computational power available or the time to run each simulation were greater, even better results would have been obtained.

## 7 Conclusions

Planning on-site measurement campaigns aimed at monitoring the condition of a structure is not a path that is always taken, especially for economic reasons. Hence the need to rely on simulations carried out on numerical models, which need to be robust and possibly computationally light to treat.

The study illustrated the methodology to be followed in order to verify and predict the ability of a railway bridge to support loads in working conditions. Taking as a reference a model developed by independent studies, a series of comparisons has been made aimed at determining the accuracy of self-made models in describing the behaviour of the structure.

An Influence Line analysis has been firstly carried out, the results of which showed an ability of the two self-made models to emulate the reference model with regard to the static behaviour of the bridge. The *MAC* method subsequently highlighted the modal incompatibility of the two models developed for this study.

In the aftermath of the determination of the extent of the damage arisen in specific sections of the bridge, sometimes overestimated and sometimes underestimated by the self-made models, it has been considered necessary to follow a model updating procedure. Then optimization process is aimed at tuning the three models in terms of damage response.

The *LAHC* algorithm has been implemented and relatively satisfactory results, based on trade-off considerations, have been obtained. However effective this approach may be, it has been shown that its efficiency depends on the complexity of the model and of the performed simulations if you have limitations in terms of computational cost or time to devote to the study.

Once the refinement of the uncertain model parameters has been completed and the model has been optimized, the numerical tool is ready to be exploited in subsequent analyses.

An assessment of the remaining service life of the bridge, using data on the historical and present rail traffic spectrum, would complement the investigation and allow maintenance plans to be established to ensure safe and durable use of the entire railway infrastructure.

---

## 8 References

- [1] B. Imam and T. D. Righiniotis, "Fatigue evaluation of riveted railway bridges through global and local analysis," *Journal of Constructional Steel Research*, no. 66, pp. 1411-1421, 2010.
- [2] G. Frøseth, "Load model of historic traffic for fatigue life estimation of Norwegian railway bridges," *PhD thesis*, Trondheim, 2019.
- [3] A. Taras and R. Greiner, "Development and Application of a Fatigue Class Catalogue for Riveted Bridge Components," *Structural Engineering International*, no. 1, pp. 91-103, 2010.
- [4] G. T. Frøseth, A. Rønnquist and O. Øiseth, "Prediction Error in Strain Response in Finite Element Simulations with Moving Load Formulation of Train Passages of Open Deck Steel Bridges," *ICRT*, pp. 766-773, 2017.
- [5] K. Solvik-Olsen, "National Transport Plan 2018-2029," *Norwegian Ministry of Transport and Communications*, 2017.
- [6] Ansys, "ANSYS Mechanical APDL Element Reference," 2019.
- [7] G. Frøseth, "thellevikmodule," *GitHub*, Trondheim.
- [8] J. Holt, "Calculation report - Fatigue calculations of older railway bridges - General project assumptions," 2018.
- [9] R. J. Allemang and D. L. Brown, "A Correlation Coefficient for Modal Vector Analysis," *International Modal Analysis Conference*, pp. 110-116, 1982.
- [10] G. Frøseth, "fatpack," *GitHub*, Trondheim.
- [11] G. Frøseth, "lahc," *GitHub*, Trondheim.

- 
- [12] Ansys, “ANSYS Mechanical APDL Command reference,” 2019.
- [13] M. Domaneschi and L. Martinelli, “Optimal passive and semi-active control of a wind excited suspension bridge,” *Structure and Infrastructure Engineering: Maintenance, Management, Life-Cycle Design and Performance*, pp. 242-259, 2013.
- [14] B. Imam, T. D. Righiniotis, M. K. Chryssanthopoulos and B. Bell, “Analytical fatigue assessment of riveted rail bridges,” *Bridge Engineering*, no. 159, p. 105-116, September 2006.
- [15] R. J. Allemang, “The Modal Assurance Criterion - Twenty Years of Use and Abuse,” *Sound and vibration*, pp. 15-17, 2003.
- [16] B. Imam, T. D. Righiniotis and M. K. Chryssanthopoulos, “Probabilistic Fatigue Evaluation of Riveted Railway Bridges,” *J. Bridge Eng.*, no. 13, pp. 237-244, 2008.
- [17] F. V. Lippi, M. Orlando and W. Salvatore, “Assessment of the dynamic and fatigue behaviour of the Panaro railway steel bridge,” *Journal of Constructional Steel Research*, no. 69, pp. 54-63, 2011.
- [18] F. Masoumi and A. Mehrabzade, “Application of Influence Lines on Static Analysis of Cable Stayed Bridges,” *International Journal of Engineering and Technology*, 2013.
- [19] A. Rageh, S. E. Azam and D. G. Linzell, “Steel railway bridge fatigue damage detection using numerical models and machine learning: Mitigating influence of modeling uncertainty,” *International Journal of Fatigue*, no. 134, 2020.
- [20] A. Somà, “*Machines construction* course notes,” Politecnico di Torino, 2020.
- [21] M. Morgese, F. Ansari, M. Domaneschi and G. P. Cimellaro, “Post-collapse analysis of Morandi’s Polcevera viaduct in Genoa Italy,” *Journal of Civil Structural Health Monitoring*, 2019.